ADAPTIVE ALGORITHMS FOR THE REJECTION OF SINUSOIDAL DISTURBANCES ACTING ON UNKNOWN PLANTS

by

Scott Anthony Pigg

A dissertation submitted to the faculty of
The University of Utah
in partial fulfillment of the requirements for the degree of

Doctor of Philosophy

Department of Electrical and Computer Engineering

The University of Utah

December 2011

The University of Utah Graduate School

STATEMENT OF DISSERTATION APPROVAL

The dissertation of _____

has been approved by the following supervisory committee members:

_____ , Chair _____
Date Approved

_____ , Member _____
Date Approved

_____ , Member _____
Date Approved

_____ , Member _____
Date Approved

_____ , Member _____
Date Approved

and by _____ , Chair of

the Department of _____

and by Charles A. Wight, Dean of The Graduate School.

ABSTRACT

The dissertation is concerned with the development and analysis of adaptive algorithms for the rejection of unknown periodic disturbances acting on an unknown system. The rejection of periodic disturbances is a problem frequently encountered in control engineering, and in active noise and vibration control in particular. A new adaptive algorithm is presented for situations where the plant is unknown and may be time-varying. Known as the adaptive harmonic steady-state or ADHSS algorithm, the approach consists in obtaining on-line estimates of the plant frequency response and of the disturbance parameters. The estimates are used to continuously update control parameters and cancel or minimize the effect of the disturbance. The dynamic behavior of the algorithm is analyzed using averaging theory. Averaging theory allows the nonlinear time-varying closed-loop system to be approximated by a nonlinear time-invariant system. Extensions of the algorithm to systems with multiple inputs/outputs and disturbances consisting of multiple frequency components are provided.

After considering the rejection of sinusoidal disturbances of known frequency, the rejection of disturbances of unknown frequency acting on an unknown and time-varying plant is considered. This involves the addition of frequency estimation to the ADHSS algorithm. It is shown that when magnitude phase-locked loop (MPLL) frequency estimation is integrated with the ADHSS algorithm, the two components work together in such a way that the control input does not prevent frequency tracking by the frequency estimator and so that the order of the ADHSS can be reduced. While MPLL frequency estimation can be combined favorably with ADHSS disturbance rejection, stability is limited due to the local convergence properties of the MPLL. Thus, a new frequency estimation algorithm with semiglobal stability properties is introduced. Based on the theory of asynchronous electric machines, the induction

motor frequency estimator, or IMFE, is shown to be appropriate for disturbance cancellation and, with modification, is shown to increase stability of the combined ADHSS/MPLL algorithm. Extensive active noise control experiments demonstrate the performance of the algorithms presented in the dissertation when disturbance and plant parameters are changing.

To my family.

CONTENTS

ACKNOWLEDGEMENTS

I would like to thank the following people. I would like to offer my sincerest gratitude to my advisor Dr. Marc Bodson, whose guidance was critical to the completion of this work. He has shown me how to pursue research with rigor and dedication. I would like to thank the members of my research committee: Prof. Behrouz Farhang-Boroujeny, Prof. Neal Patwari, Prof. Mikhail Skliar, and Prof. Mark Minor. They have made this work possible by offering many valuable suggestions and by providing a supportive environment. I would also like to thank Sandia National Labs for their financial support. Finally, I would like to thank my family for their unending support and encouragement.

CHAPTER 1

INTRODUCTION

1.1 Applications

The focus on disturbances that are known to be periodic in nature makes this research relevant to many applications involving rotating equipment, in which discrepancy between the rotor's geometric axis and inertial axis leads to unwanted vibrations. The attenuation of unwanted vibrations by adaptive means is known as active vibration control (AVC). Rotating equipment and the accompanying vibrations oftentimes lead to acoustic disturbances, which cause human discomfort and negatively affect worker productivity. The reduction of acoustic disturbances by adaptive techniques is known as active noise control (ANC). Due to the similarities involved, these fields are collectively known as active noise and vibration control (ANVC). While in some cases the frequency of the disturbance may be measurable, it is unlikely the exact phase of the disturbance will be known due to random irregularities in the source. As a result, active techniques must be used to maintain substantial attenuation of the disturbance [23].

There are many applications related to ANVC where disturbance rejection is the primary control objective. Among these applications are a variety of engineering problems. Examples include active control of noise in turboprop aircraft [9], headphones for noise cancellation [22], vibration reduction in helicopters [2] [34], reduction of optical jitter in laser communication systems [27], isolation in space structures of vibrations produced by control moment gyroscopes and cryogenic coolers [25] [46], suppression of gearbox housing vibrations [12], track following despite eccentricity in disk drives [42], [51] and CD players [8], [47].

In several of the above-mentioned applications, the tracking of time-varying parameters is essential. An example is the active control of noise, where the dynamics

of sound transmission can be considerably affected by people moving within the space where sound propagates. As another example, [45] discusses the cancellation of high-frequency noise in headsets, and reports that small movements in the headset position can create significant changes in the secondary path dynamics (*i.e.,* the plant). In particular, due to the short wavelength associated with high frequencies, the phase of the frequency response may change by more than 90 degrees with small movements of the headset. In helicopters, the plant as well as the disturbance may vary significantly due to changes in flight conditions. In applications involved with space exploration, precision is paramount, and repair is very costly. Therefore, it is preferable to have systems which can achieve optimal vibration reduction while adapting to changes caused by aging or the harsh environment.

1.2 Periodic Disturbances Acting on a Known Plant

To begin treatment of sinusoidal disturbances acting on unknown systems, it is useful to first consider algorithms for the rejection of sinusoidal disturbances acting on known systems. Perhaps the most common algorithm for ANVC applications, when the plant is known, is the filtered-X LMS (FXLMS) algorithm. Independently derived by Widrow and Burgess [23], the FXLMS algorithm is widely used in feedforward applications which rely upon an accurate measure of the uncorrupted disturbance signal. When a preview of the disturbance is available, feedforward techniques have achieved significant attenuation of unwanted disturbances. In many cases, such a preview is not available. Therefore, in this dissertation, the focus is on algorithms of the pure feedback type. These problems are more difficult to solve and less well understood.

Consider the feedback system shown in Fig. 1.1, where $P(s)$ is a known bounded-input bounded-output plant. On the figure, the desired value of y is assumed to be $y_d = 0$, and $y(t)$ is fed back in order to determine the control signal $u(t)$ needed to reject the sinusoidal disturbance $p(t)$. While the frequency of $p(t)$ may be known, it is generally assumed that the phase of $p(t)$ is not known. Adaptation is used to identify

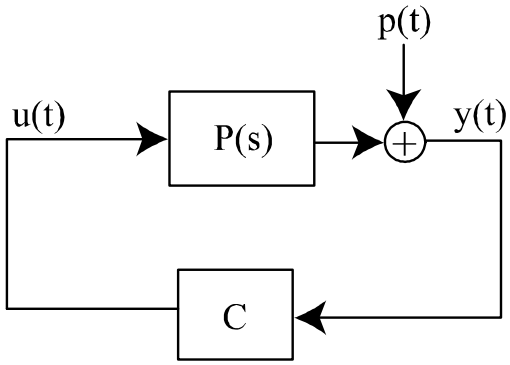

Figure 1.1. Feedback control system.

the magnitude and exact phase of $p(t)$ allowing an appropriate $u(t)$ to be obtained. Therefore, block C consists of an adaptive parameter identification scheme as well as an algebraic control law.

While FXLMS algorithms have achieved some success, they require the entire transfer function $P(s)$ be known over the frequency range of interest. Since $P(s)$ may be high-order, these algorithms can involve significant computational complexity. Other algorithms avoid this complexity by assuming that $P(s)$ can be represented by its steady-state frequency response at the disturbance frequency. This reduces the number of parameters used to represent the plant to only two parameters for each frequency component in the disturbance, namely the magnitude and phase of the frequency response, or equivalently the real and imaginary part of the frequency response.

From the steady-state assumption, a class of solutions based on the internal model principle (IMP) of control theory has arisen. IMP states that for perfect disturbance cancellation, a model of the disturbance must be embedded in the control path. This requires that the frequencies present in the disturbance be known. If the disturbance frequency is unknown or may vary with time, a reliable estimate must first be obtained before cancellation of the disturbance is possible.

1.3 Periodic Disturbance Rejection with Online Plant Estimation

As previously stated, when the plant is known (possibly measured in a preliminary experiment with white noise), a typical solution in ANVC is based on the well-known FXLMS algorithm. Therefore, it is natural that methods for time-varying plants [24] [54] [55] provide online plant estimation for this algorithm. While the adaptive methods have been shown to work, they are computationally intensive and require the injection of a significant amount of white noise to provide sufficient excitation. Stability of the algorithms is also rarely addressed, due to the difficulty in decoupling the two components of the algorithm. [52] analyzes the FXLMS algorithm with online secondary path modeling and narrowband disturbances, and derives a closed form expression for the mean squared error of the cancellation error in the presence of estimation errors. It is shown that stability requires that the phase of the frequency response of the secondary path must be within 90 degrees of the estimated path's frequency response.

A more recent and original approach can be found in [32]. Update of the controller depends upon an estimate of the complex gain of the system and is based on the recursive prediction error approach of [44]. This estimate is used to update a complex valued control signal, with only the real part of the control applied to the plant. The algorithm has been shown to work under certain random variations in the unknown parameters through simulations involving the plant of [15]. We have found in similar simulations that a large amount of measurement noise was sometimes needed to insure cancellation of the disturbance.

1.3.1 Simulation demonstrating the limits of a current method

Simulations were conducted using the same system as in [32] with a real valued disturbance of constant magnitude and unknown phase. As in [32], the frequency was taken as $\omega_0 = 0.1\ rad.$, and the system was tuned using identical parameters. The variance of the measurement noise was taken as $\sigma^2 = 0.01$. In Fig. 1.2, the output of the plant is shown. After $40,000$ samples, the control algorithm is engaged

and the disturbance is canceled. The time-varying stepsize is shown in Fig. 1.3. As an appropriate control signal for cancellation of the disturbance is determined, the stepsize converges to zero and the adaptive algorithm reaches steady-state. A drawback of the algorithm is observed when the frequency of the disturbance is decreased to $\omega_0 = 0.08\ rad.$ In Fig. 1.4, the output of the plant is shown. Even though the simulation was conducted for the same number of samples as Fig. 1.2, at approximately 3.5×10^5 samples, the output of the plant becomes undefined. In Fig. 1.5, it is seen that an internal signal of the algorithm becomes unstable. While the algorithm does take some precautions for dealing with growing signals, eventually this growth causes other signals of the algorithm to become undefined. To insure stability in this case, it was found that really large amounts of measurement noise were needed. In fact, the level of noise was so high that no observable disturbance rejection could be ascertained.

1.3.2 Internal model principle

Adaptive control theory provides another option for the control of unknown systems with unknown periodic disturbances. The idea, as proposed in [10], [11] [31], is to apply the internal model principle within a model reference or pole placement adaptive control strategy. Practically, the implementation is obtained by raising the order of the controller and forcing some poles of the controller on the unit circle (or the $j\omega$-axis in continuous-time). Global stability of such systems can be proved in theory, even allowing for unstable plants and for tracking of arbitrary reference inputs. Unfortunately, there is evidence of slow convergence and poor robustness properties of these schemes in the literature [56] [4]. It is possible that the robustness problems could be reduced or resolved using robust adaptive control methods [48], [18]. However, practical viability of these methods in disturbance rejection applications has not been demonstrated. Further, additional problems make it difficult to apply the methods to the type of problems being considered:

- the number of adaptive parameters is two times the order of the plant plus two times the number of sinusoidal components. Considering that an appropriate

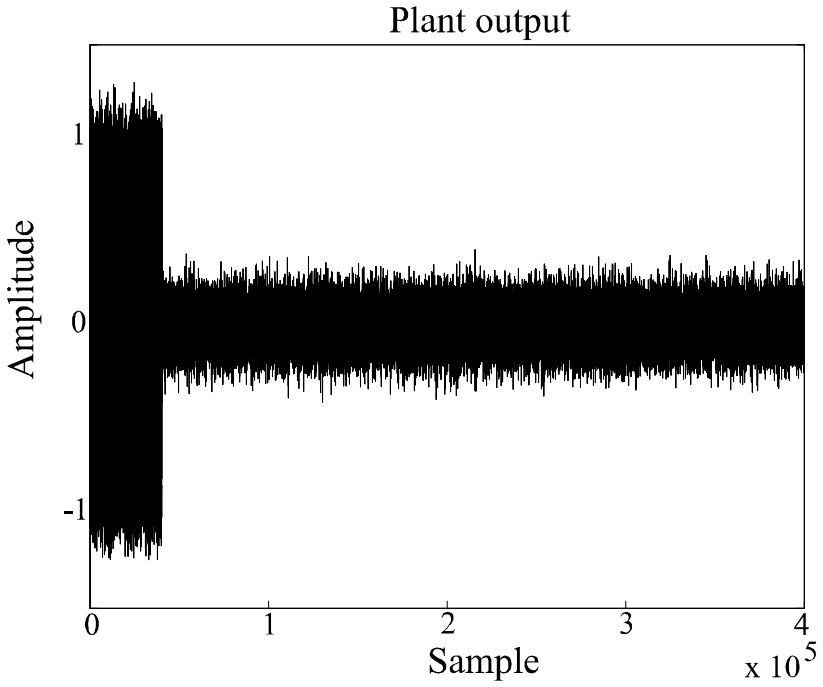

Figure 1.2. Output of plant with $\omega_0 = 0.1$ rad.

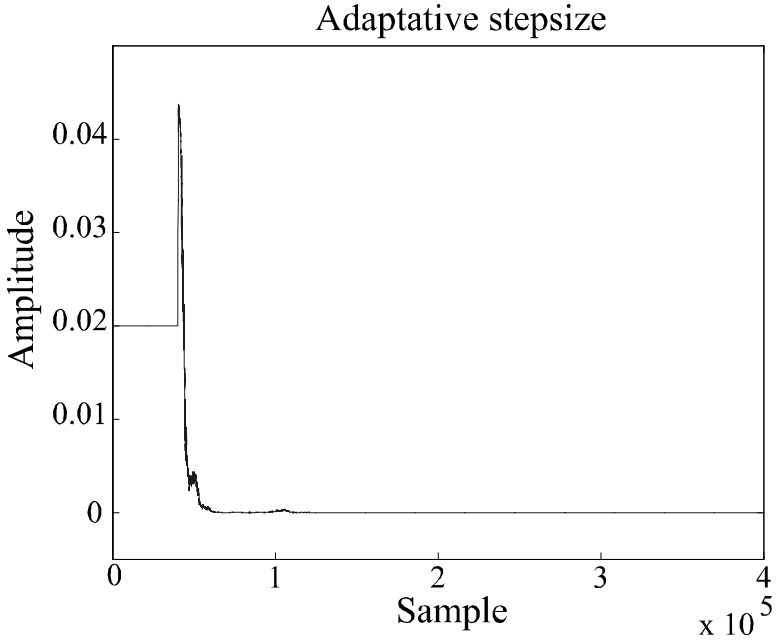

Figure 1.3. Magnitude of the time-varying stepsize with $\omega_0 = 0.1$ rad.

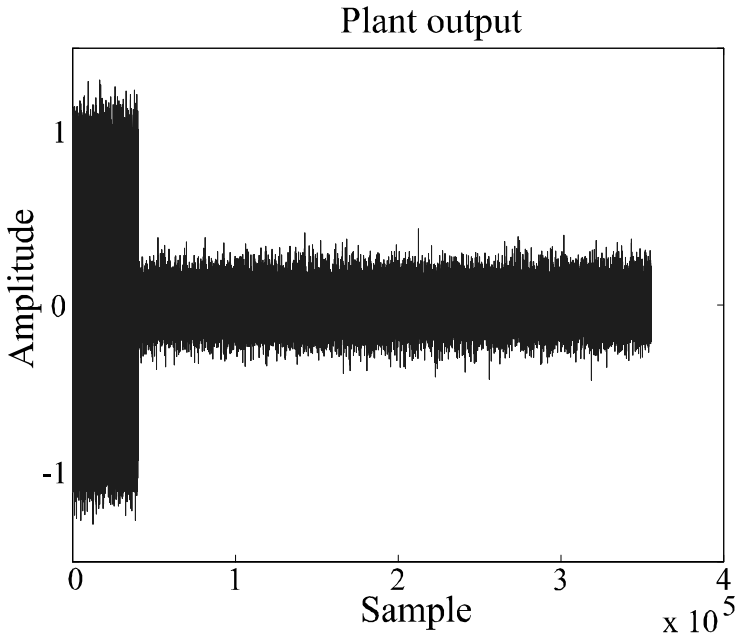

Figure 1.4. Output of plant with $\omega_0 = 0.08$ rad.

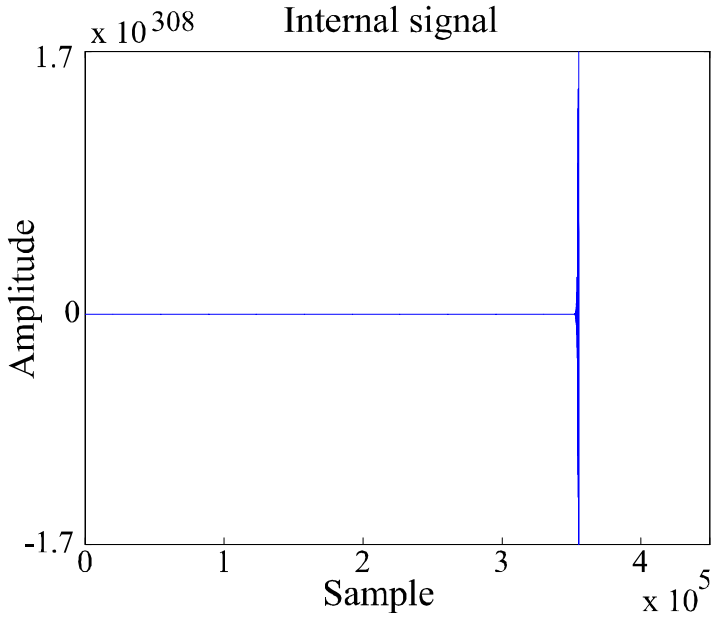

Figure 1.5. Magnitude of an internal signal with $\omega_0 = 0.1$ rad.

model for an active noise control system is a finite impulse response (FIR) system with 200 parameters or so, the adaptive controller is of very high order, and identification of the parameters is difficult.

- model reference and pole placement methods assume a known plant delay. In ANC, this delay is not known *a priori*, and may vary.

1.3.3 Harmonic steady-state

Harmonic steady-state (HSS) methods have simplified the problem by approximating the plant by its steady-state sinusoidal response. In [34], Pratt and coworkers described an HSS algorithm known as higher harmonic control (HHC), for use in the reduction of vibrations in helicopters. In [7], the algorithm was used for the cancellation of periodic noise in an acoustic drum. A proof of stability was provided in [7], although the authors assumed the injection of an excitation signal to ensure correct identification of the plant. The HSS algorithm of [7] updates an online estimate of the system's frequency response based on the processing of batches of data, which results in some delay in tracking variations in the system plant.

1.4 Research Problems Considered in the Dissertation

1.4.1 Disturbance of known frequency acting on an unknown/time-varying plant

The starting point for the rejection of sinusoidal disturbances of known frequency acting on an unknown system is the assumption that the plant can be represented by its steady-state frequency response. Inspired from the harmonic steady-state algorithm of [7], this allows a linear expression in terms of the unknown frequency response and disturbance parameters to be constructed at the output of the plant. From this linear expression, an estimate of the frequency response and disturbance parameters is obtained using a gradient or least-squares algorithm. An appropriate control signal is found by using the estimated parameters in the same controller that would be used if the parameters were known exactly. This is known as a certainty equivalence control law and, as the parameter estimates converge to their

steady-state value, the control signal converges to the nominal value needed to cancel the disturbance. The resulting algorithm is known as the so-called adaptive harmonic steady-state (ADHSS) algorithm.

The ADHSS algorithm offers several advantages over other HSS algorithms:

- a remarkably simple adaptive HSS algorithm that eliminates the need for batches of data as in [7] (control parameters are updated continuously).
- a verification of the performance of the algorithm through active noise control experiments, demonstrating the ability to track abruptly or continuously time-varying system parameters in a challenging, practical application.
- a stability analysis based on the theory of averaging that does not require the addition of external excitation signals and provides useful insight into the dynamics of the adaptive system.

Note that rigorous stability proofs have been the subject of much research in adaptive control, but often turn out to be very complicated and to provide no insight about the dynamics of the systems. As an alternative, averaging methods have provided approximate results that are far more useful [1] [43] [20]. Averaging theory shows how a set of nonlinear time-varying differential equations can be approximated by a much simpler averaged system. In [43] and other work, averaging theory was found to provide invaluable information on the dynamic properties of specific adaptive control systems. For periodic disturbance rejection problems, averaging theory is even more powerful, because the conditions for the existence of the averaged system are generally satisfied without additional assumptions, due to the periodic nature of the signals. While averaging theory requires low adaptation gains, experience shows that the approximation is useful for the typical adaptation gains used in practice, and that the loss of rigor due to the approximation is more than compensated for by the powerful insights that the approximation provides.

The averaging analysis shows that the ADHSS algorithm converges independent of initial estimation errors in phase of the plant frequency response. In other words, the algorithm converges for initial phase errors outside the 90 degree condition discussed above. Further, the ADHSS possesses a four-dimensional equilibrium surface that

can be divided into a stable half and an unstable half. Any point on the equilibrium surface leads to cancellation of the disturbance. It is shown that trajectories of the system starting near an unstable equilibrium travel along a sphere until reaching a point along the stable half of the equilibrium. While a four-dimensional equilibrium surface indicates that the system is over-parameterized, this over-parameterization is not a problem and allows the local stability problem around an unstable equilibrium point to be resolved.

1.4.2 Disturbance of unknown frequency acting on an unknown/time-varying plant

The rejection of sinusoidal disturbances of unknown frequency acting on an unknown system is a difficult problem for which few solutions exist in the literature. These few typically require the presence of a significant level of noise for identification of system dynamics. If this noise is not present, it must be artificially injected in the form of an auxiliary signal. Often, one finds oneself in a situation where this auxiliary signal is too small to enable rapid identification, or too large to avoid noticeable degradation of system performance.

To avoid this pitfall, use of the HSS assumption allows the control signal used to reject the disturbance to be used for identification of the plant. If the frequency of the disturbance is unknown or may vary with time, a common approach is the so-called indirect approach. The indirect approach is a two step procedure that first estimates the disturbance frequency and then uses this estimate in a disturbance cancellation algorithm for known frequency. Based on the ADHSS algorithm developed in Chapter 2, an indirect algorithm is developed that simultaneously updates estimates of the disturbance frequency as well as the disturbance phase and the plant frequency response. Frequency estimation is based on the magnitude phase-locked loop (MPLL) algorithm of [49]. It is shown that when the ADHSS algorithm is combined with MPLL frequency estimation, the control input does not interfere with estimation of the disturbance frequency, and the MPLL frequency estimator allows the order of the ADHSS to be decreased. As such, the additional consideration of unknown frequency entails negligible increase in algorithm complexity. Averaging theory is used to explore

the steady-state stability characteristics of the combined ADHSS/MPLL algorithm. It is shown that the algorithm possesses a two-dimensional equilibrium surface and that the allowable plant phase errors within the stable subset is reduced from the known frequency ADHSS.

1.4.3 Improving the stability of disturbance rejection algorithms for unknown frequency

In dealing with disturbances of unknown frequency using the ADHSS algorithm, reliable frequency estimation is essential. While MPLL frequency estimation led to favorable stability properties when used with disturbance cancellation algorithms, stability of the MPLL frequency estimate requires that the initial frequency estimate be sufficiently close to the true frequency [16]. This limits the stability of the overall disturbance cancellation algorithm, and constrains the allowable changes in the system parameters. A globally convergent frequency estimate could be used to solve or at least extend the stability limits inherent in the use of the MPLL.

As such, new frequency estimators are obtained from models of AC (alternating current) electric machines. Specifically, induction machines are robust devices whose mechanical speed track the angular frequency of the electric currents applied to their windings. An induction motor model can therefore form the basis of a frequency estimator where the rotor speed is the estimate of the frequency. In practice, induction machines are asynchronous, meaning that the speed is slower than the electrical frequency, due to load and friction. However, when a no-load condition is simulated, convergence of the frequency estimator can be obtained. The induction motor frequency estimation (IMFE) algorithm can also be combined with a disturbance cancellation algorithm to reject disturbances of unknown frequency. The approach is tested successfully in active noise control experiments using the disturbance cancellation algorithm of [50]. The need for an *a priori* estimate of the frequency is found to be relaxed with a negligible increase in computational complexity.

The IMFE is also used to improve stability of the ADHSS algorithm when the disturbance frequency is unknown. In Chapter 3, it is shown that even small frequency

errors cause performance issues for the ADHSS. The IMFE frequency does not lock onto the frequency of the disturbance and, in the presence of measurement noise, similar performance issues are encountered. As such, the IMFE is first used to extend the stability properties of the MPLL, and then the combined MPLL/IMFE frequency estimator is used with the ADHSS algorithm. Averaging theory is used to investigate the increase in stability of the overall algorithm over the algorithm of Chapter 3.

1.5 Contribution and Organization of the Dissertation

The dissertation can be broken down into three main parts. In Chapter 2, the rejection of sinusoidal disturbances of known frequency acting on an unknown and time-varying plant is considered [37][39][40]. Specific contributions include:

- derivation of the adaptive harmonic steady-state (ADHSS) algorithm,
- a stability proof of the ADHSS algorithm base on the theory of averaging,
- an investigation of the convergence and steady-state stability properties of the averaged ADHSS system,
- testing of the ADHSS algorithm through extensive active noise control (ANC) experiments and a comparison of performance with a gradient algorithm without online plant estimation,
- extension of the algorithm to consider multichannel systems and disturbances containing multiple frequency components.

In Chapter 3, extension of the ADHSS algorithm for the rejection of sinusoidal disturbances of unknown/time-varying frequency acting on an unknown/time-varying system is considered [38]. Specific contributions include:

- study the effect of a frequency error on the ADHSS algorithm,
- the addition of frequency estimation to the ADHSS algorithm and study the interaction of the two components. It is shown that a reduced order ADHSS with even stronger stability properties may be used,
- a stability analysis based on the theory of averaging that yields conditions for steady-state stability of the algorithm,
- testing of the ADHSS/MPLL algorithm through extensive ANC experiments.

In Chapter 4, a new frequency estimation technique based on the theory of electric drives is introduced [36]. Specific contributions of this section include:

- introduction of the induction motor frequency estimation (IMFE) for estimating the unknown frequency of a sinusoidal signal,
- an averaging analysis that establishes semiglobal convergence of the IMFE estimate to the true frequency,
- use of the IMFE in adaptive disturbance rejection for known plant with ANC experimental results demonstrating performance of the algorithm and verifying the analysis,
- modifications to the IMFE that allow it to be used with the ADHSS algorithm for unknown plant,
- a stability analysis based on the theory of averaging that yields conditions for steady-state stability of the algorithm,
- ANC experiments demonstrating the improvement resulting from the use of the modified IMFE.

Chapter 5 concludes the dissertation with general observations and offers suggestions for future work.

CHAPTER 2

SINUSOIDAL DISTURBANCES AND UNKNOWN SYSTEMS

2.1 Introduction

This chapter introduces a new algorithm for the rejection of sinusoidal disturbances of known frequency acting on systems with dynamics that are unknown and may vary in unpredictable ways. The plant is approximated by its steady-state frequency response, so that an algorithm with far fewer parameters than a filtered-X LMS algorithm is obtained. Inspired from the harmonic steady-state algorithm of [7], a linear parametrization at the output of the plant allows a gradient–based identifier to be used for estimation of both the plant frequency response and disturbance parameters. The estimated parameters are then used in determining an appropriate controller. Averaging theory is used to study the stability properties of the algorithm.

This chapter is organized as follows. After formulating the system's equations, the averaged system associated with the problem is found as defined in [43] and simulations are used to demonstrate the closeness of the responses. Next, the equilibrium points of the averaged system are determined and an eigenanalysis is used to understand the system's behavior around the equilibrium. This analysis enables one to understand how the algorithm handles uncertainty in the plant parameters in a way that a standard adaptive algorithm without plant adaptation is unable to. Further simulations illustrate the results of the analysis of the averaged system, and active noise control experiments validate the analysis further. Experimental results using a standard LMS algorithm are presented for comparison. Finally, experiments are reported using a *least-squares* identifier and demonstrate the ability of the algorithm to track time-varying parameters. For clarity the presentation is confined to a single-input single-output plant and a single tone disturbance; however, extensions

of the algorithm to multi-input multi-output plants and multitone disturbances are provided.

2.2 Adaptive Algorithm

2.2.1 System formulation

Consider the feedback system shown in Fig. 1.1. The output of the plant

$$y(t) = P(s)[u(t)] + p(t) \tag{2.1}$$

is fed back in order to determine the control signal $u(t)$ needed to reject the sinusoidal disturbance $p(t)$. The notation $P(s)[(\cdot)]$ represents the time-domain output of the system with transfer function $P(s)$. $P(s)$ is assumed to be a bounded input-bounded-output stable linear time-invariant system, but is otherwise unknown. Although the plant is fixed in the analysis, experiments show that the use of adaptation allows the plant to vary significantly over time. The compensator C is generally a nonlinear and time-varying control law consisting of a parameter identification scheme and a disturbance cancellation algorithm.

The disturbance is assumed to be a sinusoidal signal given by

$$p(t) = p_c \cos(\omega_1 t) + p_s \sin(\omega_1 t) = w_1^T(t)\pi^* \tag{2.2}$$

where

$$\pi^* = \begin{pmatrix} p_c \\ p_s \end{pmatrix}, \quad w_1 = \begin{pmatrix} \cos(\omega_1 t) \\ \sin(\omega_1 t) \end{pmatrix} \tag{2.3}$$

and ω_1 is the known frequency of the disturbance signal. Under these conditions, a control signal of the form

$$u(t) = \theta_c \cos(\omega_1 t) + \theta_s \sin(\omega_1 t) = w_1^T(t)\theta \tag{2.4}$$

is sufficient to cancel the disturbance in steady-state, provided that the controller parameter vector

$$\theta = \begin{pmatrix} \theta_c \\ \theta_s \end{pmatrix} \tag{2.5}$$

is chosen appropriately.

2.2.2 Adaptive harmonic steady-state algorithm

For the derivation of the algorithm, the response of the plant is approximated by the sinusoidal steady-state response [34]

$$y(t) \simeq y_{ss}(t) = w_1^T(t)G^*\theta + p(t) = w_1^T(t)\left(G^*\theta + \pi^*\right) \tag{2.6}$$

where

$$G^* = \begin{pmatrix} P_R^* & P_I^* \\ -P_I^* & P_R^* \end{pmatrix} \tag{2.7}$$

is a so-called frequency response matrix whose elements P_R^*, P_I^* are the real and imaginary parts of the plant's frequency response evaluated at ω_1

$$P(j\omega_1) \triangleq P_R^* + jP_I^* \tag{2.8}$$

Although the expression may not look familiar to the reader, the result is a straightforward application of the general formula for the steady-state sinusoidal response of a linear time-invariant system [19].

In the problem considered here, there are four unknowns: two are associated with the plant (P_R and P_I) and two are associated with the disturbance (p_c and p_s). The parameters, whose estimate will be part of the internal state of the controller, are collected in a vector

$$x^* = \begin{pmatrix} P_R^* & P_I^* & p_c & p_s \end{pmatrix}^T \tag{2.9}$$

so that the steady-state output of the plant (2.6) can be written as

$$y_{ss}(t) = W^T(t,\theta)x^* \tag{2.10}$$

where $W(t,\theta)$ is a so-called *regressor matrix*

$$W(t,\theta) = \begin{pmatrix} \theta_c \cos(\omega_1 t) + \theta_s \sin(\omega_1 t) \\ \theta_s \cos(\omega_1 t) - \theta_c \sin(\omega_1 t) \\ \cos(\omega_1 t) \\ \sin(\omega_1 t) \end{pmatrix}. \tag{2.11}$$

On the basis of the linear expression in (2.10), an estimate x of the unknown parameter vector x^* can be obtained using a gradient or a least-squares algorithm [43]. For example, a gradient algorithm for the minimization of the squared error $e^2 = \left(W^T x - y\right)^2$ that uses the approximation $y(t) \simeq y_{ss}(t)$ is given by

$$\dot{x}(t) = -\epsilon W(t,\theta)\left(W^T(t,\theta)x(t) - y(t)\right) \tag{2.12}$$

The parameter $\epsilon > 0$ is the adaptation gain, which will be assumed to be small in the application of the averaging theory in Sec. 2.3.

Having derived an algorithm for the estimation of the unknown parameters, it remains to define the control law. Note that, from (2.6), the disturbance is known to be cancelled exactly in steady-state for a nominal control parameter

$$\theta^* = -G^{*-1}\pi^* \tag{2.13}$$

Given an estimate of the unknown parameter vector x, a certainty equivalence control law [43] will redefine θ as $\theta(x)$, a function of the estimate x, using

$$G(x) = \begin{pmatrix} x_1 & x_2 \\ -x_2 & x_1 \end{pmatrix}, \ \pi(x) = \begin{pmatrix} x_3 \\ x_4 \end{pmatrix} \tag{2.14}$$

and

$$\begin{aligned}\theta(x) &= \begin{pmatrix} \theta_c(x) \\ \theta_s(x) \end{pmatrix} = -G^{-1}(x)\pi(x) \\ &= -\tfrac{1}{x_1^2+x_2^2} \begin{pmatrix} x_1x_3 - x_2x_4 \\ x_1x_4 + x_2x_3 \end{pmatrix}\end{aligned} \tag{2.15}$$

The nominal values satisfy

$$G^* = G(x^*),\ \pi^* = \pi(x^*),\ \text{and}\ \theta^* = \theta(x^*) \tag{2.16}$$

A state-space representation of the overall system can be obtained as follows. With x_P denoting the states of $P(s) = C(sI - A)^{-1}B$, the plant has the following state-space representation

$$\begin{aligned}\dot{x}_P(t) &= Ax_P(t) + Bu(t) \\ &= Ax_P(t) + Bw_1^T(t)\theta(x) \\ y(t) &= Cx_P(t) + p(t) = Cx_P(t) + w_1^T(t)\pi^*\end{aligned} \tag{2.17}$$

Defining

$$E(x) = \begin{pmatrix} D(x) \\ I_{2\times 2} \end{pmatrix},\ D(x) = \begin{pmatrix} \theta_c(x) & \theta_s(x) \\ \theta_s(x) & -\theta_c(x) \end{pmatrix} \tag{2.18}$$

the matrix $W(t,\theta)$ is given by

$$W(t,\theta) = E(x)w_1(t). \tag{2.19}$$

Then, the overall system is described by a set of differential equations with two vectors x and x_P composing the total state vector and

$$\begin{aligned}\dot{x}_P &= Ax_P + Bw_1^T(t)\theta(x) \\ \dot{x} &= -\epsilon E(x)w_1(t)\left(w_1^T(t)E^T(x)x - Cx_P - w_1^T(t)\pi^*\right)\end{aligned} \tag{2.20}$$

with (2.15), (2.18) giving the functions $\theta(x)$ and $E(x)$. Note that this set of differential equations is both time-varying and nonlinear, making direct analysis difficult. For-

tunately, under the assumption of small gain ϵ, the application of averaging theory produces an approximate nonlinear time-invariant system whose dynamics can be analyzed and provide interesting insights in the behavior of the system.

2.2.3 Alternative solution

In the formulation presented in the dissertation, the algorithm has the structure of Fig. 2.1, where

$$\begin{aligned} \tilde{u}(t) &= \tilde{w}_1^T(t)\theta \\ \tilde{w}_1(t) &= \begin{pmatrix} -\sin(\omega_1 t) \\ \cos(\omega_1 t) \end{pmatrix} \end{aligned} \tag{2.21}$$

In [40], a different implementation of the same concept was proposed, whereby the regressor variables would vary at a slower rate. The vector y_a was defined as

$$y_a = \begin{pmatrix} y_c \\ y_s \end{pmatrix} = AVG\left[2w_1(t)y(t)\right] = G^*\theta + \pi^*. \tag{2.22}$$

where the averaging operation AVG could be performed by averaging the signals over some multiple of the period T of the signals. Using this approach, the system was parameterized in terms of the regressor

$$W(t) = \begin{pmatrix} \theta_c(t) & \theta_s(t) & 1 & 0 \\ \theta_s(t) & -\theta_c(t) & 0 & 1 \end{pmatrix}^T \tag{2.23}$$

which corresponds to the system of Fig. 2.2. In this formulation, the regressor signals (2.23) vary at a slower rate as compared to (2.11), which varies with the periodic fluctuation of $w_1(t)$. Both approaches have been tested in experiments, with comparable results. In the implementation of [40], the averaging operation was simply neglected, on the basis that slow adaptation would provide the necessary smoothing. Here a similar argument is used for the analysis of the adaptive system, relying on a more formal application of averaging theory.

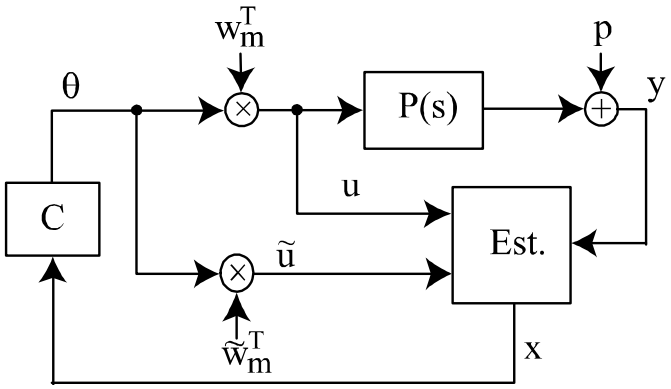

Figure 2.1. Proposed control system.

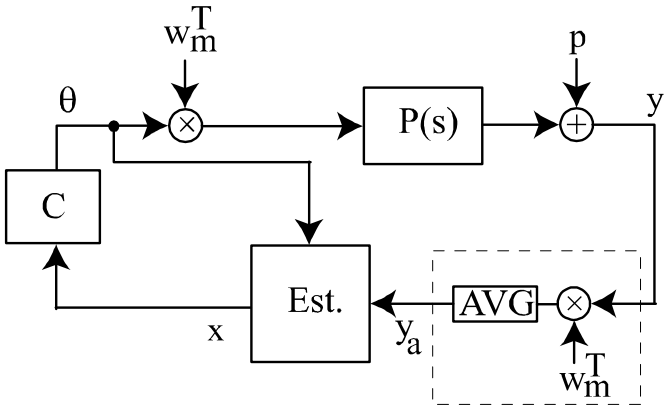

Figure 2.2. Alternative control system.

2.3 Averaging Analysis

2.3.1 Averaged system

Averaging theory allows a set of nonlinear and time-varying differential equations to be approximated by a set of nonlinear time-invariant equations and is a powerful tool in analyzing the stability of adaptive algorithms. Essential to application of the theory is the satisfaction of assumptions B1-B6 given in Appendix A. Other aspects of the relevant theory can also be found in Appendix A. The ADHSS algorithm fits into the averaging framework with the following definitions

$$\begin{aligned} f(t,x,x_P) &= -E(x)w_1(t)\left(w_1^T(t)E^T(x)x - Cx_P - w_1^T(t)\pi^*\right) \\ h(t,x) &= Bw_1^T(t)\theta(x) \end{aligned} \tag{2.24}$$

For ϵ small, x is a slow variable, while x_P varies faster, except through its dependency on x. It remains to determine what the averaged system is, whether the assumptions are satisfied, and what interesting properties the averaged system may have. The parameter vector x is frozen in the computation of the averaged system [43]. Further, all of the time variation in the functions is due to sinusoidal signals, and the systems to which they are applied are linear time-invariant systems. The outcome is that the average of the function $f(t,x,x_P)$ is well-defined and can be computed exactly. Specifically, the function

$$\begin{aligned} v(t,x) &= \int_0^t e^{A(t-\tau)}Bw_1(\tau)d\tau \cdot \theta(x) \\ &= x_{P,ss}(t) + x_{P,tr}(t) \end{aligned} \tag{2.25}$$

where $x_{P,ss}(t)$ is the steady-state response of the state of the plant to the sinusoidal excitation $w_1(t)$ and $x_{P,tr}$ is a transient response that decays to 0 exponentially, given that A is exponentially stable.

The averaged system is obtained by computing the average of

$$f_{av}(x) = -\lim_{T\to\infty}\frac{1}{T}\int_{t_0}^{t_0+T} E(x)w_1(\tau)\left(w_1^T(\tau)E^T(x)x - Cv(\tau,x) - w_1^T(\tau)\pi^*\right)d\tau \tag{2.26}$$

where

$$\begin{aligned} Cv(t,x) + w_1^T(t)\pi^* &= Cx_{P,ss}(t) + Cx_{P,tr}(t) + w_1^T(t)\pi^* \\ &= y_{ss}(t) + y_{tr}(t) \end{aligned} \tag{2.27}$$

and $y_{tr}(t) = Cx_{P,tr}(t)$. Equations (2.10) and (2.19) imply that

$$y_{ss}(t) = w_1^T(t)E^T(x)x^* \tag{2.28}$$

and since the transient response of the plant does not affect the average value of the function,

$$\begin{aligned} f_{av}(x) &= -\lim_{T\to\infty} \tfrac{1}{T} \int_{t_0}^{t_0+T} E(x)w_1(\tau)\left(w_1^T(\tau)E^T(x)x - w_1^T(\tau)E^T(x)x^*\right)d\tau \\ &= -E(x)\left(\lim_{T\to\infty} \tfrac{1}{T} \int_{t_0}^{t_0+T} w_1(\tau)w_1^T(\tau)d\tau\right)E^T(x)(x-x^*) \\ &= -\tfrac{1}{2}E(x)E^T(x)(x-x^*) \end{aligned} \tag{2.29}$$

In other words, the averaged system is simply given by

$$\dot{x} = -\frac{\epsilon}{2}\begin{pmatrix} D(x) \\ I_{2\times 2} \end{pmatrix}\begin{pmatrix} D(x) & I_{2\times 2} \end{pmatrix}(x - x^*) \tag{2.30}$$

with (2.15) and (2.18) giving

$$D(x) = \frac{1}{x_1^2 + x_2^2}\begin{pmatrix} x_1x_3 - x_2x_4 & x_1x_4 + x_2x_3 \\ x_1x_4 + x_2x_3 & -x_1x_3 + x_2x_4 \end{pmatrix} \tag{2.31}$$

Although (2.30)-(2.31) describe a nonlinear system, the method of averaging has eliminated the time variation of the original system, providing an opportunity to understand much better the dynamics of the system.

2.3.2 Application of averaging theory

The application of the theory is relatively straightforward, and verification of the assumptions is left to Appendix B. A technical difficulty is related to the fact that

both the adaptive and the averaged systems have a singularity at $x_1^2 + x_2^2 = 0$ (see equations (2.15) and (2.31)). Such singularities are quite common in adaptive control, occurring any time the estimate of the gain of the plant is zero. Here, the singularity occurs when the estimate of the plant's frequency response is zero, a problem that is somewhat unlikely to occur as *two* parameters need to be small for the singularity to be reached. Nevertheless, a cautious implementation of the algorithm would apply one of the available techniques to address singularities. For example, a simple practical fix consists in using in the control law either the parameter x if $x_1^2 + x_2^2 \geqslant \delta > 0$, where δ is a small parameter, or else the last value of the estimated parameter x that satisfied the condition. As far as the theory is concerned, given assumptions B1-B6 in Appendix A, this difficulty is avoided by adding the following assumption:

B7 Assume that trajectories of the original and averaged system are such that $x_1^2 + x_2^2 \geqslant \delta$ for some $\delta > 0$.

Using assumptions B1-B7, it is verified in Appendix B that the system given by (2.12)-(2.17) satisfies the conditions of the theory. Thus, *Lemma 1* and *Lemma 2* can be applied. In the verification of assumption B3, one finds that $d(t, x)$ has a bounded integral with respect to time, suggesting that $\xi(\epsilon)$ in *Lemma 1* is of the order of ϵ. *Lemma 2* establishes that (2.30) can be used as an order of ϵ approximation of (2.12)-(2.17) for all $t \in [0, T/\epsilon]$. Note that *Lemma 2* only shows closeness of the original and averaged systems over finite time. Any stability properties connecting the original and the averaged system would require a different theorem. The theorems of [43] do not apply because they assume a unique equilibrium point of the averaged system. As will be seen, this is not the case here.

2.3.3 Simulation example

To show the closeness of the responses (2.12)-(2.17) and (2.30), let $\omega_1 = 330\pi$ and take the plant to be a 250 coefficient FIR transfer function. The transfer function was measured from an active noise control system using a white noise input and a gradient search identification procedure. The frequency response of the system can be seen in

Fig. 2.3. The initial parameter estimate was $x(0) = x_{av}(0) = \begin{pmatrix} 1.0 & 1.0 & 0 & 0 \end{pmatrix}^T$. In Fig. 2.4, the response of the first adaptive parameter x_1 is shown. Four responses are shown: the averaged system with $\epsilon = 1$ and the actual system for $\epsilon = 100$, 50, and 1. As ϵ decreases, one finds that the trajectory of the original system approaches that of the averaged system. Note that the parameter estimates do not converge to the nominal values, indicating that the regressor (2.11) is not persistently exciting [43]. However, the control parameters θ_c and θ_s do converge to the nominal values, resulting in cancellation of the disturbance for all values of ϵ. The control parameters are shown in Fig. 2.5, along with θ^*, the nominal value that exactly cancels the disturbance (the constant line).

2.4 Properties of the Averaged System

Several properties of the averaged system can be derived from the rather simple form that was obtained in (2.30)-(2.31), enabling one to gain insight on the behavior of the closed-loop system.

2.4.1 Equilibrium surface

From the expression of the averaged system (2.30), it is deduced that an equilibrium point of the averaged system must satisfy

$$E^T(x)(x - x^*) = \begin{pmatrix} D(x) & I_{2\times 2} \end{pmatrix} (x - x^*) = 0 \tag{2.32}$$

Therefore, $x = x^*$ is an equilibrium point of the system. It is not the only one, however. Using (2.14)-(2.15)

$$\begin{aligned} \begin{pmatrix} D(x) & I_{2\times 2} \end{pmatrix} x &= \begin{pmatrix} \theta_c(x) & \theta_s(x) \\ \theta_s(x) & -\theta_c(x) \end{pmatrix} \begin{pmatrix} x_1 \\ x_2 \end{pmatrix} + \begin{pmatrix} x_3 \\ x_4 \end{pmatrix} \\ &= \begin{pmatrix} x_1 & x_2 \\ -x_2 & x_1 \end{pmatrix} \begin{pmatrix} \theta_c(x) \\ \theta_s(x) \end{pmatrix} + \begin{pmatrix} x_3 \\ x_4 \end{pmatrix} \\ &= 0 \end{aligned} \tag{2.33}$$

In other words, $E^T(x)x = 0$ and equilibrium points must satisfy

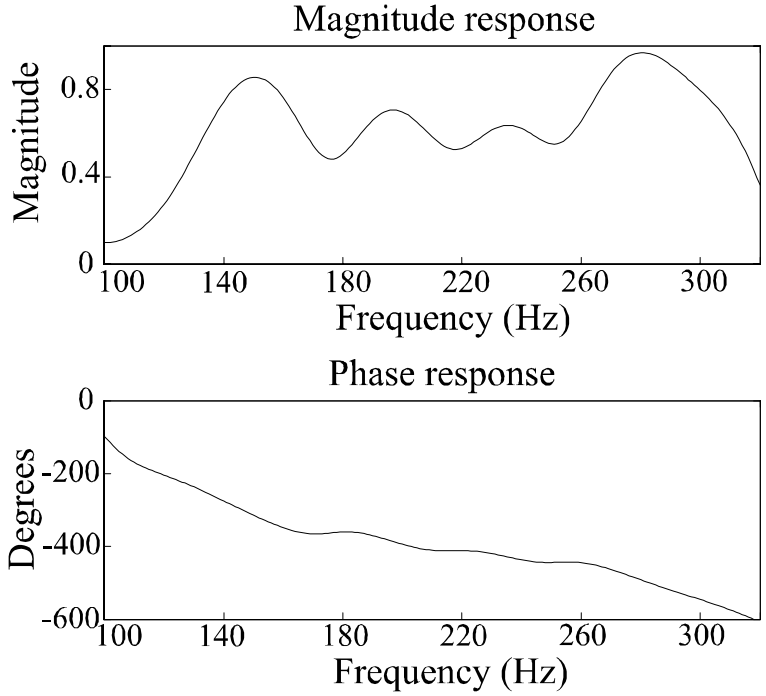

Figure 2.3. Frequency response of the plant: magnitude and phase responses.

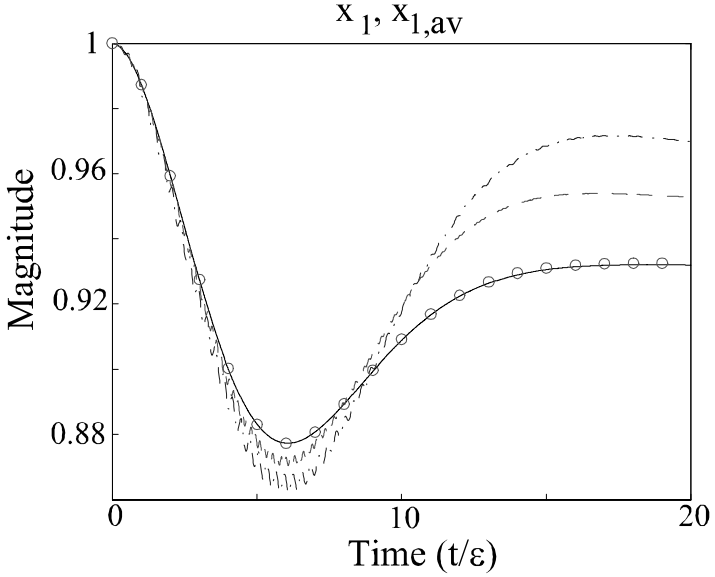

Figure 2.4. The response of the first adapted parameter x_1 for the averaged system with $\epsilon = 1$ (solid line), the actual system for $\epsilon = 100$ (dashed dot), the actual system for $\epsilon = 50$ (dashed), and the actual system for $\epsilon = 1$ (circles).

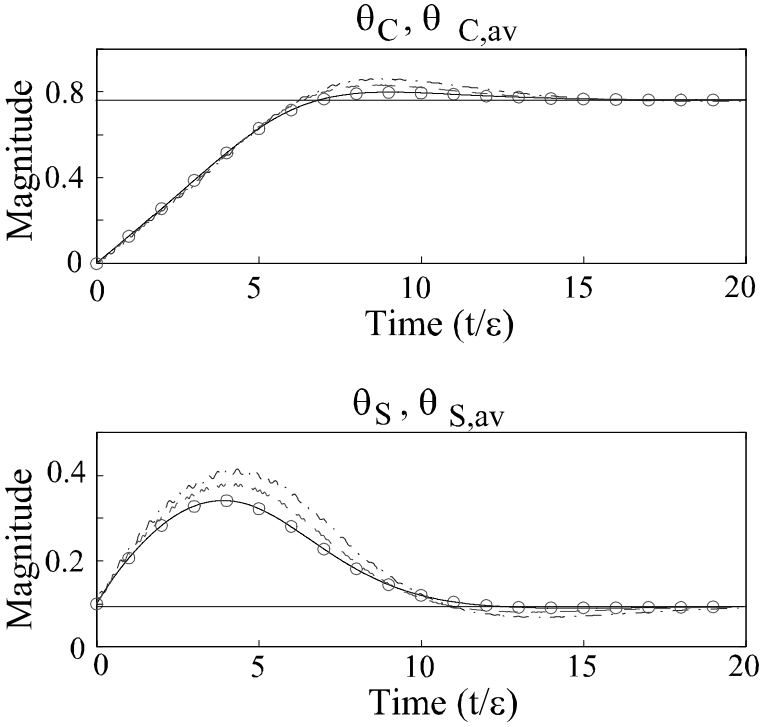

Figure 2.5. Trajectories of control parameters for the averaged system with $\epsilon = 1$ (solid line), the actual system for $\epsilon = 100$ (dashed dot), the actual system for $\epsilon = 50$ (dashed), and the actual system for $\epsilon = 1$ (circles).

$$E^T(x)x^* = 0 \tag{2.34}$$

(2.34) can be rewritten as

$$\begin{aligned}\begin{pmatrix} \theta_c(x) & \theta_s(x) \\ \theta_s(x) & -\theta_c(x) \end{pmatrix}\begin{pmatrix} x_1^* \\ x_2^* \end{pmatrix} + \begin{pmatrix} x_3^* \\ x_4^* \end{pmatrix} &= \begin{pmatrix} x_1^* & x_2^* \\ -x_2^* & x_1^* \end{pmatrix}\begin{pmatrix} \theta_c(x) \\ \theta_s(x) \end{pmatrix} + \begin{pmatrix} x_3^* \\ x_4^* \end{pmatrix} \\ &= 0\end{aligned} \tag{2.35}$$

or

$$\begin{aligned}\begin{pmatrix} \theta_c(x) \\ \theta_s(x) \end{pmatrix} &= -\begin{pmatrix} x_1^* & x_2^* \\ -x_2^* & x_1^* \end{pmatrix}^{-1}\begin{pmatrix} x_3^* \\ x_4^* \end{pmatrix} \\ &= \begin{pmatrix} \theta_c^* \\ \theta_s^* \end{pmatrix}\end{aligned} \tag{2.36}$$

The last equation shows that any equilibrium state results in the cancellation of the disturbance, confirming the observation made in Sec. 2.3.3. Equation (2.36) also implies, with (2.14)-(2.15), that

$$\begin{pmatrix} x_1 & x_2 \\ -x_2 & x_1 \end{pmatrix}^{-1}\begin{pmatrix} x_3 \\ x_4 \end{pmatrix} = -\begin{pmatrix} \theta_c^* \\ \theta_s^* \end{pmatrix} \tag{2.37}$$

or, reorganizing the terms,

$$\begin{pmatrix} x_3 \\ x_4 \end{pmatrix} = -\begin{pmatrix} \theta_c^* & \theta_s^* \\ \theta_s^* & -\theta_c^* \end{pmatrix}\begin{pmatrix} x_1 \\ x_2 \end{pmatrix} \tag{2.38}$$

In other words, the set of equilibrium points is a two-dimensional linear subspace of the four-dimensional state-space. The set includes the nominal parameter x^*. Note that, for x constant,

$$f(t, x, x_{P,ss}) = -E(x)w_1(t)w_1^T(t)E^T(x)(x - x^*). \tag{2.39}$$

Therefore, any equilibrium state of the averaged system is also an equilibrium state of the original system. This result further explains why, in Sec. 2.3.3., all the trajectories

were such that θ converged to θ^*. Further, (2.28) indicates that any equilibrium state corresponds to a perfect rejection of the disturbance. In practice, measurement noise and quantitization errors result in a small residual.

2.4.2 Local stability

The local stability of the averaged system can be determined by linearizing (2.30) around an equilibrium state x. The following eigenvalues were computed using the Maple kernel

$$\lambda = \begin{pmatrix} 0 \\ 0 \\ \left(\frac{x_2^* + jx_1^*}{x_2 + jx_1}\right)\beta \\ \left(\frac{x_2^* - jx_1^*}{x_2 - jx_1}\right)\beta \end{pmatrix} \tag{2.40}$$

where $\beta = -\frac{\epsilon}{2}\left(\frac{x_1^{*2}+x_2^{*2}+x_3^{*2}+x_4^{*2}}{x_1^{*2}+x_2^{*2}}\right)$. The two eigenvalues at zero confirm the two-dimensional nature of the linear equilibrium surface. The nonzero eigenvalues are complex conjugates that lie in the open left-half plane if and only if

$$x_1 x_1^* + x_2 x_2^* > 0 \tag{2.41}$$

or equivalently

$$x_3 x_3^* + x_4 x_4^* > 0. \tag{2.42}$$

For the reverse signs, the eigenvalues lie in the open right-half plane. The stability condition can be interpreted in the (x_1, x_2) plane, as shown in Fig. 2.6. Specifically, the line going through the origin that is perpendicular to the line joining (0, 0) and (x_1^*, x_2^*) defines the boundary between the stable and unstable states. Interestingly, this is the same boundary that delineates the stable and unstable regions of a standard LMS algorithm that does not identify the plant parameters [29], as will be discussed in Sec. 2.5.2. In this case, however, the nonlinear dynamics ensure that all trajectories eventually converge to the stable subset of the equilibrium surface.

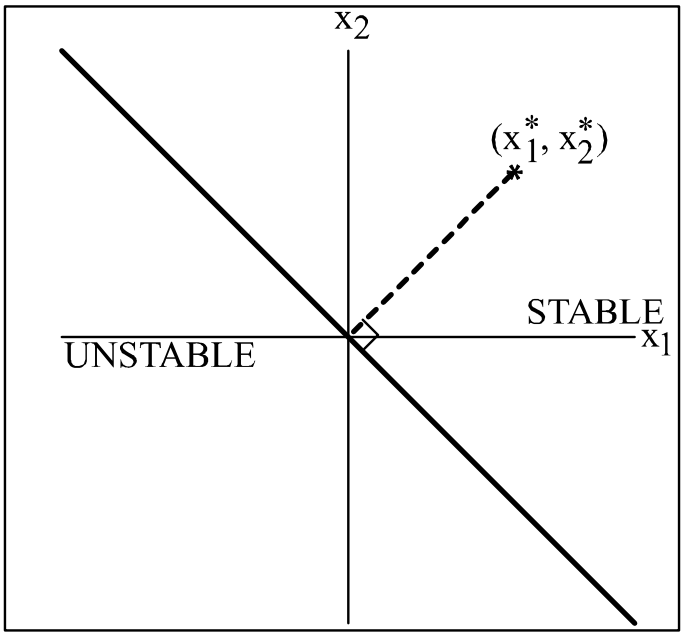

Figure 2.6. Relationship between the location on the equillibrium surface and stability

2.4.3 Lyapunov analysis

Lyapunov arguments can be used to establish further stability results for the averaged system. Specifically, the Lyapunov candidate function

$$V = \|x(t) - x^*\|^2 \tag{2.43}$$

evaluated along the trajectories of (2.30) gives

$$\dot{V} = -\epsilon \left\| E^T(x)\,(x - x^*) \right\|^2 \leq 0 \tag{2.44}$$

which implies that

$$\|x(t) - x^*\| \leq \|x(0) - x^*\| \tag{2.45}$$

for all $t > 0$. Since x and $\dot{x}$ are bounded (using (2.30) and assumption B7), one may also deduce that $E^T(x)\,(x - x^*) \to 0$ as $t \to \infty$. In turn, it can be further verified that $E^T(x)x = 0$. As such, (2.28) implies that the disturbance is asymptotically cancelled.

Further results may be obtained by noting that

$$\begin{pmatrix} -I_{2\times 2} & D(x) \end{pmatrix} E(x) = 0 \tag{2.46}$$

so that

$$\begin{pmatrix} -I_{2\times 2} & D(x) \end{pmatrix} \dot{x} = 0 \tag{2.47}$$

Using (2.14)-(2.15)

$$\begin{aligned} D(x) &= \begin{pmatrix} \theta_c(x) & \theta_s(x) \\ \theta_s(x) & -\theta_c(x) \end{pmatrix} \\ &= -\begin{pmatrix} x_1 & x_2 \\ -x_2 & x_1 \end{pmatrix}^{-1} \begin{pmatrix} x_3 & x_4 \\ x_4 & -x_3 \end{pmatrix} \end{aligned} \tag{2.48}$$

The result implies that

$$\begin{pmatrix} x_1 & x_2 & x_3 & x_4 \\ -x_2 & x_1 & x_4 & -x_3 \end{pmatrix} \dot{x} = 0 \tag{2.49}$$

From the first equation, one has that

$$\|x(t)\| = \|x(0)\| \tag{2.50}$$

for all $t > 0$. In other words, while the norm of the parameter error vector is monotonically decreasing, the norm of the parameter vector is constant. In particular, the norm of the state is bounded for all time by its initial value, regardless of the local instability around one half of the equilibrium surface. (2.50) along with (2.15) indicate that any decrease in the magnitude of the first two estimated parameters $\sqrt{x_{1,av}^2 + x_{2,av}^2}$ must result in an increase in the magnitude of the other two estimated parameters $\sqrt{x_{3,av}^2 + x_{4,av}^2}$, and vice versa. Note that if the two magnitudes changed proportionally in the same direction, there would be no change in control parameter and no impact on the output error. The second equation in (2.49) yields a further constraint on the state vector but is not as easily integrated as the first one.

2.4.4 Simulation

In this section, an example is discussed that illustrates the properties of the averaged system. Consider the nominal parameter

$$x^* = \begin{pmatrix} 1.0 & 1.0 & 1.0 & 1.0 \end{pmatrix}^T, \tag{2.51}$$

with the initial vector $x(0) = \begin{pmatrix} 1.1 & -2.0 & -2.0 & 1.0 \end{pmatrix}^T$ and the gain $\epsilon = 2.0$. The eigenvalues of (2.30) are given in (2.40). $x(0)$ was chosen in the neighborhood of an unstable equilibrium point whose eigenvalues have relatively large imaginary part. The trajectories of the parameter estimates were projected into the $(x_{1,av}, x_{2,av})$ plane for visualization in the simulation result of Fig. 2.7.

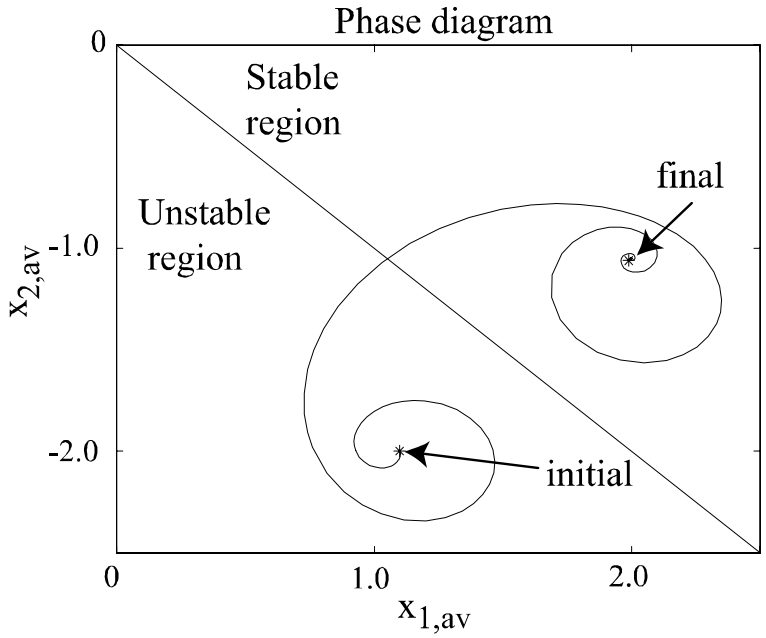

Figure 2.7. Responses of identified parameters.

With the initial conditions chosen close to the unstable region of the equilibrium surface, the trajectory spirals with exponential growth as predicted, then crosses over into the stable region. The trajectory spirals back with exponential decay towards the equilibrium surface, as the eigenvalues turn out to also have large imaginary parts in that region. The unstable, highly oscillatory initial response was obtained by setting the initial estimate of the phase of the plant at

$$\measuredangle \hat{P}(j\omega_o) = -61.2^o. \tag{2.52}$$

while the phase of the plant was

$$\measuredangle P(j\omega_o) = 45^o \tag{2.53}$$

resulting in a phase difference of $\measuredangle P(j\omega_o) - \measuredangle \hat{P}(j\omega_o) = 106^o$ (beyond the 90^o angle condition, but close to it to ensure oscillatory behavior). The 90^o angle condition pertains to the mixed time scale system (A.1) when the plant estimate is not updated online, such as the standard LMS algorithm. It states that for stability of the averaged system (A.2), it is both sufficient and necessary that $P_R\hat{P}_R + P_I\hat{P}_I > 0$, or equivalently $\left|\measuredangle P(j\omega_o) - \measuredangle \hat{P}(j\omega_o)\right| < 90^o$ [43]. Although not shown, it was verified that the norm of trajectories remained constant at $\|x(t)\| = \|x(0)\| = 3.20$.

2.5 Experiments

2.5.1 Results with the adaptive algorithm

The performance of the algorithm given by (2.11), (2.12), and (2.15) was examined through single-channel active noise control experiments. The active noise control system diagrammed in Fig. 2.8 was the same system used to identify the 250 coefficient FIR transfer function used in Sec. 2.3.3. In the experiments of this subsection and of the subsection that follows, the parameters of the plant remain unchanged. The algorithm was coded in C and implemented via a dSpace DS1104 digital signal processing board. A sampling frequency of 8 kHz was used. A constant amplitude sinusoidal disturbance with frequency of 185 Hz was generated by one

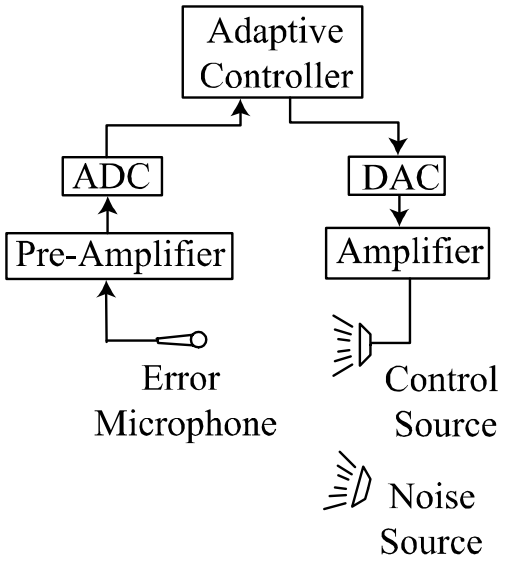

Figure 2.8. Diagram of the single channel active noise control system.

loudspeaker, while the control signal was produced by another. The phase of the plant was estimated experimentally at 93.2°. The initial plant estimate was set at $P(j\omega) = \begin{pmatrix} -0.01 & 0.1 \end{pmatrix}^T$, corresponding to a phase angle of 95.7° and a phase difference of 2.5°. Using these initial conditions along with an adaptation gain of 10, chosen to insure stability as well as quick convergence, results in the parameter convergence seen in Fig. 2.9. The corresponding error attenuation is shown in Fig. 2.10. The parameters converge to values which give significant noise attenuation.

Next, an initial plant estimate with $P(j\omega) = \begin{pmatrix} 0.1 & -0.01 \end{pmatrix}^T$ was used, corresponding to a phase angle of −5.7° and a phase difference of 98.9°, beyond the 90° phase condition. After some initial oscillations, the parameters are seen to converge in Fig. 2.11 . The corresponding error is shown in Fig. 2.12. Starting from the unstable region simply results in a slightly longer transient. Although the initial conditions of the system produce a locally unstable adaptive system, the dynamics are such that convergence to a nonunique equilibrium state is eventually achieved. In the transient, the parameter error vector and the parameter vector remain bounded by their initial value. In the steady-state, the parameter vector is such that the nominal control vector is reached.

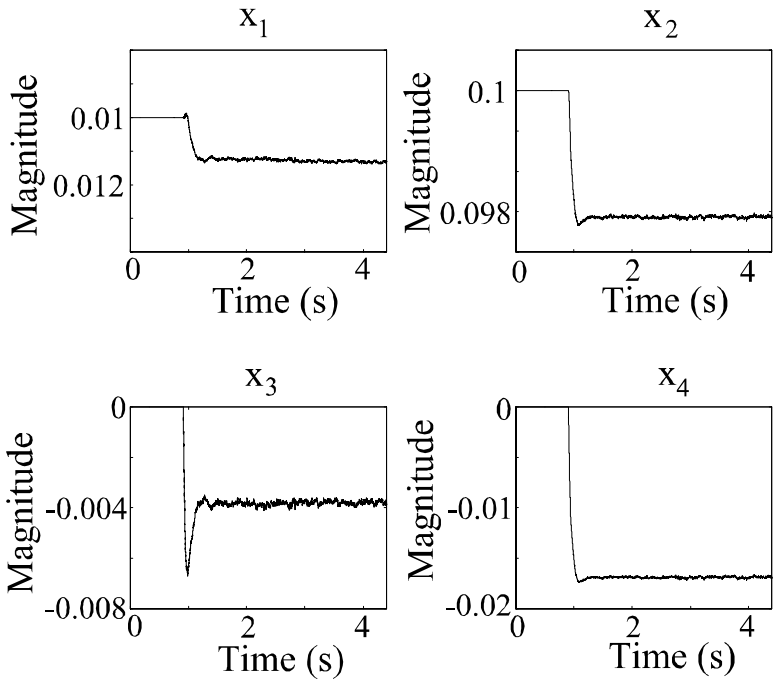

Figure 2.9. Adaptive algorithm with small initial phase difference: parameter convergence.

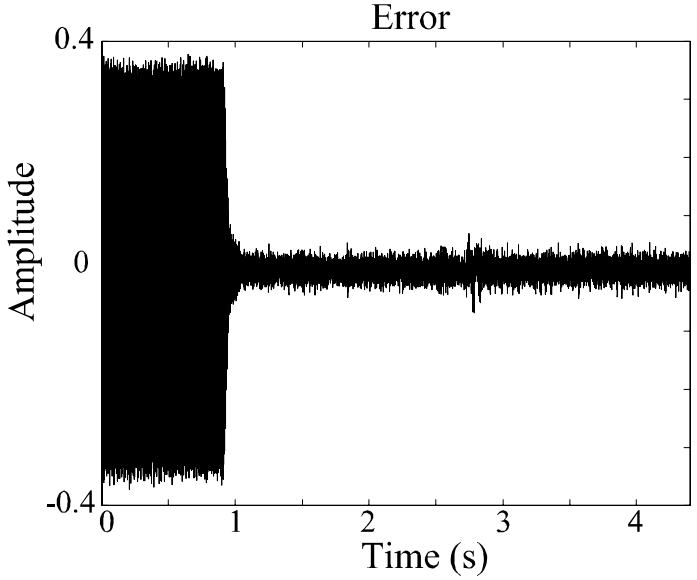

Figure 2.10. Adaptive algorithm with small initial phase difference: error attenuation.

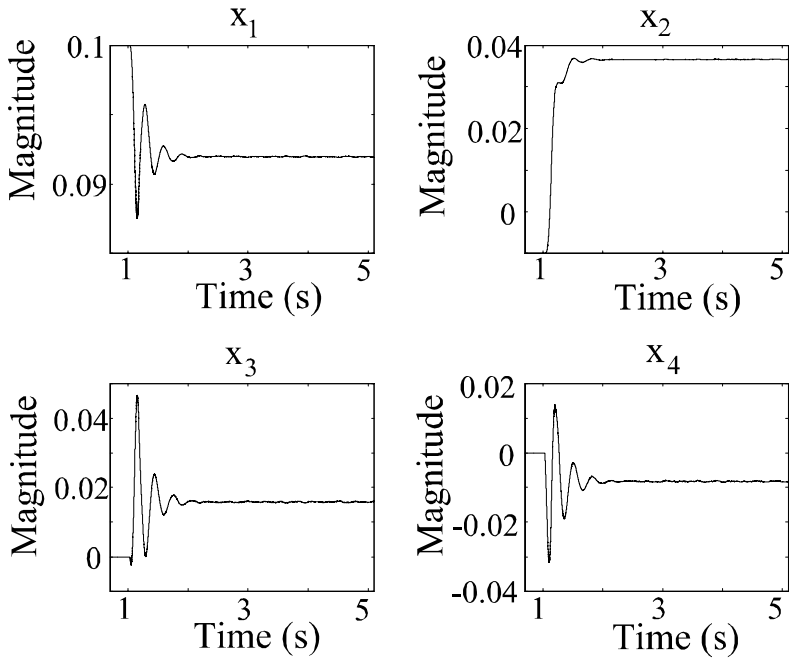

Figure 2.11. Adaptive algorithm with large initial phase difference: parameter convergence.

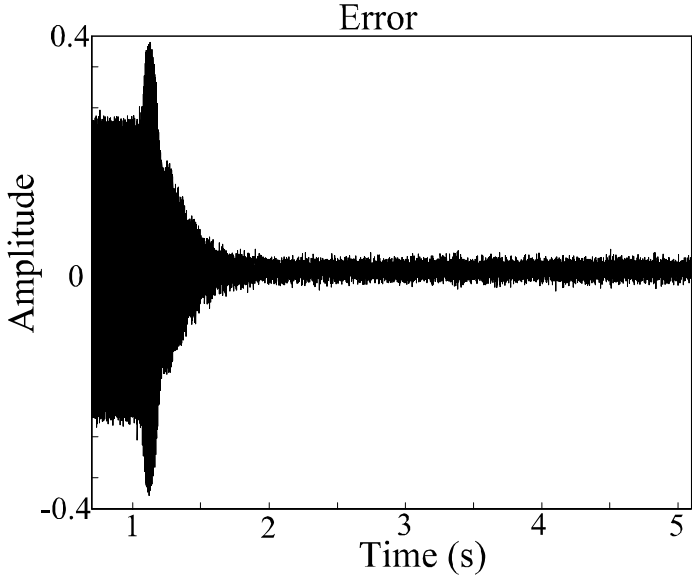

Figure 2.12. Adaptive algorithm with large initial phase difference: error attenuation.

2.5.2 Comparison to standard LMS algorithm

A standard algorithm in active noise and vibration control is the filtered-X LMS algorithm [23]. It is a gradient-type algorithm of which an implementation is presented here for the sake of comparison. Recalling (2.6), the steady-state output of the plant is

$$y = w_1^T G^* \theta + p = w_1^T G^* \left(\theta - \theta^*\right) \tag{2.54}$$

The error y^2 can be minimized by using the gradient algorithm [50]

$$\dot{\theta} = -\epsilon G^{*T} w_1 y \tag{2.55}$$

The corresponding averaged system

$$\dot{\theta} = -\frac{\epsilon}{2} G^{*T} G^* \left(\theta - \theta^*\right) \tag{2.56}$$

has a unique equilibrium at $\theta = \theta^*$ that is exponentially stable if $G^* \neq 0$. If G^* is not known, an *a priori* estimate G of G^* is used, and the averaged system becomes [50]

$$\dot{\theta} = -\frac{\epsilon}{2} G^T G^* \left(\theta - \theta^*\right) \tag{2.57}$$

$\theta = \theta^*$ is still an equilibrium, but it is unique and exponentially stable if and only if the eigenvalues of

$$G^T G^* = \begin{pmatrix} x_1 & -x_2 \\ x_2 & x_1 \end{pmatrix} \begin{pmatrix} x_1^* & x_2^* \\ -x_2^* & x_1^* \end{pmatrix} \tag{2.58}$$

lie in the open right half plane. As in Fig. 2.6, the condition for stability is again that

$$x_1 x_1^* + x_2 x_2^* > 0 \tag{2.59}$$

which requires that the phase of the initial estimate of the plant be within 90° of the true value.

Experiments with the filtered-X LMS algorithm show the benefits of the algorithm of (2.11), (2.12), and (2.15). In the first experiment, the plant estimate $P(j\omega)$ has a phase difference of 1.7° with respect to the actual plant. Using the estimate along with an adaptation gain of $\epsilon = 75$, the responses of the parameters can be seen in Fig. 2.13, and the corresponding error attenuation can be seen in Fig. 2.14. As expected, the parameters converge to values that result in significant noise cancellation. Next, a phase difference of 99.8° was applied In Fig. 2.15, the parameters are seen to experience divergence which results in the exponential growth of the error in Fig. 2.16. Comparing these results with those obtained in the previous section, one finds interesting similarities between the stability regions of the algorithms. With the algorithm of (2.11), (2.12), and (2.15), however, on-line identification produces a nonlinear system where trajectories eventually converge to the vicinity of a stable equilibrium, regardless of the initial error in the estimate of the phase of the true plant.

2.6 Experiments with Least-squares Algorithm and Time-varying Systems

In the experiments of this subsection, the parameters of the plant are allowed to change significantly with time. In some situations, it may be desirable to use a least-squares algorithm for its superior convergence properties. A discrete-time implementation [3] is available that incorporates a stabilizing mechanism to insure stability while still allowing for rapid convergence. The parameter vector x is obtained by minimizing the cost function

$$E\left[x(n)\right] = \sum_{k=1}^{n} (y(k) - W^T(k)x(n))^2 \lambda^{n-k} + \alpha \left|x(n) - x(n-1)\right|^2 \tag{2.60}$$

where λ is a forgetting factor and α is a stabilizing factor. Note that this criterion incorporates a penalty on the parameter variation, while for $\alpha = 0$, the standard

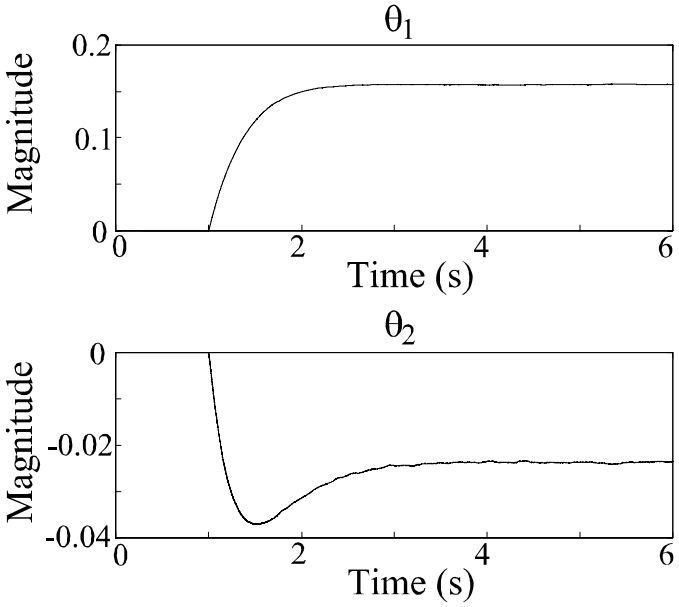

Figure 2.13. LMS algorithm with small initial phase difference: parameter convergence.

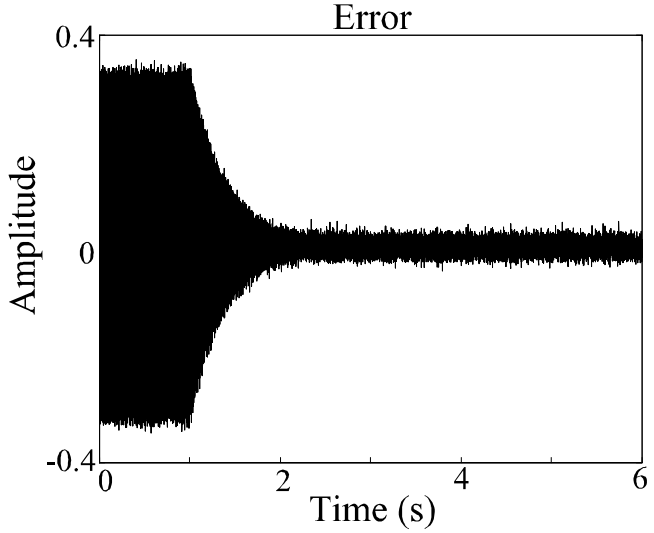

Figure 2.14. LMS algorithm with small initial phase difference: error attenuation.

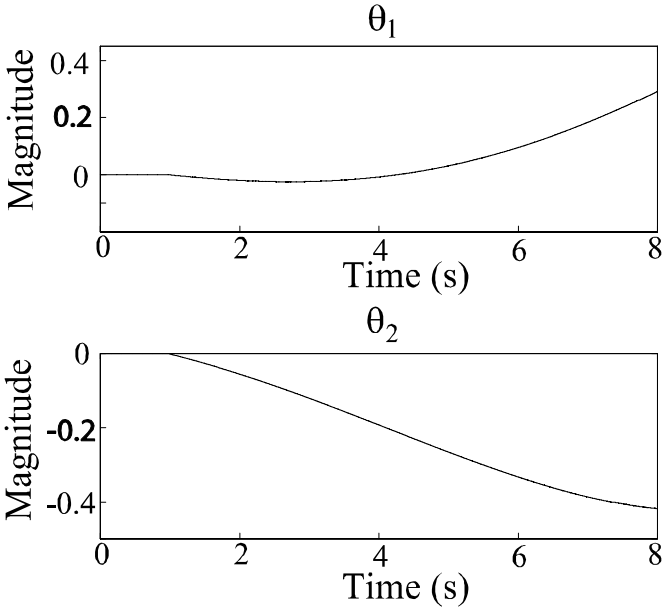

Figure 2.15. LMS algorithm with large initial phase difference: parameter convergence.

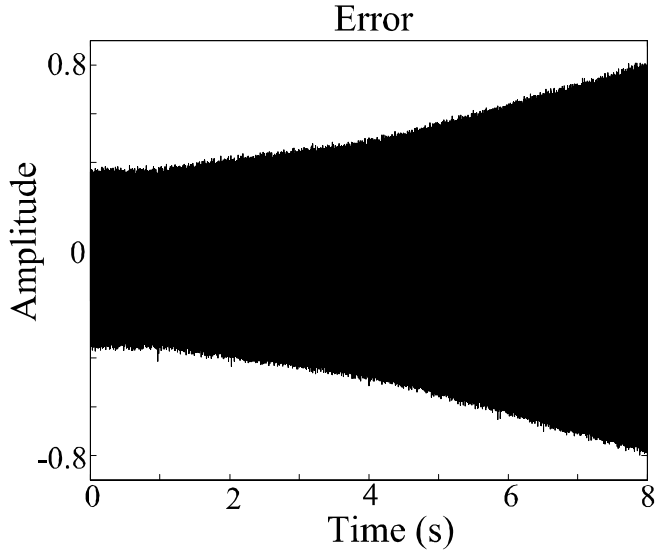

Figure 2.16. LMS algorithm with large initial phase difference: error attenuation.

least-squares with forgetting factor is recovered. Setting $\partial E/\partial \hat{x}(n) = 0$, the estimate that minimizes (2.60) is

$$\begin{aligned} x(n) &= \left(\sum_{k=1}^{n} W(k) W^T(k) \lambda^{n-k} + \alpha I_{4x4} \right)^{-1} \\ &\times \left(\sum_{k=1}^{n} W(k) y(k) \lambda^{n-k} + \alpha x(n-1) \right) \end{aligned} \tag{2.61}$$

From this batch formula, an equivalent recursive formulation can be found as

$$\begin{aligned} K^{-1}(n) &= \lambda K^{-1}(n-1) + W(n) W^T(n) + \alpha(1-\lambda) I_{4x4} \\ x(n) &= x(n-1) + K(n) W(n) (y(n) - W^T(n) x(n-1)) \\ &\quad + \alpha\lambda K(n) (x(n-1) - x(n-2)) \end{aligned} \tag{2.62}$$

where

$$K^{-1}(0) = \alpha I_{4x4}. \tag{2.63}$$

A forgetting factor $\lambda < 1$ causes the influence of old data on the identification of x to be reduced as time proceeds, enabling the algorithm to track variations in the true parameters. From [3], the averaged system corresponding to (2.62) is given by

$$\begin{aligned} K_{av}^{-1}(n) &= \lambda K_{av}^{-1}(n-1) + E(x) E^T(x) + \alpha(1-\lambda) I_{4x4} \\ x_{av}(n) &= x_{av}(n-1) - K_{av}(n) E(x) E^T(x) x_{av}(n-1) \\ &\quad + \alpha\lambda K_{av}(n) \left(x_{av}(n-1) - x_{av}(n-2) \right) \end{aligned} \tag{2.64}$$

The least-squares algorithm was tested with challenging test conditions requiring continuous adaptation. A constant amplitude sinusoidal disturbance with frequency of 185 Hz was assumed. Plant parameters were initialized at $x_1(0) = x_2(0) = 1.0$, and disturbance parameters were initialized at $x_3(0) = x_4(0) = 0$. A forgetting factor $\lambda = 0.999$ was used. This choice corresponds to a time constant of $1,000$ samples, or 0.125 seconds. A value of $\alpha = 75$ was chosen. The covariance matrix was started

at (2.63). (2.62) was used to update $K^{-1}(n)$ and the inverse was taken for use in updating x. These results were obtained using the control structure of Fig. 2.1.

An error microphone provided feedback to the algorithm, and attenuation results can be seen in Fig. 2.17. The estimated parameters can be seen in Fig. 2.18. The control algorithm was engaged after approximately $0.75s$ and convergence occurred in less than one half second. Unknown to the algorithm, the microphone used for cancellation was abruptly switched at approximately $2.75s$ to a microphone located some 4 $feet$ away. After a brief time interval, the algorithm was able to compensate for the change in plant parameters, again in less than half a second.

The ability to track slow time variations in system parameters was also explored. In Fig. 2.19 and Fig. 2.20, the results of manually moving the error sensor within the field of cancellation are shown. In these figures, the parameters were frozen after reaching the initial steady-state. The error signal is shown along with the frozen control signal. Significant errors occur once the microphone has moved sufficiently to alter the characteristics of the system in a significant way. In Fig. 2.21, the algorithm is allowed to track the time-varying parameters. Significant attenuation is now observed despite the fact that both plant and disturbance parameters are changing. The identified parameters are shown in Fig. 2.22.

2.7 Extension of the Algorithm

2.7.1 MIMO case

In the extension of the algorithm of (2.11), (2.12), and (2.15), assume that there are i outputs of $P(s)$ and j inputs. Take the disturbance as consisting of a single sinusoidal component, and apply the algorithm of (2.11), (2.12), and (2.15) at each output. At each plant output, there are $2j$ plant parameters and 2 disturbance parameters to be identified, giving a regressor at each output of the form

$$W_i(t,\theta) = \begin{pmatrix} u_v \\ \tilde{u}_v \\ \cos(\omega_1 t) \\ \sin(\omega_1 t) \end{pmatrix} \tag{2.65}$$

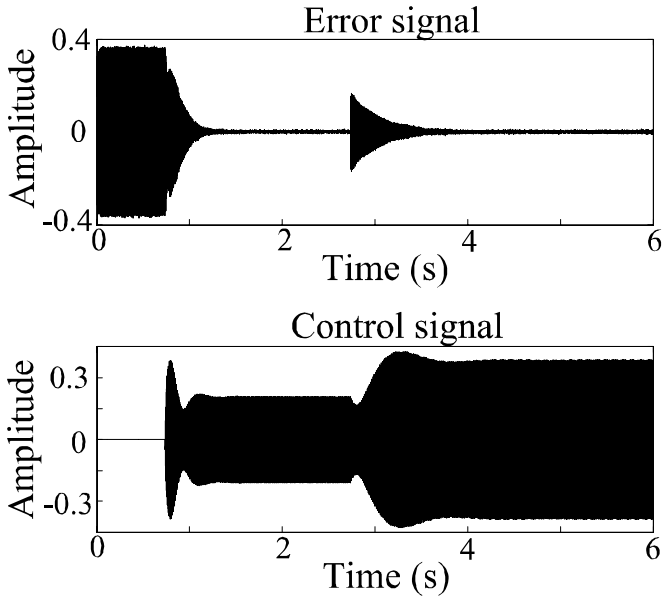

Figure 2.17. Error and control signals with fixed true parameters and microphone switched at ≈ 2.75 s.

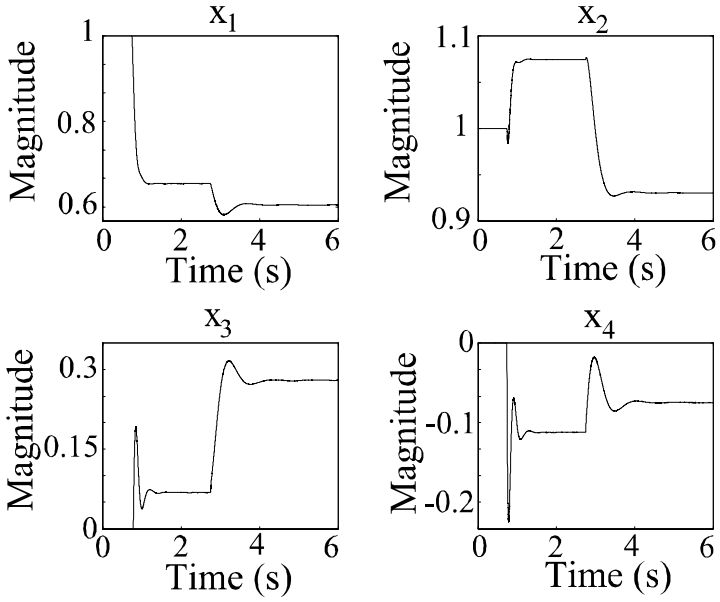

Figure 2.18. Identified parameters when true parameters suddenly change.

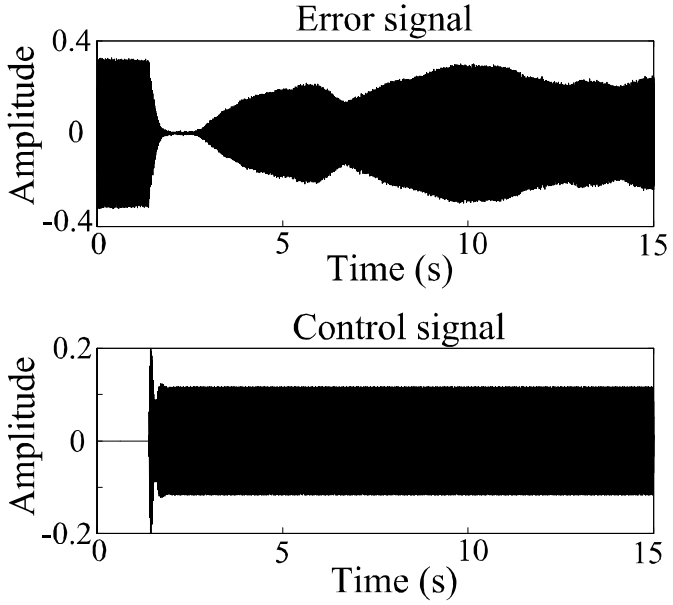

Figure 2.19. Error and control signals with continuously changing parameters but frozen estimates.

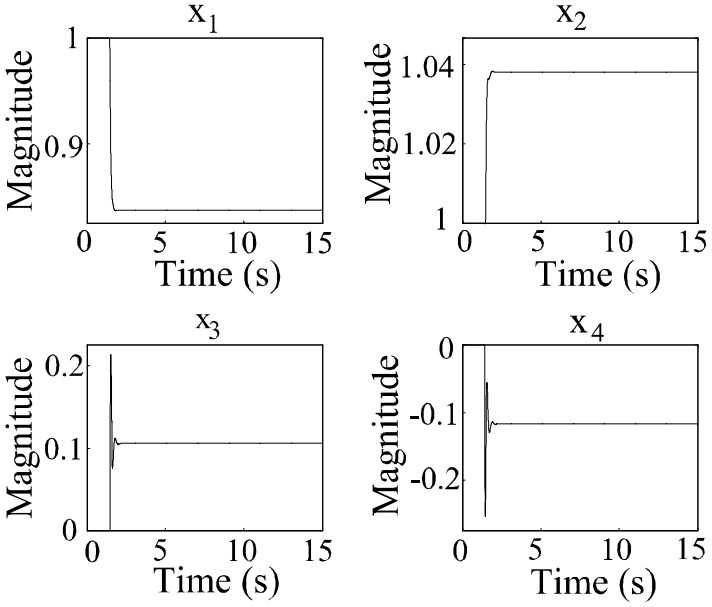

Figure 2.20. Parameter estimates frozen after reaching steady-state.

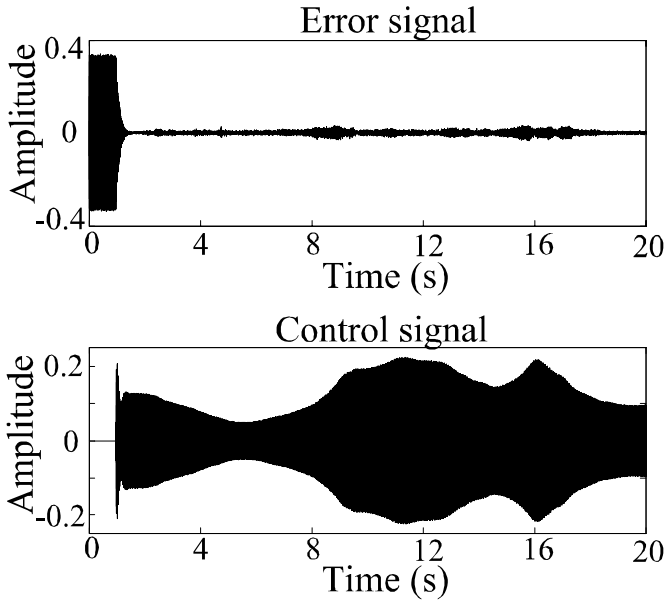

Figure 2.21. Error and control signals with continuously changing system parameters.

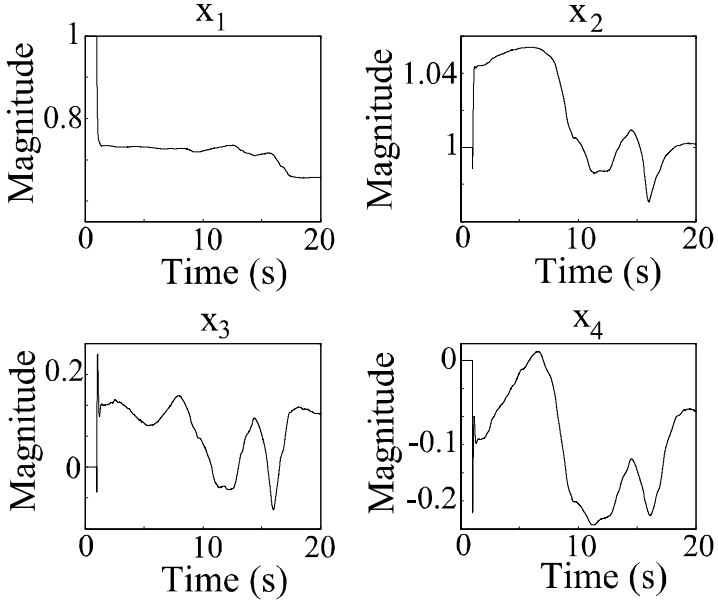

Figure 2.22. Tracking of continuously changing parameters.

where

$$u_v = \begin{pmatrix} u_1(t) \\ \vdots \\ u_j(t) \end{pmatrix}, \quad \tilde{u}_v = \begin{pmatrix} \tilde{u}_1(t) \\ \vdots \\ \tilde{u}_j(t) \end{pmatrix} \tag{2.66}$$

and each u_j, $\tilde{u}_j$ correspond to a plant input. This leads to a state vector of the form

$$x_i(t) = \begin{pmatrix} \hat{P}_{Ri1} & \cdots & \hat{P}_{Rij} & \hat{P}_{Ii1} & \cdots & \hat{P}_{Iij} & \hat{p}_{ci} & \hat{p}_{si} \end{pmatrix}^T \tag{2.67}$$

For clarity, the individual elements of the vector $x_i(t)$ are denoted by the estimate of the corresponding element of x_i^*. For calculation of the control coefficients, the states of each algorithm can be combined as

$$G = \begin{pmatrix} \hat{P}_R & \hat{P}_I \\ -\hat{P}_I & \hat{P}_R \end{pmatrix}, \pi = \begin{pmatrix} \hat{p}_c \\ \hat{p}_s \end{pmatrix} \tag{2.68}$$

where

$$\hat{P}_R = \begin{pmatrix} \hat{P}_{R11} & \cdots & \hat{P}_{R1j} \\ \vdots & \ddots & \vdots \\ \hat{P}_{Ri1} & \cdots & \hat{P}_{Rij} \end{pmatrix}, \hat{P}_I = \begin{pmatrix} \hat{P}_{I11} & \cdots & \hat{P}_{I1j} \\ \vdots & \ddots & \vdots \\ \hat{P}_{Ii1} & \cdots & \hat{P}_{Iij} \end{pmatrix} \tag{2.69}$$

and

$$\hat{p}_c = \begin{pmatrix} \hat{p}_{c1} \\ \vdots \\ \hat{p}_{ci} \end{pmatrix}, \quad \hat{p}_s = \begin{pmatrix} \hat{p}_{s1} \\ \vdots \\ \hat{p}_{si} \end{pmatrix} \tag{2.70}$$

The control coefficients are determined by

$$\theta = -G^{-1}\pi \tag{2.71}$$

where

$$\theta = \begin{pmatrix} \theta_{c1} & \cdots & \theta_{cj} & \theta_{s1} & \cdots & \theta_{sj} \end{pmatrix}^T \tag{2.72}$$

In (2.71), the appropriate pseudo-inverse should be used for cases where $i \neq j$. The initial conditions of each x_i must be chosen so that G is not singular, but all other initial conditions can be 0. The jth plant input is found as

$$u_j(t) = \theta_{cj} \cos(\omega_1 t) + \theta_{sj} \sin(\omega_1 t) \tag{2.73}$$

In order to demonstrate this extension of the algorithm, an active noise control experiment is presented. The plant consists of 2 inputs (control loudspeakers) and 2 outputs (error microphones). The disturbance is a 160 Hz sinusoid. The initial conditions of each x_i were chosen as

$$\begin{aligned} x_1(0) &= \begin{pmatrix} 1 & 1 & 0 & 0 & 0 & 0 \end{pmatrix}^T \\ x_2(0) &= \begin{pmatrix} 0 & 0 & 1 & 1 & 0 & 0 \end{pmatrix}^T \end{aligned} \tag{2.74}$$

The results of the experiment can be seen in Fig. 2.23, where significant attenuation is observed at each output of the plant.

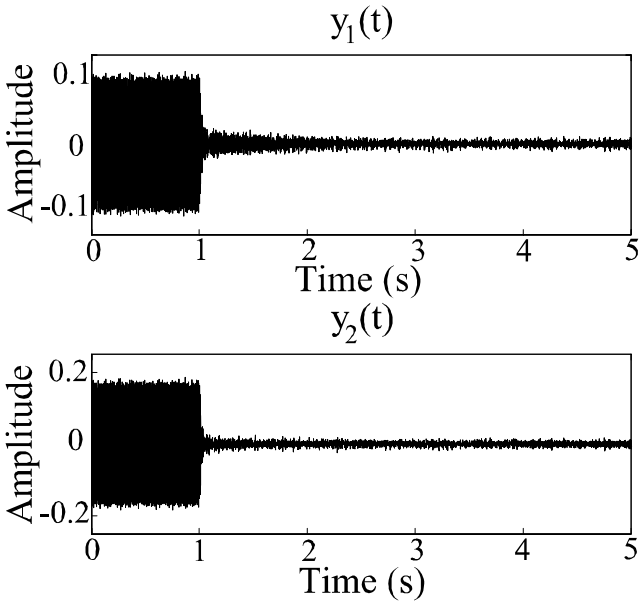

Figure 2.23. Output error with 2 inputs and 2 outputs.

2.7.2 Multiple frequency components

The algorithm of (2.11), (2.12), and (2.15) can also be extended for the rejection of a periodic disturbance consisting of multiple sinusoidal components. A disturbance consisting of m sinusoidal components is written in the form of (2.2) as

$$p(t) = w_m^T \pi^* \tag{2.75}$$

where the vector

$$w_m(t) = \begin{pmatrix} v_{\cos} \\ v_{\sin} \end{pmatrix} \tag{2.76}$$

consists of

$$v_{\cos} = \begin{pmatrix} \cos(\omega_1 t) \\ \vdots \\ \cos(\omega_m t) \end{pmatrix}, v_{\sin} = \begin{pmatrix} \sin(\omega_1 t) \\ \vdots \\ \sin(\omega_m t) \end{pmatrix} \tag{2.77}$$

and the vector

$$\pi^* = \begin{pmatrix} p_c \\ p_s \end{pmatrix} \tag{2.78}$$

consists of

$$p_c = \begin{pmatrix} p_{c,1} \\ \vdots \\ p_{c,m} \end{pmatrix}, \quad p_s = \begin{pmatrix} p_{s,1} \\ \vdots \\ p_{s,m} \end{pmatrix} \tag{2.79}$$

Each ω_m, $p_{c,m}$, $p_{s,m}$ corresponds to a specific sinusoidal component of the disturbance. The regressor is given by

$$W(t,\theta) = \begin{pmatrix} u_v \\ \tilde{u}_v \\ \cos(\omega t) \\ \sin(\omega t) \end{pmatrix} \tag{2.80}$$

where

$$u_v = \begin{pmatrix} u_{,1}(t) \\ \vdots \\ u_{,m}(t) \end{pmatrix}, \qquad \tilde{u}_v = \begin{pmatrix} \tilde{u}_{,1}(t) \\ \vdots \\ \tilde{u}_{,m}(t) \end{pmatrix} \tag{2.81}$$

and

$$\begin{aligned} u_{,m}(t) &= \theta_{c,m} \cos(\omega_m t) + \theta_{s,m} \sin(\omega_m t) \\ \tilde{u}_{,m}(t) &= \theta_{s,m} \cos(\omega_m t) - \theta_{c,m} \sin(\omega_m t) \end{aligned} \tag{2.82}$$

These definitions lead to a vector of identified parameters of the form

$$x(t) = \begin{pmatrix} \hat{P}_{R,1} & \cdots & \hat{P}_{R,m} & \hat{P}_{I,1} & \cdots & \hat{P}_{I,m} & \hat{p}_c & \hat{p}_s \end{pmatrix}^T \tag{2.83}$$

where

$$\hat{p}_c = \begin{pmatrix} \hat{p}_{c,1} \\ \vdots \\ \hat{p}_{c,m} \end{pmatrix}, \quad \hat{p}_s = \begin{pmatrix} \hat{p}_{s,1} \\ \vdots \\ \hat{p}_{s,m} \end{pmatrix} \tag{2.84}$$

Again for clarity, the individual elements of the vector $x(t)$ are denoted by the estimate of the corresponding element of x^*. Calculation of the control coefficients can be combined as

$$G = \begin{pmatrix} \hat{P}_R & \hat{P}_I \\ -\hat{P}_I & \hat{P}_R \end{pmatrix}, \pi = \begin{pmatrix} \hat{p}_c \\ \hat{p}_s \end{pmatrix} \tag{2.85}$$

where

$$\hat{P}_R = \begin{pmatrix} \hat{P}_{R,1} & 0 & 0 \\ 0 & \ddots & 0 \\ 0 & 0 & \hat{P}_{R,m} \end{pmatrix}, \hat{P}_I = \begin{pmatrix} \hat{P}_{I,1} & 0 & 0 \\ 0 & \ddots & 0 \\ 0 & 0 & \hat{P}_{I,m} \end{pmatrix} \tag{2.86}$$

The control coefficients are found similar to (2.71) by

$$\theta = -G^{-1}\pi \tag{2.87}$$

but now

$$\theta = \begin{pmatrix} \theta_{c,1} & \cdots & \theta_{c,m} & \theta_{s,1} & \cdots & \theta_{s,m} \end{pmatrix}^T \tag{2.88}$$

The control signal is found as

$$u(t) = u_{,1}(t) + u_{,2}(t) + \cdots + u_{,m}(t) = w_m^T \theta \tag{2.89}$$

In order to demonstrate this extension of the algorithm, an active noise control experiment is presented. The plant consists of a single input (loudspeaker) and a single output (microphone). The disturbance consisted of two sinusoidal components of 180 Hz and 160 Hz, respectively. The initial x was

$$x = \begin{pmatrix} -0.04 & -0.7 & 1.04 & 1.4 & 0 & 0 & 0 & 0 \end{pmatrix}^T \tag{2.90}$$

The result of the experiment can be seen in Fig. 2.24, where significant attenuation is observed.

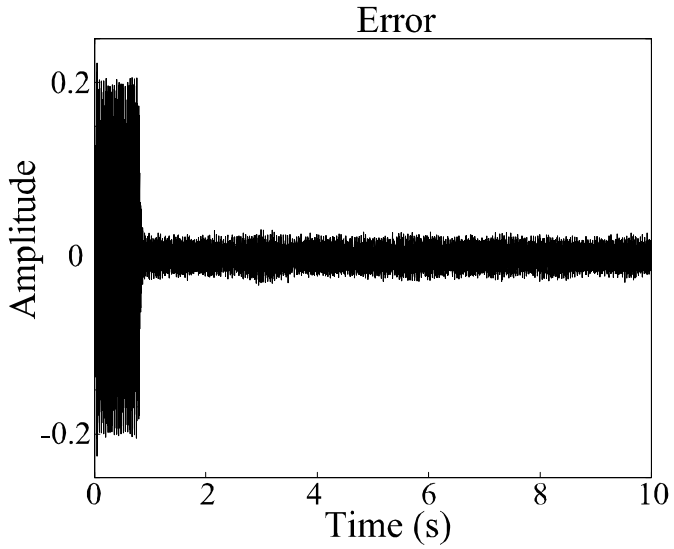

Figure 2.24. Plant output with disturbance consisting of 2 frequency components.

2.8 Conclusions

An adaptive algorithm for the rejection of periodic disturbances of known frequency affecting unknown plants was considered. Typically, in active noise and vibration control applications, the plant is approximately linear, allowing a linear expression at the output of the plant to be derived. The unknown parameters were collected in a vector, and an estimate of this vector formed the states of a nonlinear controller. Since the overall closed-loop system was nonlinear and time-varying, averaging theory was applied to analyze the system. By averaging over time, a much simpler time-invariant system was obtained, whose dynamics closely approximated the dynamics of the actual system. It was shown that the averaged system for the algorithm under consideration was a four-dimensional nonlinear system with a two-dimensional equilibrium surface. Half of the surface was locally stable and the other half was unstable. Generally, trajectories converged to the stable subset of the equilibrium surface, resulting in cancellation of the disturbance. Further properties of the trajectories of the system were obtained from an analysis of the averaged system. A lyapunov analysis showed that trajectories of the averaged system traveled along a path of constant norm. Simulations and single-channel active noise control experiments illustrated the results. It was found that stability was achieved in situations that would be unstable with simpler algorithms that do not provide plant adaptation. In addition, the ability to track abruptly or continuously time-changing system parameters was demonstrated. While disturbances of known frequency have been considered, many real-world scenarios contain unknown frequencies that may drift over time. In the next chapter, disturbances of unknown and time-varying frequency acting on unknown and time-varying systems are considered.

CHAPTER 3

UNKNOWN DISTURBANCES AND UNKNOWN SYSTEMS

3.1 Introduction

This chapter introduces a new algorithm for the rejection of sinusoidal disturbances of unknown frequency acting on an unknown system. The algorithm builds on the ADHSS algorithm of the previous chapter by adding *magnitude/phase-locked loop* (MPLL) frequency estimation [49]. It is shown that the MPLL algorithm combines favorably with the ADHSS algorithm. However, combination of the two components of the algorithm is not trivial. Indeed, combination of the two algorithms is where the challenge begins. Specifically, the ADHSS algorithm injects a control signal in the plant that adds itself to the disturbance signal measured by the MPLL and interferes with its operation. Conversely, any frequency error in the MPLL contributes a disturbance in the ADHSS which results in bursting, unless eliminated. Fortunately, analysis shows that the MPLL is able to lock on the unknown frequency despite the presence of the control signal and further enables a reduction of the order of the ADHSS system. Thus, the reduced-order ADHSS is investigated, after which the overall system consisting of the reduced-order ADHSS and the MPLL is considered. Equilibrium points of the system are found that ensure perfect rejection of the disturbance in ideal conditions, and local stability is guaranteed under certain conditions. Finally, multiple active noise control experiments with variations in plant and disturbance parameters demonstrate the performance of the algorithm under challenging conditions.

3.1.1 Effect of a frequency error

While it was shown in the last chapter that the ADHSS algorithm possesses desirable convergence and stability properties when the frequency of an unwanted sinusoidal disturbance is known, unfortunately, the ADHSS algorithm does not tolerate well a frequency error. To explain this characteristic, account for a frequency error by introducing a new definition of the disturbance

$$p(t) = m^* \cos(\alpha_1^*(t)) \tag{3.1}$$

where

$$\alpha_1^*(t) = \alpha_1^*(0) + \int_0^t \omega_1^* d\tau \tag{3.2}$$

and ω_1^* is the true frequency of the disturbance. With the phase

$$\alpha_1(t) = \int_0^t \omega_1(\tau) d\tau \tag{3.3}$$

where ω_1 is the frequency estimate used by the adaptive algorithm, and its equations remain unchanged. Note that the disturbance can be written as

$$\begin{aligned} p(t) &= m^* \cos(\alpha_1(t) + (\alpha_1^*(t) - \alpha_1(t))) \\ &= w_1^T(t)\pi(t) \end{aligned} \tag{3.4}$$

where

$$\pi(t) = \begin{pmatrix} p_c(t) \\ p_s(t) \end{pmatrix} = m^* \begin{pmatrix} \cos(\alpha(t) - \alpha_1^*(t)) \\ \sin(\alpha_1(t) - \alpha_1^*(t)) \end{pmatrix} \tag{3.5}$$

Thus, (2.2) and (2.6) remain valid, but with the vector π and its components p_c and p_s becoming functions of time. For small frequency error, the disturbance vector π slowly rotates in the two-dimensional space.

The effect of such rotation is illustrated through a simulation. The plant $P(s)$ is taken to be a 250 coefficient FIR transfer function identified from an active noise control system. The frequency of the disturbance is $\omega_1^* = 160\ Hz$, while the estimate is $\omega_1 = 159\ Hz$. The frequency error creates a drift of x with time. Its components rotate to follow the rotation of the disturbance vector, while staying within the equilibrium surface where the disturbance is cancelled. Unfortunately, the unstable subset of the equilibrium surface is encountered eventually, causing a bursting of the control signal $u(t)$ and of the error $e(t)$, as shown in Fig. 3.1 from the simulation. Fig. 3.2 shows the left side of (2.41), which verifies that the system bursts when the expression becomes negative. While the system returns to the stable subset of the equilibrium surface, bursting of the control and error signals is undesirable and repeats indefinitely. This demonstrates the necessity of obtaining an accurate estimate of the disturbance frequency if the adaptive harmonic steady-state algorithm is to be used for disturbances of unknown frequency, and is to track this frequency if the frequency varies.

3.2 Use of Frequency Estimation

3.2.1 Magnitude/phase-locked loop frequency estimator

In this section, the MPLL frequency estimator of [49], which was further analyzed in [16], is reviewed. The algorithm was successfully used in active noise control applications, and achieves the continuous tracking of time-varying frequencies. As opposed to a conventional phase-locked loop, the magnitude of the signal is also tracked, which yields the property that, under ideal conditions, all signals converge to their nominal values without residual oscillations.

First assume that the control signal is equal to zero. Then, the output $y(t)$ is equal to the disturbance, which is assumed to be of the form (3.1). The algorithm reconstructs estimates $m(t)$, $\alpha_1(t)$ and $\omega_1(t)$ that yield an estimate of the output

$$\hat{y}(t) = m(t)\cos(\alpha_1(t)) \tag{3.6}$$

Defining the signal estimation error

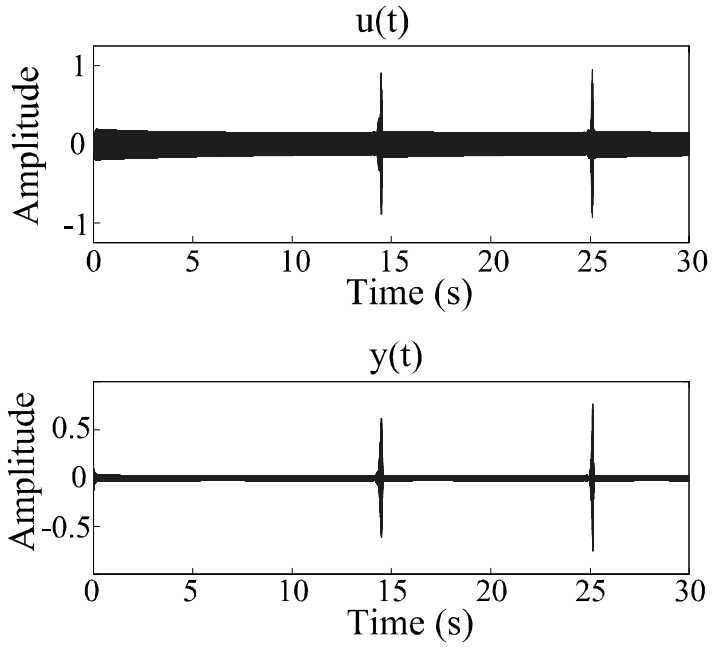

Figure 3.1. Control and error signals exhibiting bursting due to a constant frequency error.

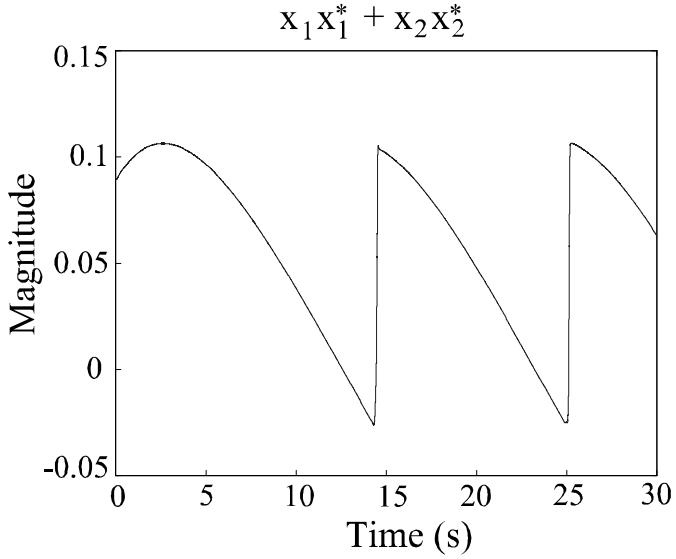

Figure 3.2. The expression $x_1x_1^* + x_2x_2^*$ versus time.

$$e(t) = y(t) - \hat{y}(t) \tag{3.7}$$

and the vector

$$\begin{pmatrix} e_c(t) \\ e_s(t) \end{pmatrix} = 2 \begin{pmatrix} \cos(\alpha_1(t)) \\ -\sin(\alpha_1(t)) \end{pmatrix} e(t) \tag{3.8}$$

the rest of the MPLL algorithm is given in the Laplace domain by

$$\begin{aligned} m(s) &= \tfrac{g_m}{s} e_c(s) \\ \omega_1(s) &= \tfrac{g_\omega}{s} e_s(s) \\ \alpha_1(s) &= \tfrac{ks+1}{s} \omega_1(s) \end{aligned} \tag{3.9}$$

where g_m, g_ω, and k are positive constants. Note that (3.3) is now replaced by

$$\alpha_1(t) = k\omega_1(t) + \int_0^t \omega_1(\tau) d\tau \tag{3.10}$$

Other equations remain the same and, except for a bias, the phase estimate α_1 is the integral of the frequency estimate in steady-state. The benefit of a nonzero k will become obvious later. Fig. 3.3 shows the structure of the MPLL algorithm.

The averaging analysis of [49] is similar to the conventional method of analysis of phase-locked loops and starts by computing the average values of the error signals assuming constant parameters

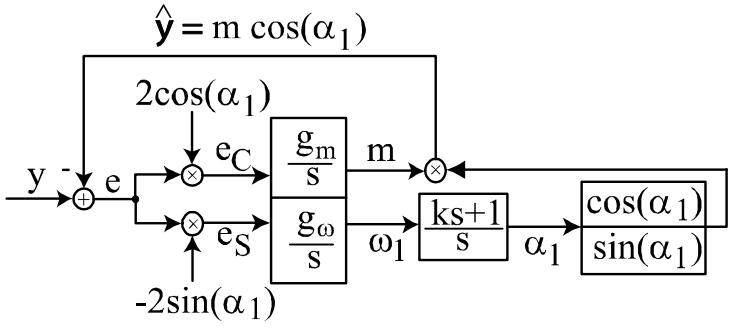

Figure 3.3. Diagram of MPLL frequency estimator.

$$AVE\left[\begin{pmatrix} e_c \\ e_s \end{pmatrix}\right] = \begin{pmatrix} m^* \cos(\alpha_1 - \alpha_1^*) - m \\ m^* \sin(\alpha_1^* - \alpha_1) \end{pmatrix} \simeq \begin{pmatrix} m^* - m \\ m^*(\alpha_1^* - \alpha_1) \end{pmatrix} \tag{3.11}$$

where the second approximation results from linearization of the first around the nominal trajectories. The equilibrium is at $m = m^*$ and $\alpha_1 = \alpha_1^*$ and, with (3.9), the approximation leads to the conclusion that the linearized system is the combination of two linear time-invariant systems whose poles are the roots of

$$s + g_m = 0 \tag{3.12}$$

$$s^2 + kg_\omega m^* s + g_\omega m^* = 0 \tag{3.13}$$

From this, one can conclude that the linearized system is stable for all positive values of the design parameters k, g_ω g_m.

3.2.2 Interaction of MPLL with ADHSS algorithm

Combination of the MPLL estimator with the ADHSS algorithm brings significant issues. Similar problems are found in other approaches that try to solve the difficult problem involving both an unknown plant and an unknown disturbance frequency. Interestingly, the MPLL and ADHSS algorithms have specific features that allow them to be integrated successfully. The main issue to consider is that the output signal $y(t)$ is composed not only of the disturbance, but also of the effect of the control input. When control is applied, the output signal contains two sinusoids with distinct frequencies: one at the disturbance frequency and one at the estimated frequency. When the frequency estimate is exact, the frequencies are the same, but the output converges to zero (if all goes well), leaving no signal for frequency estimation. Guaranteeing that the components of a combined algorithm interact favorably in such conditions is nontrivial. In other situations, the effect of the control input has been eliminated by subtracting from the plant output a signal equal to the contribution of the control signal to the output. However, this approach is not feasible if the plant is unknown.

The averaging analysis of the MPLL can be extended when the plant output includes the effect of a control input of the form (2.4). With constant parameters,

the nonlinear and linear approximations of (3.11) become

$$\begin{aligned} AVE\left[\begin{pmatrix} e_c \\ e_s \end{pmatrix}\right] &= \begin{pmatrix} m^* \cos(\alpha_1 - \alpha_1^*) - m + x_1^*\theta_c + x_2^*\theta_s \\ m^* \sin(\alpha_1^* - \alpha_1) + x_2^*\theta_c - x_1^*\theta_s \end{pmatrix} \\ &\simeq \begin{pmatrix} m^* - m + x_1^*\theta_c + x_2^*\theta_s \\ m^*(\alpha_1^* - \alpha_1) + x_2^*\theta_c - x_1^*\theta_s \end{pmatrix} \end{aligned} \tag{3.14}$$

As a result, the linearized system is described by the same characteristic polynomials and is stable under the same conditions. A remarkable property of the MPLL is that the frequency estimate converges to the true frequency despite the presence of an additional component on the output signal at a different frequency. As long as the second component is at the MPLL frequency, however, it is rejected by the MPLL. Nevertheless, there is a catch, in that the equilibrium state is shifted and m and α_1 satisfy different nonlinear equations

$$\begin{aligned} m - m^* \cos(\alpha_1 - \alpha_1^*) &= x_1^*\theta_c + x_2^*\theta_s \\ m^* \sin(\alpha_1 - \alpha_1^*) &= x_2^*\theta_c - x_1^*\theta_s \end{aligned} \tag{3.15}$$

Therefore, a new necessary and sufficient condition for the existence of an equilibrium of the MPLL is that

$$\left| \frac{x_2^*\theta_c - x_1^*\theta_s}{m^*} \right| < 1 \tag{3.16}$$

In other words, the effect of the control signal on the output must not be greater than the disturbance magnitude for phase-lock to be possible.

The derivations bring another interesting result regarding the interactions between the two algorithms. Specifically, (3.15) and (3.5) indicate that, if phase-lock occurs,

$$-P_I^*\theta_c + P_R^*\theta_s + p_S = 0 \tag{3.17}$$

This equation is the second equation of $G^*\theta + \pi^* = 0$, which guarantees perfect disturbance cancellation. The first equation is

$$P_R^*\theta_c + P_I^*\theta_s + p_c = 0 \tag{3.18}$$

and does not involve p_s. In other words, cancellation of the disturbance can be achieved in a combined algorithm regardless of x_4, the estimate of p_s. In particular, the parameter x_4 can be set to zero, which is equivalent to assuming that $p_s = 0$. In reality, p_s is not zero, but the phase of the MPLL converges to a value such that one may make this assumption in the ADHSS. For this reason, now consider an ADHSS algorithm with 3 parameters instead of 4, *i.e.,* an ADHSS algorithm that assumes a known phase of the disturbance signal.

3.2.3 ADHSS with known frequency and phase

3.2.3.1 Adaptive algorithm and averaged system

The algorithm is obtained by dropping the parameter x_4 in the previous algorithm. The result is a simpler algorithm, with even stronger properties. The vector of control parameters becomes

$$\theta(x) = \begin{pmatrix} \theta_c(x) \\ \theta_s(x) \end{pmatrix} = -\frac{1}{x_1^2 + x_2^2} \begin{pmatrix} x_1 x_3 \\ x_2 x_3 \end{pmatrix} \tag{3.19}$$

The vector of unknowns is

$$x^* = \begin{pmatrix} P_R^* & P_I^* & m^* \end{pmatrix}^T \tag{3.20}$$

and the regressor used for adaptation is

$$W(t, \theta) = E(x) w_1(t) \tag{3.21}$$

where

$$E(x) = \begin{pmatrix} \theta_c(x) & \theta_s(x) \\ \theta_s(x) & -\theta_c(x) \\ 1 & 0 \end{pmatrix} \tag{3.22}$$

Other equations of the algorithm remain the same.

Taking A, B, and C to be the matrices of a minimal state-space realization of the plant, so that $P(s) = C(sI - A)^{-1}B$, the overall equations describing the system are given by

$$\begin{aligned} \dot{x}_P &= Ax_P + Bw_1^T(t)\theta(x) \\ \dot{x} &= -gE(x)w_1(t)\left(w_1^T(t)E^T(x)x - Cx_P - \cos(\alpha_1)x_3^*\right) \end{aligned} \tag{3.23}$$

where the fact that $m^* = x_3^*$ and

$$p(t) = \cos(\alpha_1^*)x_3^* = \cos(\alpha_1)x_3^* \tag{3.24}$$

were used when the frequency and phase of the disturbance are known.

Averaging theory can be used to analyze this system as in [37]. The averaged system corresponding to the adaptive system is simply

$$\dot{x} = -\frac{g}{2}E(x)E^T(x)\left(x - x^*\right) \tag{3.25}$$

The applicable theory is given in Appendix A. The Basic Averaging Lemma can be applied so that the averaged system (3.25) can be used as an approximation of (3.23) over any time interval of fixed length (after rescaling by a factor of g). Verification of assumptions B1-B7 is required, which mostly guarantee certain boundedness and continuity conditions. B7 is an assumption related to the fact that both the adaptive and the averaged systems have a singularity at $x_1^2 + x_2^2 = 0$ (see equation (3.19)). Such singularities are quite common in adaptive control, occurring any time the estimate of the gain of the plant is zero. Here, the singularity occurs when the estimate of the plant's frequency response is zero, a problem that is somewhat unlikely to occur, because *two* parameters need to be zero for the singularity to be reached. Nevertheless, a cautious implementation of the algorithm would apply one of the available techniques to address singularities. For example, a simple practical fix consists in using in the control law either the parameter x if $x_1^2 + x_2^2 \geqslant \delta > 0$, where δ is a small parameter, or else the last value of the estimated parameter x that satisfied the condition.

3.2.3.2 Equilibrium subset

Because $EE^T x = 0$ if and only if $E^T x = 0$, and since

$$E^T(x)x = -\frac{1}{x_1^2 + x_2^2} \begin{pmatrix} x_1 x_3 & x_2 x_3 \\ x_2 x_3 & -x_1 x_3 \end{pmatrix} \begin{pmatrix} x_1 \\ x_2 \end{pmatrix} + \begin{pmatrix} x_3 \\ 0 \end{pmatrix} = 0$$

equilibrium points of the averaged system are determined by

$$E^T(x)x^* = 0 \tag{3.26}$$

Reorganizing terms, one finds that

$$E^T(x)x^* = \begin{pmatrix} x_1^* & x_2^* \\ -x_2^* & x_1^* \end{pmatrix} \begin{pmatrix} \theta_c(x) \\ \theta_s(x) \end{pmatrix} + \begin{pmatrix} x_3^* \\ 0 \end{pmatrix} \tag{3.27}$$

so that equilibrium points are also such that

$$\begin{pmatrix} \theta_c(x) \\ \theta_s(x) \end{pmatrix} = -\frac{1}{x_1^{*2} + x_2^{*2}} \begin{pmatrix} x_1^* x_3^* \\ x_2^* x_3^* \end{pmatrix} = \begin{pmatrix} \theta_c^* \\ \theta_s^* \end{pmatrix} \tag{3.28}$$

In other words, an equilibrium point corresponds to a control parameter vector equal to the nominal one, and results in exact cancellation of the disturbance.

From (3.26), one can also conclude that any equilibrium point satisfies

$$\begin{aligned} (x_1 x_1^* + x_2 x_2^*)x_3 &= x_3^*(x_1^2 + x_2^2) \\ x_2 x_1^* - x_1 x_2^* &= 0 \end{aligned} \tag{3.29}$$

so that the equilibrium set can be parameterized as a function of a single variable. For example, if $x_1^* \neq 0$, one can express x_2 and x_3 as functions of x_1 with

$$x_2 = \frac{x_2^* x_1}{x_1^*}, \quad x_3 = \frac{x_3^* x_1}{x_1^*} \tag{3.30}$$

In general, the set of equilibrium points is a line connecting the origin of the three-dimensional state-space and the nominal parameter x^*. For x constant and $x_P = x_{P,ss}$, (3.23) becomes

$$E(x)w_1(t)w_1^T(t)E^T(x)(x - x^*) = 0 \tag{3.31}$$

so that any equilibrium of the averaged system is also an equilibrium of the original system.

3.2.3.3 Local stability of equilibrium points

Linearizing (3.25) with (3.22) around an equilibrium state x, the following eigenvalues can be computed

$$\lambda_1 = 0, \quad \lambda_2 = -g\frac{x_i^*}{x_i}\frac{x_3^{*2}}{x_1^{*2} + x_2^{*2}}, \quad \lambda_3 = -g\frac{x_i^*}{x_i}\left(1 + \frac{x_3^{*2}}{x_1^{*2} + x_2^{*2}}\right) \tag{3.32}$$

where $i = 1, 2$, or 3 (whichever corresponds to a nonzero x_i). Thus, the condition for stability of an equilibrium point is that

$$\text{sign}(x_i) = \text{sign}(x_i^*) \tag{3.33}$$

which means that the equilibrium point is stable if it is on the same side of the origin as the nominal parameter x^*. A corresponding orthogonal set of eigenvectors is given by

$$v_1 = \begin{pmatrix} x_1^* \\ x_2^* \\ x_3^* \end{pmatrix}, v_2 = \begin{pmatrix} -x_2^* \\ x_1^* \\ 0 \end{pmatrix}, v_3 = \begin{pmatrix} x_1^* x_3^* \\ x_2^* x_3^* \\ -x_1^{*2} - x_2^{*2} \end{pmatrix} \tag{3.34}$$

Note that $|\lambda_2| < |\lambda_3|$ and may be much smaller if $x_3^{*2} \ll x_1^{*2} + x_2^{*2}$. In such cases, convergence of the state x_3 (the estimate of the disturbance magnitude) occurs fast, followed by a slower convergence within the $x_1 - x_2$ plane.

3.2.3.4 Trajectories of the averaged system

Using the Lyapunov function $V = \|x(t) - x^*\|^2$, one finds that $\dot{V} \leq 0$ and

$$\|x(t) - x^*\| \leq \|x(0) - x^*\| \tag{3.35}$$

Since x and $\dot{x}$ are bounded (using (3.25) and assumption B7), one may again deduce that $E^T(x)\,(x - x^*) \to 0$ as $t \to \infty$. Also, $E^T(x)x = 0$ and (2.28) with $x_4^* = 0$ imply that the disturbance is asymptotically cancelled. Therefore the equilibrium line is reached, and the disturbance is asymptotically cancelled. Using $V = \|x(t)\|^2$ and $E^T(x)x = 0$, one finds that $\dot{V} = 0$, so that

$$\|x(t)\| = \|x(0)\| \tag{3.36}$$

for all t. Because all trajectories converge to the equilibrium line, the steady-state value of x must satisfy (3.29) as well as (3.36). Combining the equations, one gets the remarkable property that, asymptotically

$$x_i = x_i^* \frac{\|x(0)\|}{\|x^*\|}, \quad \text{for all } i \tag{3.37}$$

The reverse sign is also allowed by the equations, but the stability property determines that the positive sign must be used. Thus, trajectories of x travel along the sphere that is centered at the origin and includes $x(0)$, and eventually converge to the intersection of the sphere with the line connecting the origin to x^*, on the same side as x^*.

3.2.3.5 Illustrative simulations

The first set of simulations shows the closeness of (3.23) and (3.25). The plant is the 250 coefficient FIR transfer function used in the previous simulation and the disturbance frequency is $\omega_1^* = 330\pi$. The initial parameter estimate is $x(0) = \begin{pmatrix} 1.0 & 1.0 & 0 \end{pmatrix}^T$. The adaptation gain takes the place of the parameter ϵ in the averaging theory, so $g = \epsilon$. The response of x_1 is shown in Fig. 3.4. Four simulations are plotted: the averaged system with $\epsilon = 1$ (solid line), the actual system for $\epsilon = 100$

(dashed dot), the actual system for $\epsilon = 50$ (dashed), and the actual system for $\epsilon = 1$ (circles). As ϵ decreases, one finds that the trajectory of the adaptive system approaches that of the averaged system. The parameter estimates do not converge to the nominal values: however, they converge to the same steady-state value for all ϵ (as expected since the initial condition remains the same). As seen in Fig. 3.5, the control parameters θ_c and θ_s converge to their nominal values, resulting in cancellation of the disturbance for all values of ϵ.

The second set of simulations highlights the stability properties of the adaptive system. The disturbance frequency is now $\omega_1^* = 320\pi$. The plant is the same, the adaptive gain $g = 100$ and

$$x^* = \begin{pmatrix} 0.7471 & .1548 & 0.1 \end{pmatrix}^T \tag{3.38}$$

The initial vector is

$$x(0) = \begin{pmatrix} -1 & 1 & 0 \end{pmatrix}^T \tag{3.39}$$

and corresponds to an initial estimate of the phase of the plant

$$\tan^{-1}(x_2(0)/x_1(0)) = 135^o \tag{3.40}$$

while the actual phase of the plant is

$$\tan^{-1}(x_2^*/x_1^*) = \measuredangle P(j\omega_1^*) = 11.7^o \tag{3.41}$$

The phase difference of 123.3^o is beyond the 90^o angle condition. The state trajectory can be seen in Fig. 3.6. Although initially diverging from the unstable half of the line, the trajectory eventually reaches the stable side. As predicted from the stability analysis, there is a slower mode of convergence within the $x_1 - x_2$ plane that corresponds to a near constant value of x_3. Although not shown, it was verified that $\|x(t)\| = \|x(0)\|$.

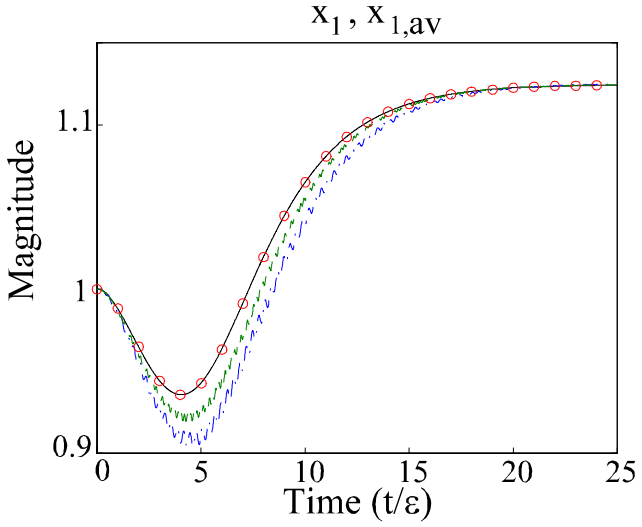

Figure 3.4. Responses of x_1 for the averaged system with $\epsilon = 1$ (solid) and for the actual system with $\epsilon = 100$ (dashed dot), $\epsilon = 50$ (dashed), and $\epsilon = 1$ (circles).

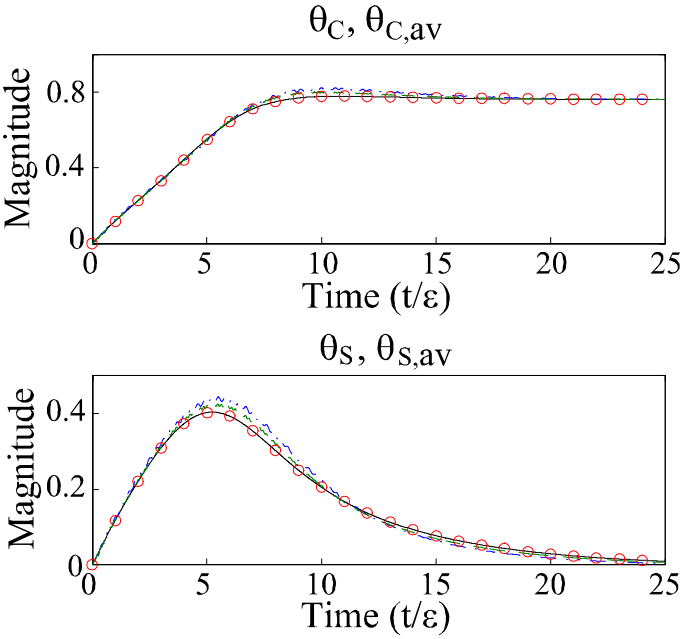

Figure 3.5. Responses of control parameters for the averaged system with $\epsilon = 1$(solid) and for the actual system with $\epsilon = 100$ (dashed dot), $\epsilon = 50$ (dashed), and $\epsilon = 1$ (circles).

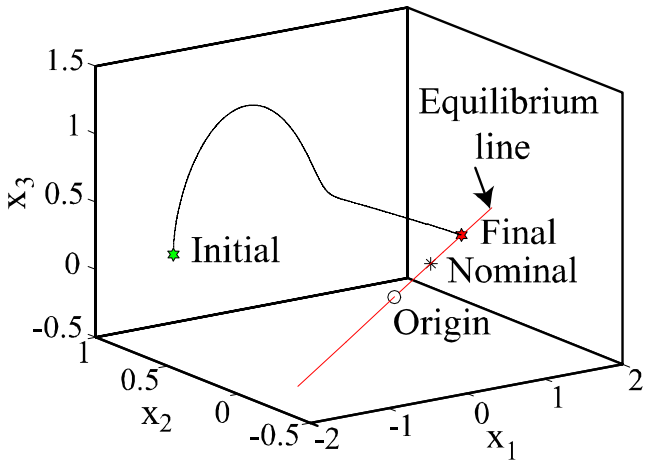

Figure 3.6. State trajectory and relation to the line equilibrium.

3.3 Adaptive Algorithm with Unknown Frequency and Unknown Plant

3.3.1 Adaptive algorithm and averaged system

The algorithm for the general problem of unknown frequency and plant is obtained by combining the MPLL algorithm with the (reduced) ADHSS algorithm for known phase and frequency, resulting in the differential equations

$$\begin{aligned} \dot{x} &= -gE(x)w_1(t)\left(w_1^T(t)E^T(x)x - y\right) \\ \dot{m} &= 2g_m\cos(\alpha_1)(y - m\cos(\alpha_1)) \\ \dot{\omega}_1 &= -2g_\omega\sin(\alpha_1)(y - m\cos(\alpha_1)) \\ \dot{\alpha}_1 &= \omega_1 - 2kg_\omega\sin(\alpha_1)(y - m\cos(\alpha_1)) \end{aligned} \tag{3.42}$$

with positive constants g, g_m, g_ω, and k, and the algebraic equations

$$\begin{aligned} u &= w_1^T(t)\theta(x) \\ w_1(t) &= \begin{pmatrix} \cos(\alpha_1) \\ \sin(\alpha_1) \end{pmatrix} \\ \theta(x) &= -\tfrac{1}{x_1^2+x_2^2}\begin{pmatrix} x_1x_3 \\ x_2x_3 \end{pmatrix} \\ E(x) &= \begin{pmatrix} \theta_c(x) & \theta_s(x) \\ \theta_s(x) & -\theta_c(x) \\ 1 & 0 \end{pmatrix} \end{aligned} \tag{3.43}$$

The plant and the disturbance are described by the equations

$$\begin{aligned} \dot{x}_P &= Ax_P + Bu = Ax_P + Bw_1^T(t)\theta(x) \\ y &= Cx_P + m^*\cos(\alpha_1^*) = Cx_P + m^*w_1(t)\begin{pmatrix} \cos(\alpha_1 - \alpha_1^*) \\ \sin(\alpha_1 - \alpha_1^*) \end{pmatrix} \\ \dot{\alpha}_1^* &= \omega_1^* \end{aligned} \tag{3.44}$$

The overall system is described by complex, nonlinear time-varying differential equations, so it is not very hopeful that a rigorous stability proof could be developed for this system. Again, averaging theory presents the best prospect for an approximation that would give insight into the dynamics of the system. The two

components of the controller were already studied using averaging and were shown to possess desirable stability properties. It remains to show that their combination, including coupling effects, does not produce undesirable interactions (at least close to the nominal operating mode).

The system fits the averaging theory for mixed time scales systems, where the plant state x_P varies fast and the controller states vary slowly. This assumes that the gains g, g_m, g_ω are small enough. Averaging analysis of the MPLL alone is found in [16], and may be combined with the ADHSS. In order for the theory to work, the adaptive gains are defined as functions of ϵ through

$$g = \epsilon, \quad g_m = \epsilon \bar{g}_m, \quad g_\omega = \epsilon^2 \bar{g}_\omega, \quad k = \frac{\bar{k}}{\epsilon} \tag{3.45}$$

where $\bar{g}_m$, $\bar{g}_\omega$, $\bar{k}$ are arbitrary positive values of the MPLL gains for $\epsilon = 1$. The initial error $\omega_1(0) - \omega_1^*$ must also be of the order of ϵ, due to the presence of the integrator. Omitting the tedious details of a formal averaging analysis, focus instead on the interesting properties of the averaged system.

In previous analyses, the effect of the ADHSS on the MPLL was included in the averaging analysis, but the effect of a phase error on the known phase ADHSS was not. A correction term must be added in the averaged system, similar to what was done to study the effect of a frequency error on the 4-parameter ADHSS algorithm. Since

$$p(t) = m^* w_1^T(t) \begin{pmatrix} \cos(\alpha_1 - \alpha_1^*) \\ \sin(\alpha_1 - \alpha_1^*) \end{pmatrix} \tag{3.46}$$

instead of

$$p(t) = m^* \cos(\alpha_1) \tag{3.47}$$

the correction term to be added to the steady-state output is

$$\Delta y_{ss} = m^* w_1^T(t) \begin{pmatrix} \cos(\alpha_1 - \alpha_1^*) - 1 \\ \sin(\alpha_1 - \alpha_1^*) \end{pmatrix} \tag{3.48}$$

Adding the correction term to $y_{ss}$and substituting $\delta\alpha_1 = \alpha_1 - \alpha_1^*$, and $\delta\omega_1 = \omega_1 - \omega_1^*$, the overall averaged system becomes

$$\begin{aligned}
\dot{x} &= -\tfrac{g}{2}E(x)\left(E^T(x)\left(x - x^*\right) - m^*\begin{pmatrix}\cos(\delta\alpha_1) - 1\\ \sin(\delta\alpha_1)\end{pmatrix}\right)\\
\dot{m} &= g_m\left(m^*\cos\left(\delta\alpha_1\right) - m + x_1^*\theta_c + x_2^*\theta_s\right)\\
\delta\dot{\omega}_1 &= -g_\omega\left(m^*\sin\left(\delta\alpha_1\right) - x_2^*\theta_c + x_1^*\theta_s\right)\\
\delta\dot{\alpha}_1 &= \delta\omega_1 - kg_\omega\left(m^*\sin\left(\delta\alpha_1\right) - x_2^*\theta_c + x_1^*\theta_s\right)
\end{aligned} \tag{3.49}$$

3.3.2 Equilibrium points

Since $E^T(x)x = 0$, the equilibrium points are determined by

$$E^T(x)x^* + m^*\begin{pmatrix}\cos(\delta\alpha_1) - 1\\ \sin(\delta\alpha_1)\end{pmatrix} = 0 \tag{3.50}$$

as well as

$$\begin{aligned}
m^*\cos\left(\delta\alpha_1\right) - m + x_1^*\theta_c + x_2^*\theta_s &= 0\\
m^*\sin\left(\delta\alpha_1\right) - x_2^*\theta_c + x_1^*\theta_s &= 0\\
\delta\omega_1 &= 0
\end{aligned} \tag{3.51}$$

Overall, there are 5 equations to determine 6 variables (3 variables in x plus m, $\delta\omega_1$, $\delta\alpha_1$): the equilibrium subset must be (at least) one-dimensional. Expanding (3.50) and using $x_3^* = m^*$, one finds that (3.50) is equivalent to

$$\begin{aligned}
\theta_c x_1^* + \theta_s x_2^* + m^*\cos\left(\delta\alpha_1\right) &= 0\\
\theta_s x_1^* - \theta_c x_2^* + m^*\sin\left(\delta\alpha_1\right) &= 0
\end{aligned} \tag{3.52}$$

which brings two interesting observations: (3.51) implies that $m = 0$, and the first equation of (3.51) and the second equation of (3.52) are identical. The first conclusion is not surprising, in hindsight. If the control signal cancels the disturbance, then the output of the plant including the disturbance should converge to zero. Therefore, the disturbance is cancelled in the equilibrium subset. The second conclusion means that

the equilibrium set, instead of being one-dimensional, is actually two-dimensional, similarly to the ADHSS for known frequency and unknown phase. This is perhaps more surprising.

Using the expression for (3.43), the conditions for the equilibrium points can be written as

$$\begin{aligned} x_3 \frac{x_1 x_1^* + x_2 x_2^*}{x_1^2 + x_2^2} &= m^* \cos(\delta\alpha_1) \\ x_3 \frac{x_2 x_1^* - x_1 x_2^*}{x_1^2 + x_2^2} &= m^* \sin(\delta\alpha_1) \end{aligned} \tag{3.53}$$

Define $\|P\|$, $\|P^*\|$, ϕ, and ϕ^* so that

$$\begin{aligned} x_1 &= \|P\| \cos(\phi) \\ x_2 &= \|P\| \sin(\phi) \end{aligned} \tag{3.54}$$

and

$$\begin{aligned} x_1^* &= \|P^*\| \cos(\phi^*) \\ x_2^* &= \|P^*\| \sin(\phi^*) \end{aligned} \tag{3.55}$$

the conditions become

$$\begin{aligned} x_3 \frac{\|P^*\| \cos(\phi - \phi^*)}{\|P\|} &= m^* \cos(\delta\alpha_1) \\ x_3 \frac{\|P^*\| \sin(\phi - \phi^*)}{\|P\|} &= m^* \sin(\delta\alpha_1) \end{aligned} \tag{3.56}$$

Due to the two-dimensional nature of the equilibrium subset, one can pick two free variables. If $\|P\|$ and ϕ are picked , x_1 and x_2 are given by (3.54) and $\delta\alpha_1$ and x_3 can take one of two possible values

$$\begin{aligned} \delta\alpha_1 &= \phi - \phi^* + n\pi \\ x_3 &= (-1)^n \; m^* \frac{\|P\|}{\|P^*\|} \end{aligned} \tag{3.57}$$

with $n = 0$ or 1. Note that, for $n = 0$, the estimate of the magnitude of the disturbance is correct and the PLL phase error is zero if the estimate of the plant is exact. In

general, the estimate of the magnitude of the disturbance is weighted by the ratio of the plant magnitude to the plant magnitude estimate, and the PLL phase error is equal to the plant phase error $\phi - \phi^*$. For $n = 1$, the magnitude estimate changes sign and the phase simply shifts by 180° to compensate for it.

3.3.3 Local stability of equilibrium points

The local stability of the equilibrium points can be obtained by linearizing (3.49) around an equilibrium state. This computation and others to follow are best performed using a symbolic computation engine. With the following definitions

$$\begin{aligned} a_1 &= \tfrac{m^{*2}}{\|P\|\|P^*\|}, \quad a_2 = \tfrac{m^*}{\|P\|} \\ a_3 &= \tfrac{m^{*2}}{\|P^*\|}, \quad a_4 = \tfrac{\|P^*\|}{\|P\|} \end{aligned} \tag{3.58}$$

the Jacobian of the system evaluated around an equilibrium point can be computed to be

$$J = \begin{pmatrix} -\frac{g}{2}a_1\cos(\phi-\phi^*) & -\frac{g}{2}a_1\sin(\phi-\phi^*) & (-1)^n\frac{g}{2}a_2\cos(\phi^*) \\ \frac{g}{2}a_1\sin(\phi-\phi^*) & -\frac{g}{2}a_1\cos(\phi-\phi^*) & (-1)^n\frac{g}{2}a_2\sin(\phi^*) \\ (-1)^n\frac{g}{2}a_2\cos(2\phi-\phi^*) & (-1)^n\frac{g}{2}a_2\sin(2\phi-\phi^*) & -\frac{g}{2}a_4\cos(\phi-\phi^*) \\ (-1)^n g_m a_2\cos(2\phi-\phi^*) & (-1)^n g_m a_2\sin(2\phi-\phi^*) & -g_m a_4\cos(\phi-\phi^*) \\ (-1)^{n+1} g_\omega a_2\sin(2\phi-\phi^*) & (-1)^n g_\omega a_2\cos(2\phi-\phi^*) & g_\omega a_4\sin(\phi-\phi^*) \\ (-1)^{n+1} k g_\omega a_2\sin(2\phi-\phi^*) & (-1)^n k g_\omega a_2\cos(2\phi-\phi^*) & k g_\omega a_4\sin(\phi-\phi^*) \end{pmatrix}$$

$$\cdots \begin{pmatrix} 0 & 0 & -\frac{g}{2}a_3\sin(\phi^*) \\ 0 & 0 & \frac{g}{2}a_3\cos(\phi^*) \\ 0 & 0 & (-1)^{n+1}\frac{g}{2}m^*\sin(\phi-\phi^*) \\ -g_m & 0 & (-1)^{n+1} g_m m^*\sin(\phi-\phi^*) \\ 0 & 0 & (-1)^{n+1} g_\omega m^*\cos(\phi-\phi^*) \\ 0 & 1 & (-1)^{n+1} k g_\omega m^*\cos(\phi-\phi^*) \end{pmatrix} \tag{3.59}$$

The characteristic equation $\det(\lambda I - J) = 0$ has the following form

$$\lambda^2(\lambda + g_m)\left(c_3\lambda^3 + c_2\lambda^2 + c_1\lambda + c_0\right) = 0. \tag{3.60}$$

The 2 eigenvalues at $\lambda = 0$ are associated with the two-dimensional equilibrium subset, and the stable eigenvalue at $\lambda = -g_m$ is associated with the state m, which

depends on but does not influence other states. The stability of the three remaining eigenvalues can be ascertained by considering the third-order polynomial with coefficients

$$\begin{aligned} c_3 &= 1 \\ c_2 &= \cos(\phi-\phi^*)\left(ga_1+\tfrac{1}{2}ga_4+(-1)^n 2kg_\omega m^*\right) \\ c_1 &= (-1)^n \tfrac{1}{2}gkg_\omega m^*(a_1+a_4)+\tfrac{g^2}{4}(a_1^2+a_2^2)+(-1)^n g_\omega m^*\cos(\phi-\phi^*) \\ c_0 &= (-1)^n \tfrac{1}{2}gg_\omega m^*(a_1+a_4) \end{aligned} \tag{3.61}$$

By application of the Routh-Hurwitz test [35], when $n=1$, c_0 is negative indicating there are always eigenvalues in the right-half plane. If $n=0$, the stability of the system is guaranteed if and only if

$$|\phi-\phi^*|<90^\circ \quad \text{and } c_2c_1-c_3c_0>0 \tag{3.62}$$

The condition $c_2c_1-c_3c_0>0$ is equivalent to

$$\cos^2(\phi-\phi^*)+b_1\cos(\phi-\phi^*)-b_0>0 \tag{3.63}$$

where (reintroducing the original variables)

$$\begin{aligned} b_1 &= g\left(\|P^*\|^2+m^{*2}\right)\tfrac{2kg_\omega\|P\|\|P^*\|+gm^*}{4g_\omega\|P\|^2\|P^*\|^2} \\ b_0 &= \tfrac{g\left(\|P^*\|^2+m^{*2}\right)}{g\left(\|P^*\|^2+m^{*2}\right)+gm^{*2}+2kg_\omega m^*\|P\|\|P^*\|} \end{aligned} \tag{3.64}$$

Therefore, (3.62) is satisfied if and only if

$$|\phi-\phi^*|<\bar{\phi} \tag{3.65}$$

where

$$\bar{\phi}=\cos^{-1}\left(\frac{\sqrt{b_1^2+4b_0}-b_1}{2}\right) \tag{3.66}$$

$\bar{\phi}$ is well-defined and less than 90° because $b_1 > 0$ and $1 > b_0 > 0$.

In conclusion, there is always a positive range of angle ϕ around the nominal angle ϕ^* for which the system is stable. The range is reduced from the previous range of $\pm 90°$. It depends in a complicated manner on the system parameters, and also on the location on the equilibrium surface through the parameter $\|P\|$. The range becomes $\pm 90°$ again if $b_0 \to 0$ or $b_1 \to \infty$. These conditions are guaranteed as $k \to \infty$. Thus, for k chosen sufficiently large, the stability region of the averaged system approaches the same region as the ADHSS with known frequency.

3.3.4 Simulations

In order to demonstrate the closeness of the responses of the adaptive system and of the averaged system, a simulation is presented. The plant is the 250 coefficient transfer function used in the simulation of Sec. 2.3 and the disturbance frequency is $\omega_1^* = 320\pi$. The initial conditions are $x = (\ 0.1 \quad 0.1 \quad 0\ )$, $m = 0$, $\omega_1 = 310\pi$. The difference between the actual system response and the averaged system response is shown in Fig. 3.7, where the first three states are plotted. The three other states are plotted on Fig. 3.8. Results corresponding to values of $\epsilon = 1$ (solid line) and $\epsilon = 10$ (dashed line) are shown. For the smaller value of $\epsilon = 1$, the difference between the values of the actual and averaged systems settles more quickly and approaches a steady-state value of zero. For the larger value $\epsilon = 10$, the difference settles more slowly and, in the case of the first two responses, in Fig. 3.7, approach a nonzero steady-state value. This result is consistent with the assumption that, as ϵ decreases, the response of the actual system and the averaged system approach each other.

3.4 Experiments

3.4.1 Practical considerations

If the initial parameters $x_1(0)$ and $x_2(0)$ satisfy the stability condition of the adaptive HSS given by (2.41) and the initial frequency estimate is sufficiently close to the true frequency, convergence of the algorithm is immediately observed. However, for larger initial errors, the frequency must be identified before convergence of the adaptive HSS is observed. Thus, it is useful to use a two-phase start-up routine.

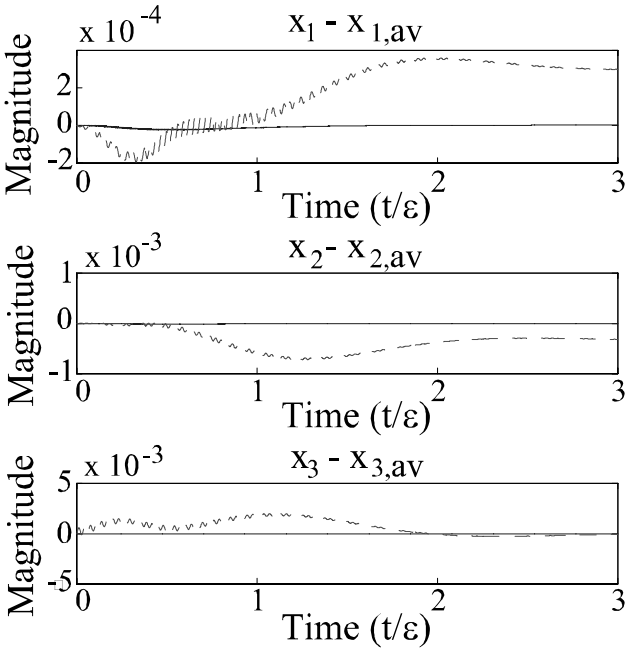

Figure 3.7. Difference between actual states of ADHSS and the averaged states for $\epsilon = 1$ (solid line) and $\epsilon = 10$ (dashed line).

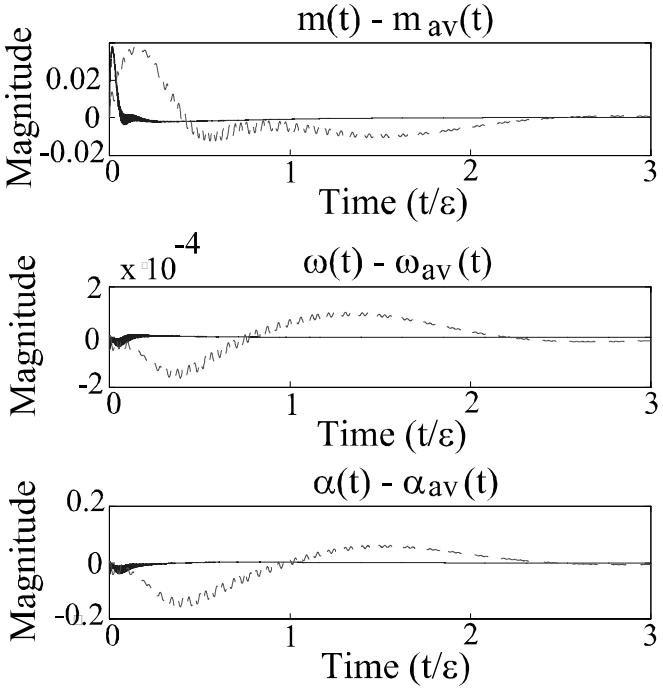

Figure 3.8. Difference between the actual states of the MPLL and the averaged states for $\epsilon = 1$ (solid line) and $\epsilon = 10$ (dashed line).

After start-up, the full algorithm is engaged and can track parameter variations. The two-phase start-up proceeds as follows: over the time interval $t \in [t_0, t_1]$, the control signal $u(t) = 0$ and the MPLL is engaged. For $t = t_1$ large enough, an accurate estimate of the frequency is obtained and $\alpha_1 - \alpha_1^* \simeq 0$. For $t \in [t_1, t_2]$, the frequency estimate is frozen, and the adaptive HSS is engaged. With the phase correctly identified and the frequency estimate frozen, the ADHSS converges, resulting in the cancellation of the disturbance. For $t > t_2$, the MPLL is re-engaged, and the 6 states of the controller are updated continuously.

Another issue is that the ADHSS with known phase may result in quick convergence of x_3 followed by slower convergence within the $x_1 - x_2$ plane. This property sometimes results in a large transients when the initial phase of the plant estimate is large. To avoid this situation, the gain g may be replaced by a gain matrix of the form

$$\Gamma = \begin{pmatrix} g_{12} & 0 & 0 \\ 0 & g_{12} & 0 \\ 0 & 0 & g_3 \end{pmatrix} \tag{3.67}$$

For small g_3, the eigenvalues become closer to each other and the system dynamics are improved.

3.4.2 Experiments with plant changes

The performance of the algorithm was examined through single-channel active noise control experiments. The system was diagrammed in Fig. 2.8 and is the same system as was identified to produce the 250 coefficient FIR transfer function used in simulations. The algorithm was coded in C and implemented in a dSpace DS1104 digital signal processing board. A sampling frequency of 8 kHz was used. A constant amplitude sinusoidal disturbance with frequency of 180 Hz was generated by a loudspeaker, while the control signal was produced by another loudspeaker. A microphone was used to measure the cancellation error. The plant consists of the hardware and transmission in the environment from the control signal output to the error microphone input, including the propagation effects of the surrounding air.

The experiments were conducted in a small room where many signal reflections are present. This is a challenging problem that helps to illustrate the performance of the algorithm in difficult conditions. Gains $g_{12} = 100$ and $g_3 = 1$ were used.

In the experiments of this section, the disturbance remained constant and the effect of a time-varying plant was investigated. During the first 0.8 seconds of operation, the control was not engaged, and the disturbance frequency was identified. Afterwards, the control signal was engaged, and the states of the ADHSS were allowed to converge. After reaching steady-state, the MPLL was engaged, and the frequency response of the plant was changed by manually moving the error microphone. In Fig. 3.9, the control signal is seen to change to compensate for the moving microphone and disturbance rejection is maintained. The states of the adaptive HSS can be seen in Fig. 3.10. In contrast, Fig. 3.11 shows the control signal and the resulting output error when the same procedure is used but the MPLL is not re-engaged. One finds that $y(t)$ varies widely and the disturbance is poorly rejected. In Fig. 3.12, the states are plotted for this experiment.

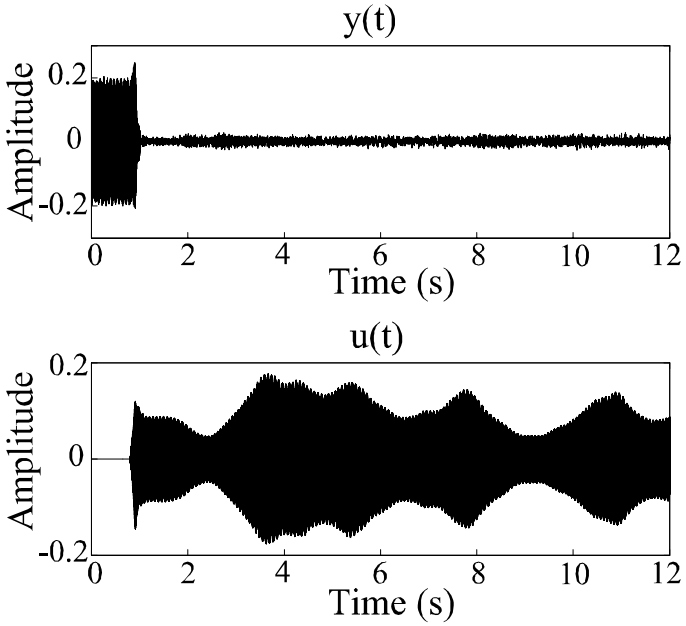

Figure 3.9. The output of the plant $y(t)$ and the control signal $u(t)$ when the estimate x is free to track time variation in the plant.

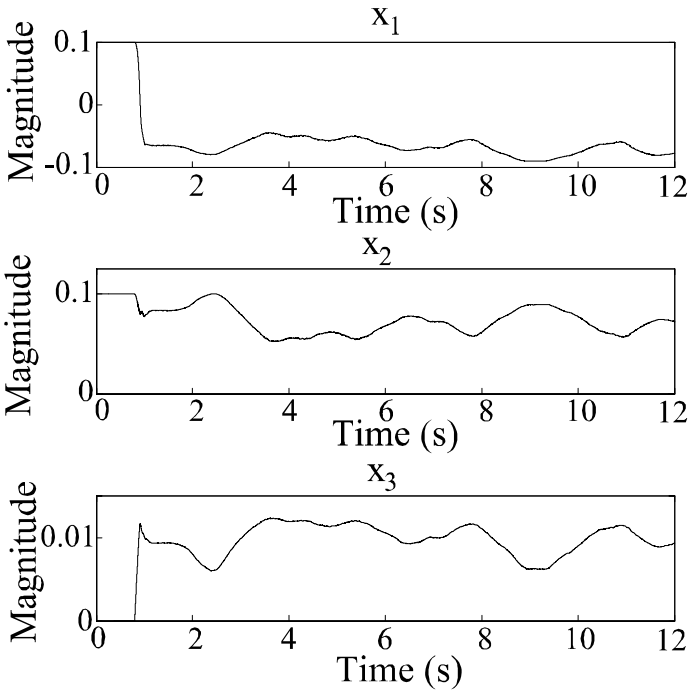

Figure 3.10. The states of the adaptive HSS are free to track time variation in the plant.

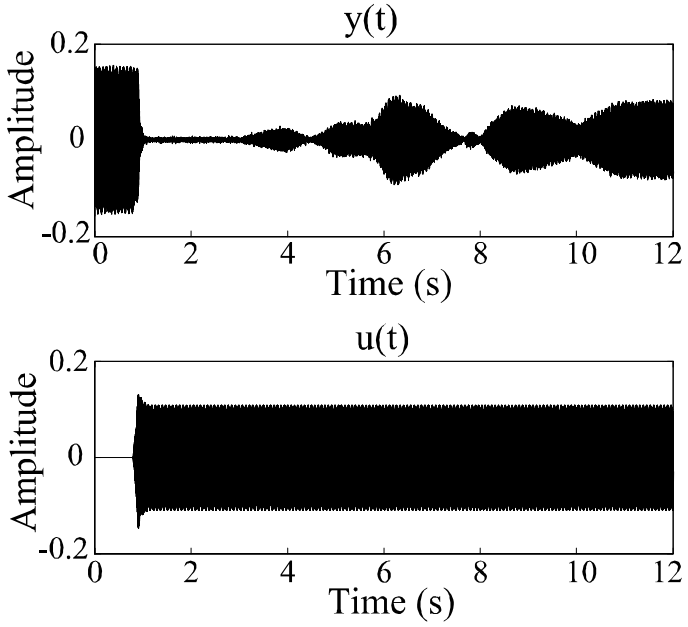

Figure 3.11. The output of the plant $y(t)$ and the control signal $u(t)$ when the estimate x is frozen.

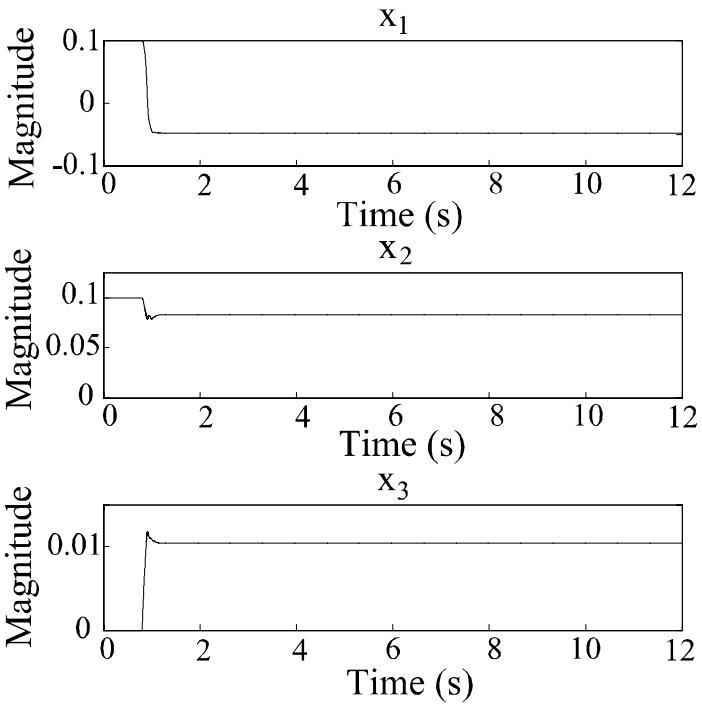

Figure 3.12. The frozen states of the adaptive HSS.

3.4.3 Experiments with disturbances of time-varying magnitude

In the following two experiments, the frequency of the disturbance and the plant were fixed, but the magnitude of the disturbance m^* varied significantly. First, results are shown where the disturbance magnitude goes to zero in three steps. Fig. 3.13 shows the disturbance, whose magnitude goes to zero and then returns to its value roughly 1 second later. The control signal changes in equal proportion, and disturbance cancellation is maintained. Fig. 3.14 shows the states of the adaptive HSS. As one would expect, the decrease in m^* is reflected primarily in x_3. Fig. 3.15 shows the frequency estimate ω_1. Fig. 3.16, Fig. 3.17, and Fig. 3.18 show similar results when the disturbance suddenly goes away in one step. From the oscillations in the frequency estimate of Fig. 3.15 and Fig. 3.18, it is observed that the MPLL does not loose phase-lock until the disturbance has gone completely away.

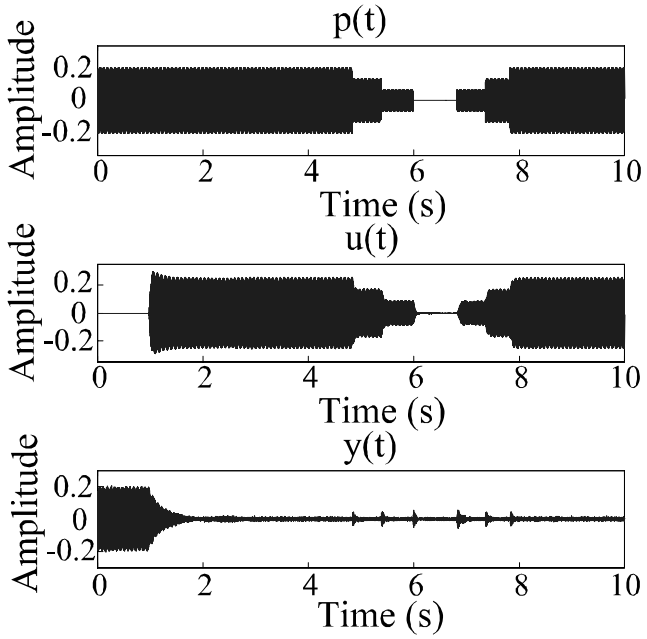

Figure 3.13. Disturbance, control signal, and the output of the plant when the disturbance goes away in three steps and then comes back.

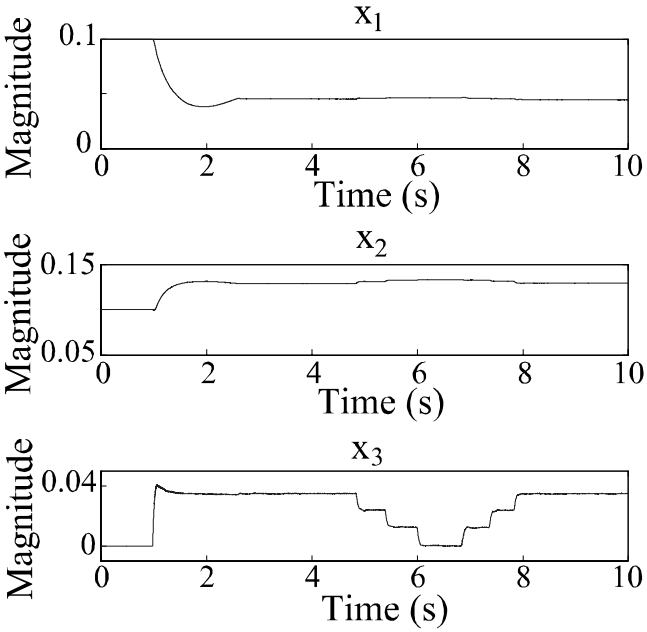

Figure 3.14. The states of the adaptive HSS when the disturbance goes away in three steps and then comes back.

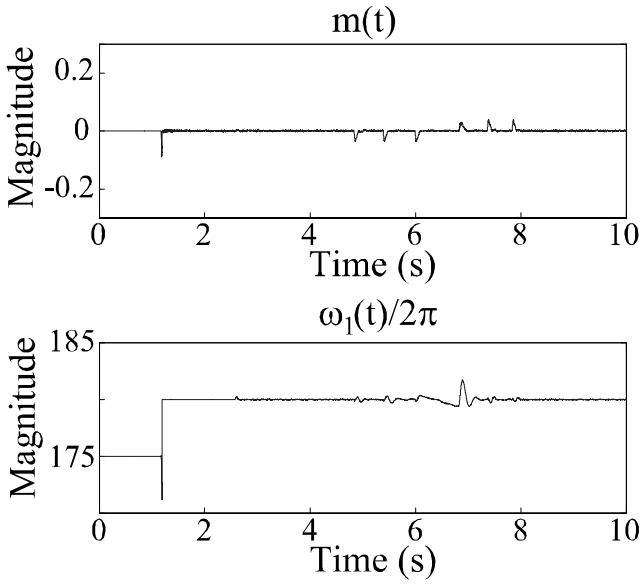

Figure 3.15. The MPLL frequency estimate when the disturbance goes away in three steps and then comes back.

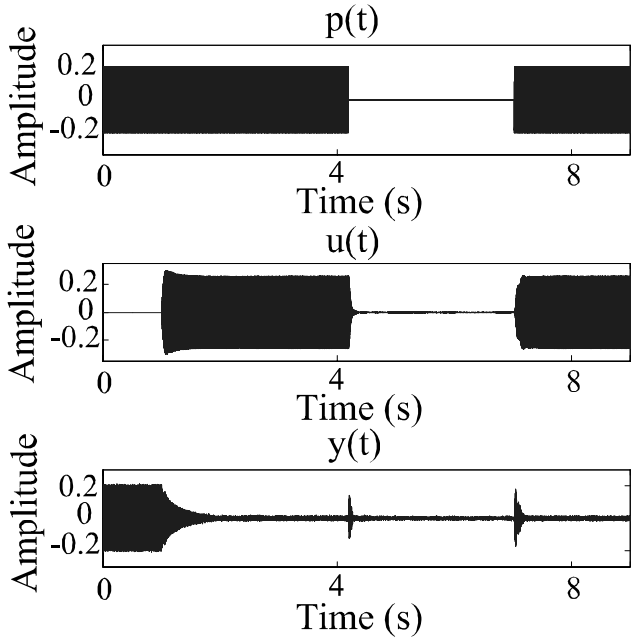

Figure 3.16. Disturbance, control signal, and output of the plant when the disturbance suddenly goes away and comes back.

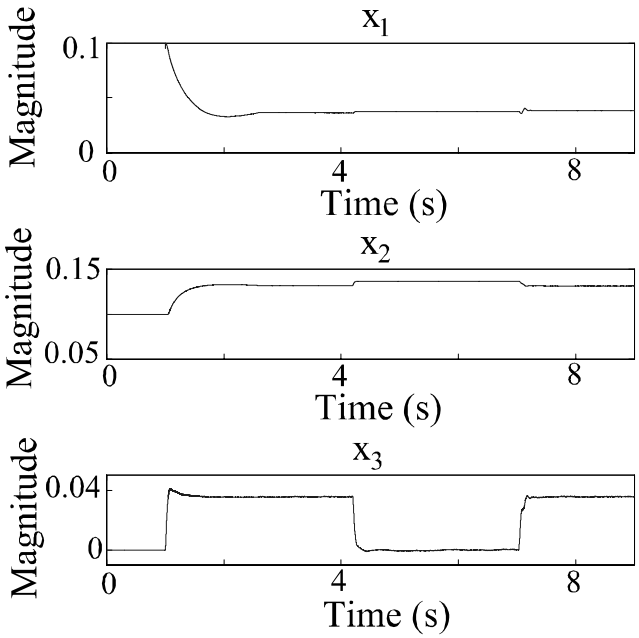

Figure 3.17. The states of the adaptive HSS when the disturbance suddenly goes away and then comes back.

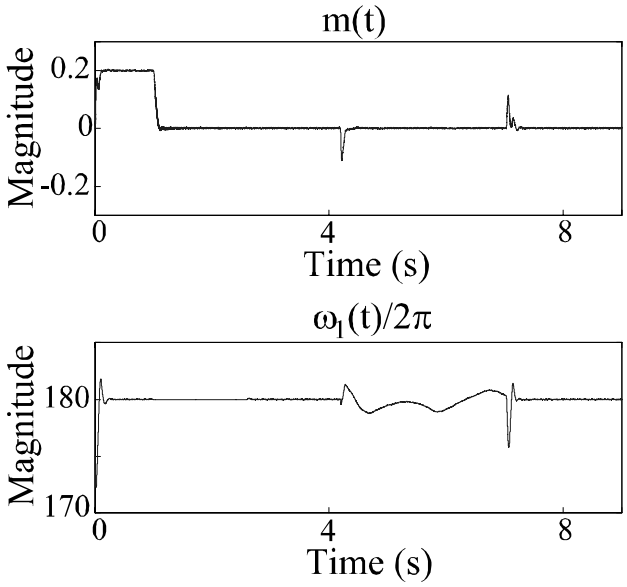

Figure 3.18. The MPLL magnitude and frequency estimate when the disturbance suddenly goes away and then comes back.

3.4.4 Experiments with disturbances of time-varying frequency

In these experiments, the frequency changed linearly from $180Hz$ to $200Hz$ in approximately 6 seconds. Note that a change in frequency of the disturbance produces a change in the plant frequency response. The magnitude of the disturbance was held constant and the algorithm was allowed to reach steady-state in the first 5 seconds. Then, the frequency change was initiated. Fig. 3.19 shows the frequency estimate ω_1 along with the true value ω_1^*. The estimate is directly on top of the true value. Fig. 3.20, shows the control signal $u(t)$, which varies to maintain significant disturbance rejection. The variation in the magnitude of $u(t)$ is indicative of the change of the frequency response of the plant $P(j\omega_1)$ as ω_1 tracks ω_1^*. Fig. 3.21 shows the states of the adaptive HSS which vary in order to produce an appropriate $u(t)$ and reduce $y(t)$.

In the next experiment, the ability to deal with a step change in the disturbance frequency was investigated. Once the system reached steady-state, the disturbance frequency was abruptly changed from $180Hz$ to $185Hz$. Fig. 3.22 shows the frequency estimate, which tracks the sudden change in the disturbance frequency. Fig. 3.23 shows the output of the plant. When the disturbance frequency changes, a small spike in $y(t)$ is noted. However, the system quickly recovers, and significant disturbance rejection is maintained.

3.5 Conclusions

An adaptive algorithm for the rejection of a sinusoidal disturbance of unknown/time-varying frequency acting at the output of an unknown and time-varying plant was presented. The algorithm had a disturbance rejection component based on an adaptive harmonic steady-state algorithm that estimates the plant frequency response at the disturbance frequency along with the disturbance parameters. Because this component required that the frequency be known exactly, a second component providing frequency estimation was added. It was found that the magnitude/phase-locked loop algorithm used for frequency estimation was able to deal with the effect of the control signal on the plant output. Under steady-state approximations, the MPLL was found

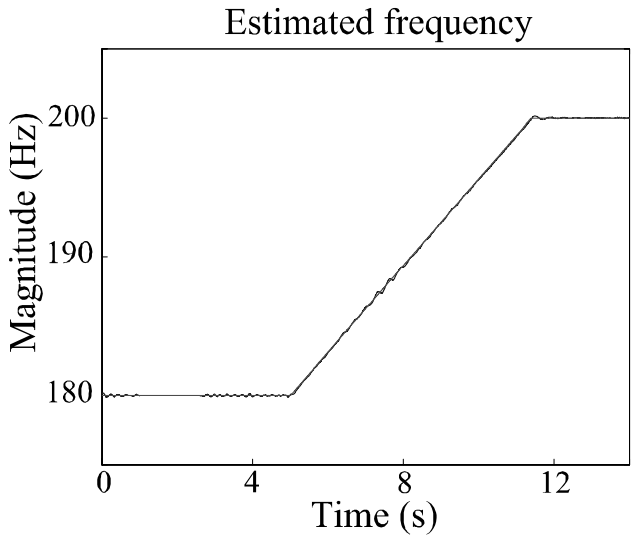

Figure 3.19. MPLL frequency estimate tracking when the time-varying disturbance frequency changes linearly from $180Hz$ and $200Hz$ over approximately 6 seconds.

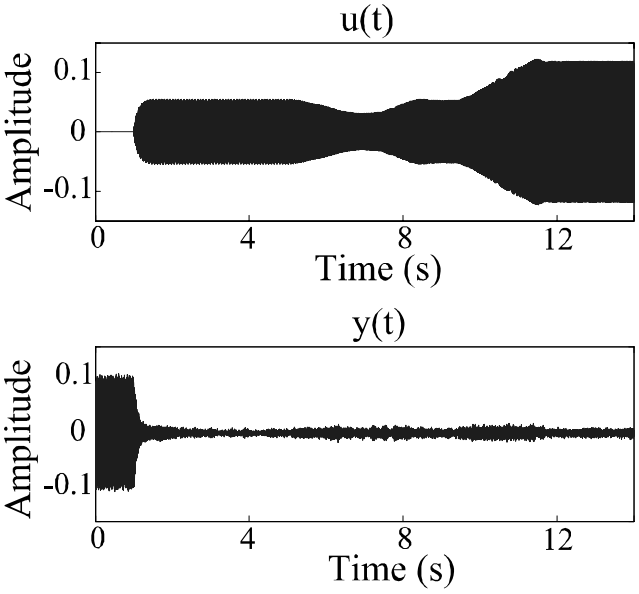

Figure 3.20. Control signal and output of the plant when the disturbance frequency changes linearly from $180Hz$ and $200Hz$ over approximately 6 seconds.

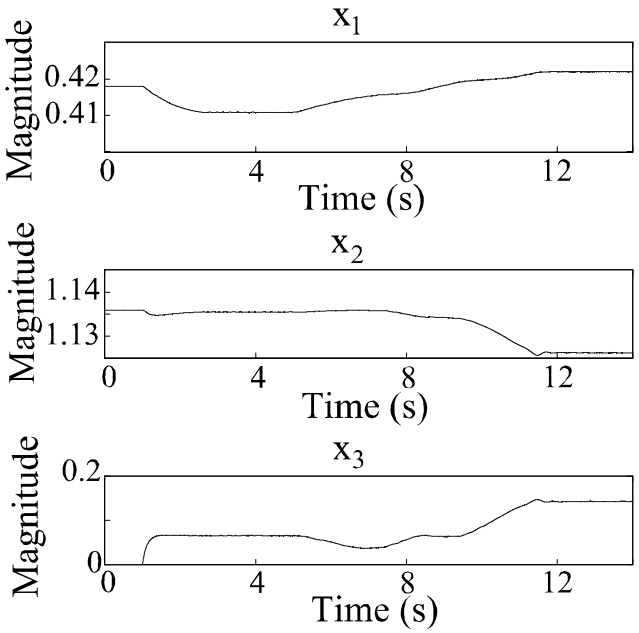

Figure 3.21. States of the adaptive HSS when the time-varying disturbance frequency changes linearly from $180Hz$ and $200Hz$ over approximately 6 seconds.

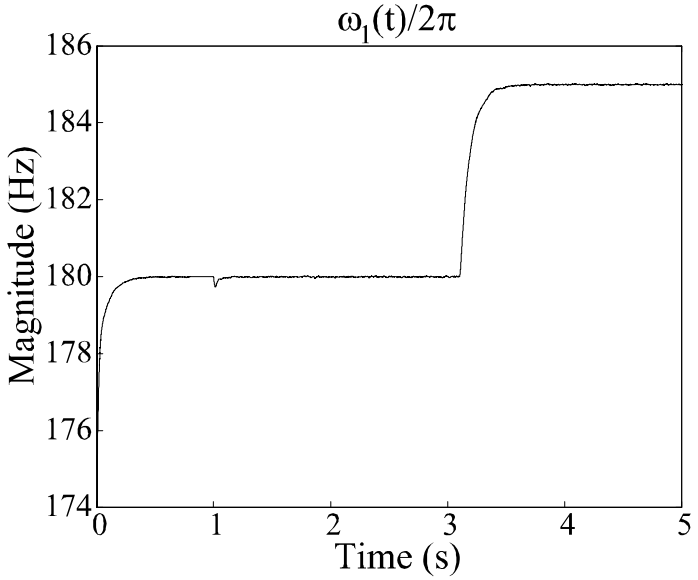

Figure 3.22. Frequency estimate when the disturbance frequency is stepped from $180Hz$ to $185Hz$.

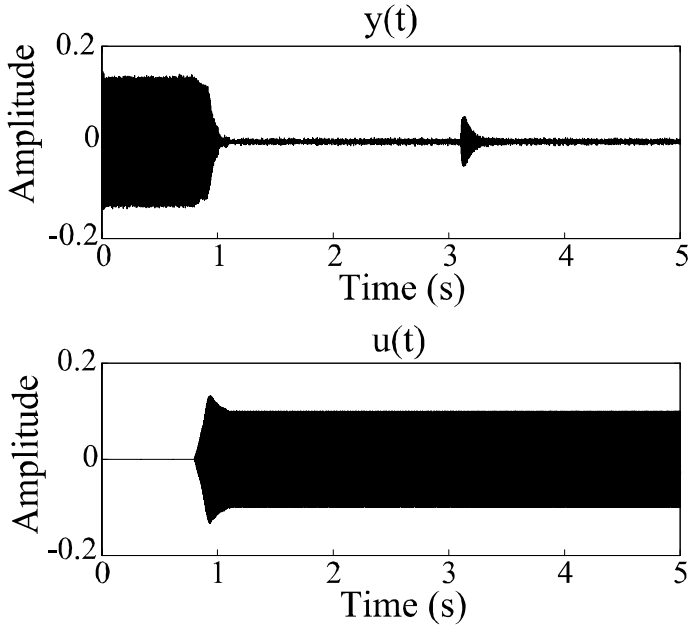

Figure 3.23. The plant output and control signal when the disturbance frequency is stepped from $180Hz$ to $185Hz$.

to be locally stable, while the ADHSS was globally stable.

Further analysis showed that the properties of the MPLL enabled a simplification of the ADHSS algorithm. Instead of the four ADHSS parameters needed in Chapter 2, only three parameters were needed. It was shown that the simplified ADHSS in the ideal case is equivalent to assuming that the exact phase of the disturbance is known. The properties of the simplified ADHSS in the ideal case were studied using an analysis similar to the one used to study the averaged ADHSS algorithm in Chapter 2. Similar properties were observed, but the simplified system dynamics allowed further insight into the convergence of the algorithm. It was found that convergence of the third adapted parameter occurred much faster than convergence of the first two adapted parameters. This fact was used later in the chapter to show the importance of using a gain with the structure of a matrix.

The combination of the ADHSS and MPLL resulted in an overall system described by 6 nonlinear time-varying differential equations. The theory of averaging was applied to find that the equilibrium of the system was a two-dimensional surface.

Any point on the surface resulted in cancellation of the disturbance. The Jacobian matrix of the averaged system linearized around the equilibrium surface revealed that a subset of the surface was locally stable. This subset was described by a bound on the allowable steady-state phase error of the plant estimate. Various ANC experiments demonstrated the ability of the algorithm to track variations in both system and disturbance parameters. A two-phase start-up procedure was used to be sure that the stable subset of the equilibrium surface was reached.

CHAPTER 4

FREQUENCY ESTIMATION BASED ON ELECTRIC MACHINES

4.1 Introduction

The main objective of this chapter is to show that a new type of frequency estimator can be obtained from models of AC (alternating current) electric machines [6]. After reviewing the relevant theory from electric drives, the induction motor frequency estimation (IMFE) equations are presented. Averaging theory is used to show that the algorithm possesses three equilibrium points and, for positive initial frequency estimate, the algorithm is guaranteed to converge to the disturbance frequency. For negative initial estimate, the algorithm converges to the negative of the disturbance frequency. It is further shown that in the context of averaging, the IMFE is semi-globally stable and locally exponentially stable.

IMFE frequency estimation is used in two distinct disturbance rejection schemes. In the first, the IMFE algorithm is combined with a disturbance cancellation algorithm to reject disturbances of unknown frequency acting on a known system. The approach was tested successfully in active noise control experiments using the disturbance cancellation algorithm of [50]. The need for an *a priori* estimate of the frequency was found to be relaxed with a negligible increase in computational complexity. However, to avoid a bias in the frequency estimate, the effect of the control signal at the input to the estimator must be eliminated. Practically, this involves subtracting the effect of the control signal at the output of the plant from the input to the IMFE and requires the frequency response of the plant at the control signal frequency be known.

In the second disturbance rejection scheme, the IMFE algorithm is combined with a disturbance cancellation algorithm to reject disturbances of unknown frequency

acting on an unknown system. The benefits of the IMFE algorithm are used to improve the stability of the ADHSS algorithm with frequency estimation presented in Chapter 3. In Chapter 2, it was shown that the ADHSS algorithm obtains estimates of the plant and disturbance that result in cancellation of the disturbance but that it is unlikely the estimated values will be equal to the true values. As such, eliminating the effect of the control signal at the input to the IMFE is not possible. Therefore, modifications to the original IMFE equations are given that lead to an unbiased frequency estimate. Namely, any signal that varies at the modified IMFE frequency is rejected allowing the frequency of the disturbance to be identified. However, the phase corresponding to the modified IMFE frequency estimate does not lock onto the phase of the disturbance, causing minor perturbations in the frequency estimate to interact unfavorably with the ADHSS. Thus, the dynamics of the modified IMFE are combined with those of the MPLL. This dramatically improves stability of the MPLL frequency estimator so that larger initial frequency errors can be tolerated. Averaging theory is used to explore the effect of combining the modified IMFE with the ADHSS/MPLL algorithm of the previous chapter. It is found that through appropriate selection of the fixed parameters of the modified IMFE the local stability of the algorithm is improved.

4.2 Induction Motor Frequency Estimation Algorithm

4.2.1 Model of a two-phase induction motor

The model of a two-phase induction motor with one pole pair and current command is given by the equations

$$\begin{aligned} \frac{d\psi_{RA}}{dt} &= -\tfrac{1}{T_R}\psi_{RA} + \tfrac{M}{T_R} i_{SA} - \omega\psi_{RB} \\ \frac{d\psi_{RB}}{dt} &= -\tfrac{1}{T_R}\psi_{RB} + \tfrac{M}{T_R} i_{SB} + \omega\psi_{RA} \\ \frac{d\omega}{dt} &= \tfrac{M}{JL_R}\left(i_{SB}\ \psi_{RA} - i_{SA}\ \psi_{RB}\right) \end{aligned} \tag{4.1}$$

where ψ_{RA} and ψ_{RB} are the total rotor flux linkages along phases A and B, i_{SA} and i_{SB} are the currents in the phase windings A and B, T_R is the rotor time constant, M is the mutual inductance between the stator and the rotor, ω is the mechanical speed of the rotor, J is the inertia of the rotor, and L_R is the rotor self-inductance. The model assumes that there is no load or friction torque.

The currents in the stator windings are assumed to be of the form

$$\begin{pmatrix} i_{SA} \\ i_{SB} \end{pmatrix} = I_m \begin{pmatrix} \cos(\omega_e t) \\ \sin(\omega_e t) \end{pmatrix} \tag{4.2}$$

where ω_e is the (angular) electrical frequency of the sinusoidal currents. The difference between the two frequencies, $S = \omega_e - \omega$, is an important quantity known as the *slip frequency*. The torque generated by the motor is a nonlinear function of the slip frequency, but is approximately linear for small slip. Thus, for small S, induction motor theory predicts that

$$\frac{d\omega}{dt} \simeq k(\omega_e - \omega) \tag{4.3}$$

for some constant k. Therefore, the rotor speed converges to the electrical frequency with the desirable dynamics of a first-order system. For large slip, the torque is reduced, but remains of the same sign, so that global convergence of ω to ω_e is ensured.

4.2.2 IMFE algorithm

Consider now the task of estimating the frequency ω_1^* of a sinusoidal signal

$$y(t) = m^* \cos(\alpha_1^*(t)) \tag{4.4}$$

where $\alpha_1^*(t) = \omega_1^* t$. The proposed method is to solve this problem by implementing an induction motor model with ω becoming the estimate ω_1 of ω_1^*. Thus, the algorithm will be given by

$$\begin{aligned} \dot{x}_{1F}(t) &= -a_1 x_{1F} + a_1 x_1 - \omega_1 x_{2F} \\ \dot{x}_{2F}(t) &= -a_1 x_{2F} + a_1 x_2 + \omega_1 x_{1F} \end{aligned} \tag{4.5}$$

and

$$\dot{\omega}_1 = g_\omega \left(x_2(t) x_{1F}(t) - x_1(t) x_{2F}(t) \right) \tag{4.6}$$

where a_1 and g_ω are positive constants. Note that x_1 can be defined as Mi_{SA} so that the two constants in (4.5) can be assumed to be equal.

The signal x_1 is simply

$$x_1(t) = y(t) \tag{4.7}$$

but a difficulty is that the signal x_2 associated with the second winding is not available. The situation has a parallel in induction machines operated on residential single-phase supplies. In such cases, single-phase induction motors are two-phase motors where the second winding is connected in series to a capacitor, and then in parallel with the first winding. The capacitor is selected so that the current in the second winding is approximately 90° out of phase with the first winding.

In the context of a numerical frequency estimator, the limitations of a physical implementation can be avoided, and other means of shifting the phase by 90° can be used. For example, a possible choice is the filter

$$H_1(s) = \frac{\omega_1 - s}{s + \omega_1} \tag{4.8}$$

which has a gain of 1 and a phase lead of 90° at the frequency ω_1. An approximation of the second winding current is the signal $x_2(t)$ defined through

$$x_2(t) = H_1(s) \left[x_1(t) \right] \tag{4.9}$$

where the notation $H_1(s)[\cdot]$ represents the time domain output of the system with transfer function $H_1(s)$. (4.9) can be implemented as

$$\begin{aligned} \dot{x}_3 &= -\omega_1 x_3 + \omega_1 x_1 \\ x_2 &= 2x_3 - x_1 \end{aligned} \tag{4.10}$$

The overall frequency estimator is defined by (4.5), (4.6), and (4.10). Note that the algorithm is quite different from other frequency estimation algorithms, such as [30], [41].

4.2.3 Stability analysis of the IMFE algorithm using averaging

The system can be fitted in the averaging theory for mixed time scales systems [43], where the frequency estimate (4.6) varies slowly, and the signals (4.7), (4.9), and (4.5) vary at a faster or mixed time scale. In finding the averaged system, the frequency estimate is held constant, and the responses of the fast variables are approximated by their steady-state responses. Then, the signals x_1 and x_3 become

$$\begin{aligned} x_1 &= m^* \cos(\alpha_1^*) \\ x_3 &= \tfrac{m^*}{\omega_1^2+\omega_1^{*2}} \left(\omega_1^2 \cos(\alpha_1^*) + \omega_1 \omega_1^* \sin(\alpha_1^*)\right) \end{aligned} \tag{4.11}$$

To find the steady-state values of the filtered signals (4.5), rewrite the equations as

$$\begin{aligned} x_{1F} &= H_2(s)[x_1] - H_3(s)[2x_3 - x_1] \\ x_{2F} &= H_2(s)[2x_3 - x_1] + H_3(s)[x_1] \end{aligned} \tag{4.12}$$

where

$$\begin{aligned} H_2(s) &= \tfrac{a_1(s+a_1)}{(s+a_1)^2+\omega_1^2} \\ H_3(s) &= \tfrac{a_1\omega_1}{(s+a_1)^2+\omega_1^2} \end{aligned} \tag{4.13}$$

Next, define the real and imaginary parts of the frequency responses of (4.8) and (4.13) with

$$\begin{aligned} H_1(j\omega_1^*) &= H_{R1} + jH_{I1} \\ H_2(j\omega_1^*) &= H_{R2} + jH_{I2} \\ H_3(j\omega_1^*) &= H_{R2} + jH_{I2} \end{aligned} \tag{4.14}$$

The steady-state values of (4.12) are then given by

$$\begin{aligned} x_{1F} &= m^* w_1^{*T}(t) \left(\begin{pmatrix} H_{R2} \\ H_{I2} \end{pmatrix} - \begin{pmatrix} H_{R3} & -H_{I3} \\ H_{I3} & H_{R3} \end{pmatrix} \right. \\ &\qquad \left. \times \begin{pmatrix} H_{R1} \\ H_{I1} \end{pmatrix} \right) \\ x_{2F} &= m^* w_1^{*T}(t) \left(\begin{pmatrix} H_{R2} & -H_{I2} \\ H_{I2} & H_{R2} \end{pmatrix} \begin{pmatrix} H_{R1} \\ H_{I1} \end{pmatrix} \right. \\ &\qquad \left. + \begin{pmatrix} H_{R3} \\ H_{I3} \end{pmatrix} \right) \end{aligned} \tag{4.15}$$

where

$$w_1^*(t) = \begin{pmatrix} \cos(\alpha_1^*(t)) \\ -\sin(\alpha_1^*(t)) \end{pmatrix} \tag{4.16}$$

Given the steady-state values, the right side of the frequency estimator equation (4.6) can be averaged with

$$\begin{aligned} AVE\left[x_2 x_{1F} - x_1 x_{2F}\right] &= \tfrac{m^{*2}}{2} \left(2H_{I1}H_{I2} - H_{R3} \right. \\ &\qquad \left. \times (H_{R1}^2 + H_{I1}^2 + 1)\right) \end{aligned} \tag{4.17}$$

Using (4.14), the averaged system is then given by

$$\dot{\omega}_1 = -g_\omega f_{av}(\omega_1) \tag{4.18}$$

with

$$\begin{aligned} f_{av}(\omega_1) &= \tfrac{m^{*2} a_1 \omega_1}{\left(\omega_1^2 + \omega_1^{*2}\right)} \tfrac{3\omega_1^{*2} + \omega_1^2 + a_1^2}{\left(\omega_1^2 - \omega_1^{*2} + a_1^2\right)^2 + \left(2a_1\omega_1^*\right)^2} \\ &\qquad \times (\omega_1^2 - \omega_1^{*2}) \end{aligned} \tag{4.19}$$

To assess the stability of (4.18), note that $f_{av}(\omega_1) = 0$ implies the existence of three real equilibrium points at $\omega_1 = 0$ and $\omega_1 = \pm\omega_1^*$. Evaluating $\partial f_{av}/\partial\omega_1$ at the equilibrium points gives

$$\begin{aligned} \left.\frac{\partial f_{av}}{\partial \omega_1}\right|_{\omega_1=0} &= g_\omega m^{*2} \frac{a_1\left(3\omega_1^{*2}+a_1^2\right)}{\left(\omega_1^{*2}+a_1^2\right)^2} \\ \left.\frac{\partial f_{av}}{\partial \omega_1}\right|_{\omega_1=\pm\omega_1^*} &= -g_\omega m^{*2} \frac{1}{a_1} \end{aligned} \tag{4.20}$$

indicating that the equilibrium point $\omega_1 = 0$ is repulsive, while $\omega_1 = \pm\omega_1^*$ are both attractive. Thus, with a positive initial estimate $\omega_1(0)$, ω_1 will converge to ω_1^*. As $\omega_1 \to \omega_1^*$ (4.18) becomes, approximately

$$\dot{\omega}_1 \simeq -\frac{g_\omega m^{*2}}{2a_1}\left(\omega_1 - \omega_1^*\right) \tag{4.21}$$

so that convergence is exponential in the vicinity of ω_1^*. In Fig. 4.1, a typical plot of the right side of (4.18) is shown. The linear convergence around ω_1^* is comparable to the linear convergence of the induction motor for small slip. The quadrature filter (4.8) is the source of the two additional equilibrium points, which are not useful, but do not cause any problem either.

4.2.4 Discrete-time implementation

The implementation of the estimator on a microprocessor requires the derivation of a set of difference equations that can be used to recursively update the system states. It was found that direct implementation of the algorithm using an Euler approximation resulted in a bias of the frequency estimate. Thus, an equivalent discrete-time algorithm was derived that did not suffer from this problem. The input of the estimator is the discrete-time signal

$$x_1(k) = y(k) \tag{4.22}$$

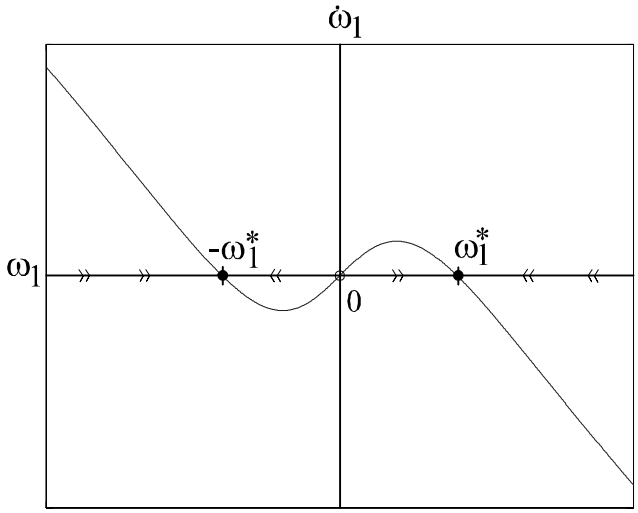

Figure 4.1. Phase plot of (4.18).

Let $\Omega_1(k)$ be the estimate of the discrete-time frequency $\Omega_1^* = \omega_1^* T_S$, where T_S is the sampling period. Define the auxiliary signal

$$r(k) = \cos(\Omega_1(k)) / \left(1 + \sin(\Omega_1(k))\right) \tag{4.23}$$

The discrete-time algorithm is given by

$$\begin{aligned} x_3(k) &= r(k)x_3(k-1) + x_1(k-1) \\ x_{1F}(k+1) &= a_{d1}x_{1F}(k) + (1-a_{d1})\, x_1(k) \\ &\quad - \sin\left(\Omega_1(k)\right) x_{2F}(k) \\ x_{2F}(k+1) &= a_{d1}x_{2F}(k) + (1-a_{d1})\, x_2(k) \\ &\quad + \sin\left(\Omega_1(k)\right) x_{1F}(k) \end{aligned} \tag{4.24}$$

where $a_{d1} = 1 - a_1 T_S$ and

$$x_2(k) = \left(1 - r(k)^2\right) x_3(k) - r(k)x_1(k) \tag{4.25}$$

The frequency update is given by

$$\Omega_1(k+1) = \Omega_1(k) + g_d f_d \tag{4.26}$$

with

$$\begin{aligned} f_d &= x_2(k)x_{1F}(k+1) - x_1(k)x_{2F}(k+1) \\ g_d &= g_\omega T_S^2 \end{aligned} \tag{4.27}$$

4.3 Application of the IMFE Algorithm in Sinusoidal Disturbance Cancellation

4.3.1 Gradient-based disturbance cancellation

The IMFE can be combined with a gradient-based disturbance cancellation algorithm to reject sinusoidal disturbances of unknown frequency. The system under consideration is shown in Fig. 4.2, where $d(t)$ is an unknown sinusoidal disturbance and the output of the plant is given by

$$y(t) = P(s)\left[u(t) + d(t)\right] \tag{4.28}$$

The goal is to find an appropriate $u(t)$ such that $y(t)$ is minimized. Expressing the disturbance in terms of its sin and cos components gives

$$d(t) = w_1^{*T}(t)\pi, \quad \pi = \begin{pmatrix} d_c \\ d_s \end{pmatrix} \tag{4.29}$$

d_c and d_s are unknown parameters. w_1^* is given by (4.16) where $\alpha_1^*(t) = \omega_1^* t$ and ω_1^* is the frequency of the disturbance. The control signal is chosen to be

$$u(t) = w_1^T(t)\theta, \quad \theta = \begin{pmatrix} \theta_c \\ \theta_s \end{pmatrix} \tag{4.30}$$

where

$$w_1(t) = \begin{pmatrix} \cos(\alpha_1(t)) \\ -\sin(\alpha_1(t)) \end{pmatrix} \tag{4.31}$$

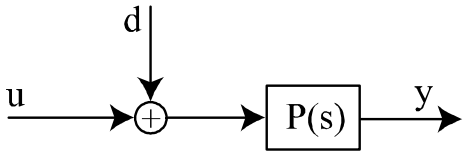

Figure 4.2. Diagram of the disturbance rejection problem.

and the phase

$$\alpha_1(t) = \int_0^t \omega_1 d\tau \tag{4.32}$$

where ω_1 is an estimate of the frequency of the disturbance.

The so-called inverse-G algorithm [50] is a gradient-based algorithm that updates θ using

$$\dot{\theta}(t) = -gG^T w_1(t) y(t). \tag{4.33}$$

where $g > 0$ is an adaptation gain,

$$G = \begin{pmatrix} P_R & -P_I \\ P_I & P_R \end{pmatrix} \tag{4.34}$$

and P_R, P_I are the real and imaginary parts of the frequency response at the estimated frequency, *i.e.*, $P(j\omega_1) = P_R + jP_I$.

The disturbance cancellation algorithm can be combined with the IMFE algorithm by using the frequency estimate ω_1 of the IMFE in the reconstruction of the angle α_1. One difficulty is that the control signal produces an output that interferes with the frequency estimator. The problem can be avoided by using in the IMFE a modified signal

$$x_1 = y(t) - P(s)[u(t)] = P(s)[d(t)] \tag{4.35}$$

so that the signal used by the IMFE is the same as if the control input was zero. Alternatively, the signal x_1 can be replaced by the simpler expression

$$x_1 = y(t) - w_1^T G\theta \tag{4.36}$$

which corresponds to a steady-state approximation with slowly varying parameter θ. The implementation is especially useful in cases where the plant is difficult to model with a finite-order transfer function (due to delays, resonances,...). A frequency response can often be obtained accurately in practice, even when a good finite-order fit cannot be obtained. Fig. 4.3 shows a diagram of the overall closed-loop system (with $y_u = w_1^T \hat{G}\theta$ and $\hat{G}$ is an estimate of G).

4.3.2 Averaging analysis of the overall adaptive system

The states of the closed-loop system can be divided into two sets, a set of slow variables and a set of fast variables. Assuming that the adaptive gains g and g_ω are small, the slow variables are the control parameter vector and the frequency estimate, described by

$$\begin{aligned} \dot{\theta} &= -gG^T w_1 y \\ \dot{\omega}_1 &= g_\omega \left(x_2 x_{1F} - x_1 x_{2F} \right) \end{aligned} \tag{4.37}$$

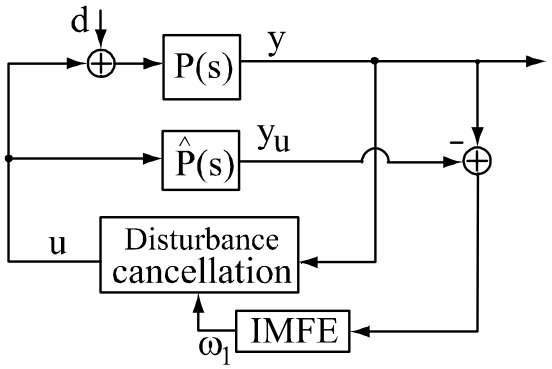

Figure 4.3. Diagram of indirect disturbance cancelation with IMFE frequency estimation.

With x_P denoting the internal states of $P(s)$, the fast variables consist of the plant states

$$\begin{aligned} \dot{x}_P &= Ax_P + B\left(w_1^{*T}\pi - w_1^T\theta\right) \\ y &= Cx_P \end{aligned} \tag{4.38}$$

as well as the IMFE dynamics

$$\begin{aligned} \dot{x}_3 &= -\omega_1 x_3 + \omega_1 x_1 \\ \dot{x}_{1F} &= -a_1 x_{1F} + a x_1 - \omega_1 x_{2F} \\ \dot{x}_{2F} &= -a_1 x_{2F} + a x_2 + \omega_1 x_{1F} \\ x_1 &= y - w_1^T G\theta \\ x_2 &= 2x_3 - x_1 \end{aligned} \tag{4.39}$$

Using the technique of [13], the angle α_1 can also be treated as a slow variable.

In finding the averaged system corresponding to (4.37)-(4.39), the responses of the fast variables are taken as the steady-state responses, and the dynamics of the slow variables are averaged over time. Thus, the frequency estimate and the control vector θ are assumed to be constant in calculating the responses of the fast variables. The averaged system for the IMFE is the same as was derived in Sec. 4.2.3 because, in steady-state

$$x_1 = y_{ss} + P(s)[d(t)] - w_1^T G\theta = P(s)[d(t)] \tag{4.40}$$

The stability result from Sec. 4.2.3 applies: for g_ω sufficiently small, the frequency estimate ω_1 converges to the disturbance frequency ω_1^*. Close to the disturbance frequency, convergence is exponential.

For the disturbance cancellation component, the steady-state output of the plant can be written

$$y_{ss} = w_1^T G\left(\theta - \theta^*\right) \tag{4.41}$$

where

$$\theta^* = -G^{-1} \begin{pmatrix} \cos(\tilde{\alpha}) & \sin(\tilde{\alpha}) \\ -\sin(\tilde{\alpha}) & \cos(\tilde{\alpha}) \end{pmatrix} G^* \pi \tag{4.42}$$

and $\tilde{\alpha} = \alpha_1 - \alpha_1^*$. As in Sec 2.2.2, the matrix

$$G^* = \begin{pmatrix} P_R^* & -P_I^* \\ P_I^* & P_R^* \end{pmatrix} \tag{4.43}$$

is a matrix whose elements correspond to the frequency response of $P(s)$ at the disturbance frequency ω_1^*. The averaged dynamics of the control parameter update are given by

$$\dot{\theta}(t) = -gG^T G(\theta - \theta^*) \tag{4.44}$$

For $\omega_1 = \omega_1^*$, the control signal converges to

$$u(t) = -w_1^{*T} \pi \tag{4.45}$$

Thus, as the frequency error $\omega_1 \rightarrow \omega_1^*$, θ converges exponentially to a value θ^*such that the disturbance is exactly canceled. Note that the equilibrium θ^* is not unique, as it depends on the phase associated with the integration of the frequency estimate. However, this nonuniqueness simply produces a rotation of the control vector without the dangers normally associated with nonuniqueness and parameter drift.

4.3.3 Experimental results

The performance of the inverse-G/IMFE algorithm was examined through single-channel active noise control experiments. (4.37) was discretized using the Euler approximation so that

$$\theta(k) = \theta(k-1) - g_\theta G^T w_1(k-1) y(k). \tag{4.46}$$

where $g_\theta = gT_S$, and the IMFE was discretized as described in Sec. 4.2.4. The algorithm was coded in C and implemented in a dSPACE DS1104 digital signal processing board. A sampling frequency of 8 kHz was used. A constant amplitude sinusoidal disturbance with frequency of 160 Hz was generated by a loudspeaker, while the control signal was produced by another loudspeaker. A microphone was used to measure the cancellation error. The plant consists of the hardware and transmission in the environment from the control signal output to the error microphone input, including the propagation effects of the surrounding air. The experiments were conducted in a small room where many signal reflections were present. In all experiments, the following parameters were used: $a_{d1} = 0.6875$, $g_d = 31.25 \times 10^{-6}$, $g_\theta = 0.001875$.

In the first experiment, the initial IMFE frequency was $f_1(0) = 130$ Hz for an initial frequency error of 50 Hz. After 2 seconds, the inverse-G and the IMFE were engaged simultaneously, and the algorithm was allowed to reach steady-state. After approximately 3.5 seconds, the frequency of the disturbance was increased by an additional 50 Hz. Fig. 4.4 shows the frequency estimate and Fig. 4.5 shows the measured output y. The figures show that the algorithm is able to adjust for the change in frequency while maintaining significant rejection of the disturbance. The components of the control vector θ are shown in Fig. 4.6.

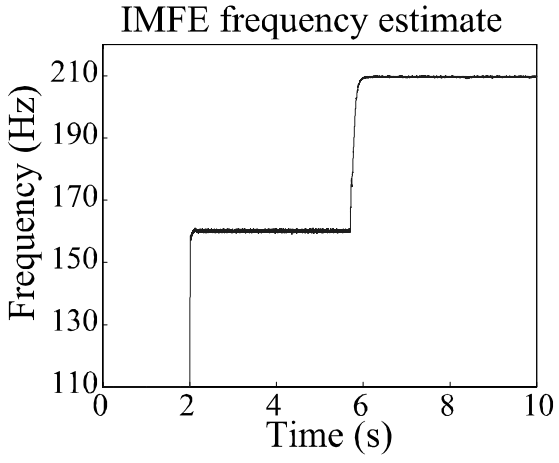

Figure 4.4. IMFE frequency estimate.

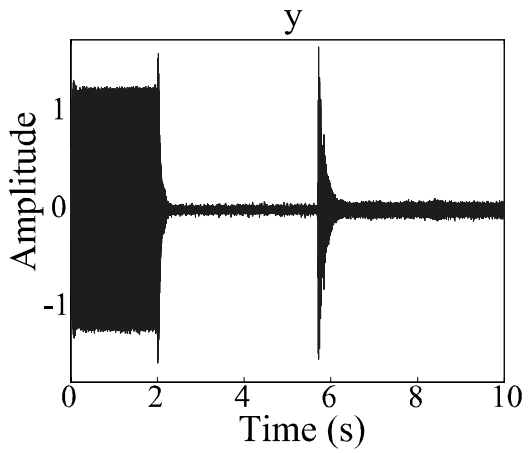

Figure 4.5. Measured output with inverse-G disturbance cancelation and IMFE frequency estimation.

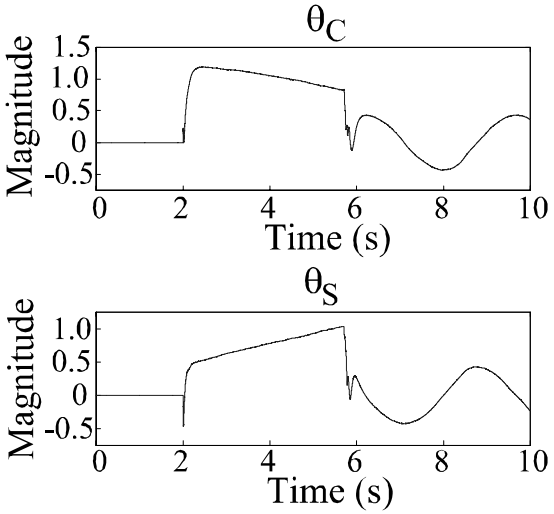

Figure 4.6. θ with IMFE frequency estimation.

In the second experiment, the IMFE frequency estimator track a slowly varying disturbance frequency. After 2 seconds, the inverse-G and the IMFE were engaged simultaneously, and the algorithm was allowed to reach steady-state. Approximately 3 seconds later, the frequency of the disturbance was increased at a rate of 15 Hz per 10 seconds. In Fig. 4.7, the ability of the algorithm to track a slowly varying frequency is shown, and in Fig. 4.8, significant attenuation of the disturbance is seen despite the changing frequency. The components of the control vector θ are shown in Fig. 4.9.

In the next experiment, results using the inverse-G disturbance cancellation algorithm and a MPLL frequency estimator are shown for comparison (implementing the algorithm of [13]). The initial frequency estimate was set at $f_1(0) = 150\ Hz$, closer to the true value to insure convergence of the MPLL algorithm. After 2 seconds, the algorithm was engaged, resulting in significant attenuation of the disturbance. After an additional 4 seconds, the frequency of the disturbance was increased by 50 Hz. Fig. 4.10 shows the MPLL frequency. The MPLL frequency estimator was not able to compensate for the change in frequency. Fig. 4.11 shows the measured output y, which exhibits good reduction under tracking conditions, but large errors otherwise.

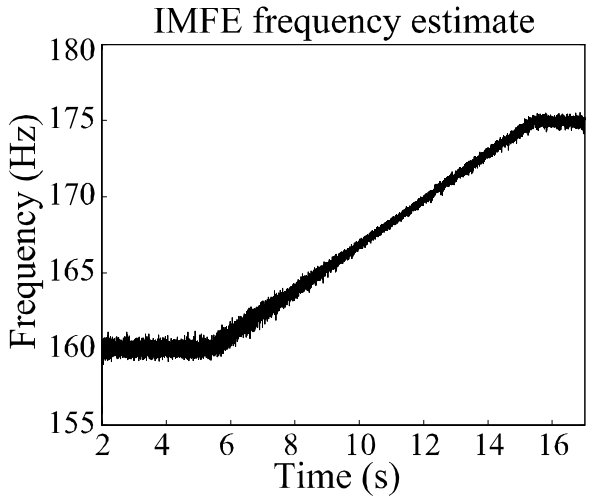

Figure 4.7. IMFE frequency estimate tracking changes in the disturbance frequency.

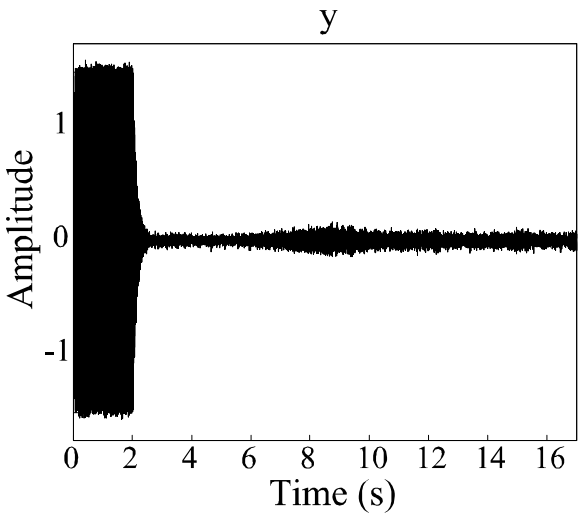

Figure 4.8. Measured output with inverse-G disturbance cancelation and IMFE frequency tracking.

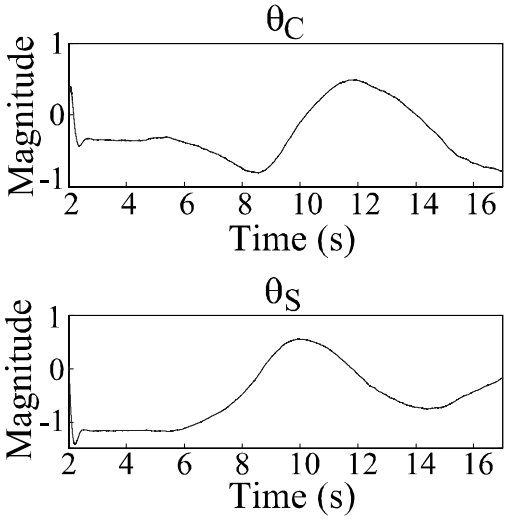

Figure 4.9. θ with IMFE frequency tracking.

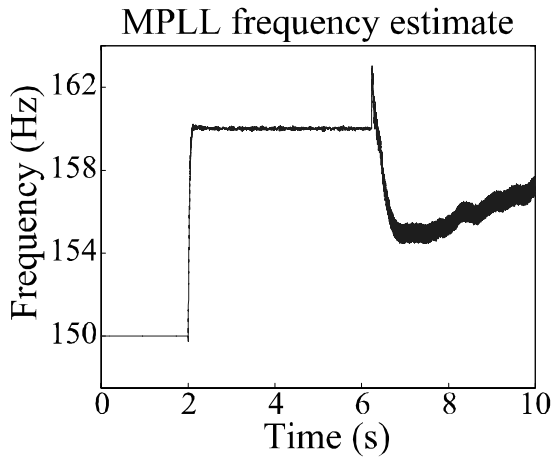

Figure 4.10. MPLL frequency estimate.

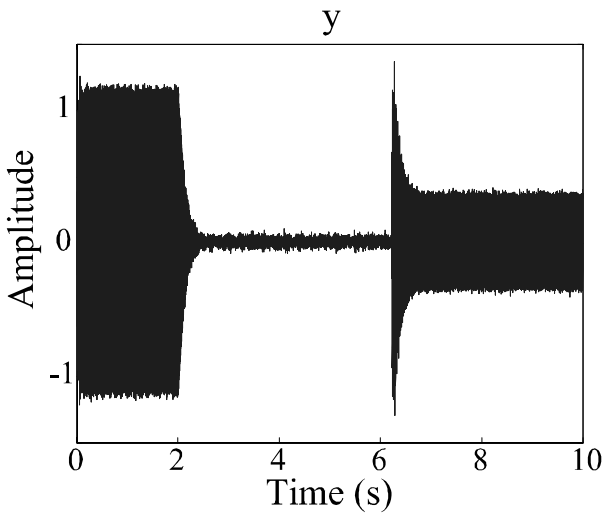

Figure 4.11. Measured output with inverse-G disturbance cancelation and MPLL frequency estimation.

4.4 Modified IMFE

4.4.1 Changes to the model

An alternative frequency estimator is possible by relaxing the present analogy and departing slightly from the equations of the induction motor. Neglecting the coupling between the phases of the rotor, the model equations (4.1) become

$$\begin{aligned} \frac{d\psi_{RA}}{dt} &= -\tfrac{1}{T_R}\psi_{RA} + \tfrac{M}{T_R} i_{SA} \\ \frac{d\psi_{RB}}{dt} &= -\tfrac{1}{T_R}\psi_{RB} + \tfrac{M}{T_R} i_{SB} \\ \frac{d\omega}{dt} &= \tfrac{M}{JL_R}\left(i_{SB}\ \psi_{RA} - i_{SA}\ \psi_{RB}\right) \end{aligned} \tag{4.47}$$

(4.47) describes a theoretical motor that generates no torque and whose slip frequency S is always zero. A reliable frequency estimate can be designed to mimic this behavior.

4.4.2 Frequency estimation equations

In Sec. 4.2.2, signals corresponding to the stator currents were constructed using a special filter to shift the input signal by 90°. Here, a different technique is used. Define the vector

$$\begin{pmatrix} x_C(t) \\ x_S(t) \end{pmatrix} = 2 \begin{pmatrix} \cos(\alpha_1(t)) \\ \sin(\alpha_1(t)) \end{pmatrix} y(t) \tag{4.48}$$

where

$$\alpha_1(t) = \int_0^t \omega_1 d\tau \tag{4.49}$$

with ω_1 an estimate of unknown frequency ω_1^*.(4.48) contains components at two different frequencies. One component varies at the difference between the actual and assumed frequencies, and the second higher frequency component varies at the sum of the actual and assumed frequencies. The high frequency component of (4.48) must be eliminated through filtering. Consider the SISO first-order system

$$H_4(s) = \frac{a_2}{s + a_2} \tag{4.50}$$

with pole $a_2 > 0$, whose output is given by

$$\begin{pmatrix} x_1(t) \\ x_2(t) \end{pmatrix} = H_4(s) \left[\begin{pmatrix} x_C(t) \\ x_S(t) \end{pmatrix} \right] \tag{4.51}$$

The notation $H_4(s)[\cdot]$ represents the time domain output of the system with transfer function $H_4(s)$ applied to the elements of (4.48) separately. $H_4(s)$ acts as a lowpass filter needed to remove the high frequency components from (4.48).

Next, consider the system

$$H_5(s) = \frac{a_3}{s + a_3} \tag{4.52}$$

with pole $a_3 > 0$, whose output is given by

$$\begin{pmatrix} x_{1F}(t) \\ x_{2F}(t) \end{pmatrix} = H_5(s) \left[\begin{pmatrix} x_1(t) \\ x_2(t) \end{pmatrix} \right] \tag{4.53}$$

The IMFE frequency estimate is updated using

$$\dot{\omega}_1 = g'_\omega \left(x_2(t) x_{1F}(t) - x_1(t) x_{2F}(t) \right) \tag{4.54}$$

where g'_ω is a positive constant. The time domain signals of the modified IMFE are diagramed in Fig. 4.12.

4.4.3 Stability analysis of the modified IMFE using averaging

The system fits the averaging theory for mixed time scales systems, where the frequency update (4.54) varies slowly, and the vectors of signals (4.51) and (4.53) vary more quickly. In finding the averaged system, the frequency estimate is held constant, and the response of the fast variables are approximated by their corresponding steady-state response. Using the steady-state responses, the dynamics of the frequency estimate are averaged over time.

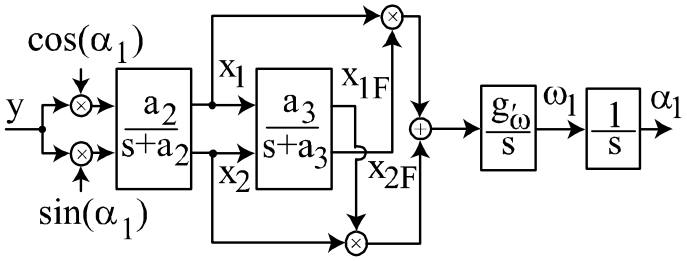

Figure 4.12. Diagram of the IMFE estimator.

Write (4.48) as

$$\begin{pmatrix} x_C(t) \\ x_S(t) \end{pmatrix} = m^* \begin{pmatrix} \cos(\alpha_1 - \alpha_1^*) + \cos(\alpha_1 + \alpha_1^*) \\ \sin(\alpha_1 - \alpha_1^*) + \sin(\alpha_1 + \alpha_1^*) \end{pmatrix} \tag{4.55}$$

whose components vary at the frequencies $\omega_1 - \omega_1^*$ and $\omega_1 + \omega_1^*$. Due to the lowpass nature of $H_4(s)$, the high frequency components can be neglected so that at steady-state the vector (4.51) is given by

$$\begin{pmatrix} x_1 \\ x_2 \end{pmatrix} = m^* \begin{pmatrix} H_{4R} & H_{4I} \\ -H_{4I} & H_{4R} \end{pmatrix} \begin{pmatrix} \cos(\tilde{\alpha}) \\ \sin(\tilde{\alpha}) \end{pmatrix} \tag{4.56}$$

where

$$\begin{aligned} H_4(j\,(\omega_1 - \omega_1^*)) &= H_{4R} + jH_{4I} \\ &= \tfrac{a_2^2 - ja_2\left(\omega_1 - \omega_1^*\right))}{\left(\omega_1 - \omega_1^*\right)^2 + a_2^2} \end{aligned} \tag{4.57}$$

The filtered signals are given by

$$\begin{pmatrix} x_{1F} \\ x_{2F} \end{pmatrix} = m^* \begin{pmatrix} H_{5R} & H_{5I} \\ -H_{5I} & H_{5R} \end{pmatrix} \begin{pmatrix} H_{4R} & H_{4I} \\ -H_{4I} & H_{4R} \end{pmatrix} \begin{pmatrix} \cos(\tilde{\alpha}) \\ \sin(\tilde{\alpha}) \end{pmatrix} \tag{4.58}$$

where

$$\begin{aligned} H_5(j\,(\omega_1 - \omega_1^*)) &= H_{5R} + jH_{5I} \\ &= \tfrac{a_3^2 - ja_3\left(\omega_1 - \omega_1^*\right)}{\left(\omega_1 - \omega_1^*\right)^2 + a_3^2} \end{aligned} \tag{4.59}$$

Applying the averaging operator

$$AVE\left[x_2 x_{1F} - x_1 x_{2F}\right] = m^{*2}\left(H_{4R}^2 + H_{4I}^2\right) H_{5I} \tag{4.60}$$

The averaged system corresponding to (4.54) can now be written as

$$\dot{\omega}_1 = -\frac{g'_\omega a_2^2 a_3 m^{*2}}{\left(\left(\omega_1 - \omega_1^*\right)^2 + a_2^2\right)\left(\left(\omega_1 - \omega_1^*\right)^2 + a_3^2\right)}\left(\omega_1 - \omega_1^*\right) \tag{4.61}$$

To access stability of the modified IMFE, consider the Lyapunov candidate

$$v = \tilde{\omega}^2 \tag{4.62}$$

where $\tilde{\omega} = \omega_1 - \omega_1^*$. In terms of this frequency error, the first derivative with respect to time evaluated along the trajectories of (4.61) is given by

$$\frac{dv}{dt} = -\frac{2g'_\omega a_2^2 a_3 m^{*2}}{\left(\tilde{\omega}^2 + a_2^2\right)\left(\tilde{\omega}^2 + a_3^2\right)}\tilde{\omega}^2 \leq 0 \tag{4.63}$$

For finite $\tilde{\omega}$, (4.63) indicates that $\omega_1 = \omega_1^*$ is a stable equilibrium point of (4.61). As $\omega_1 \to \omega_1^*$, (4.63) becomes approximately

$$\frac{dv}{dt} \simeq -\frac{2g'_\omega m^{*2}}{a_3}\tilde{\omega}^2 \leq 0 \tag{4.64}$$

so that convergence is exponential. In Fig. 4.13, a plot of the right side of (4.61) using the error $\tilde{\omega} = \omega_1 - \omega_1^*$ as $\tilde{\omega}$ is varied in the range $\tilde{\omega} \in [-500, 500]$ is shown. The plot confirms the analysis. Implicit in the analysis is the assumption of a positive initial frequency estimate. This assumption is a result of the form of (4.55) and is hidden in the assumption that the $\omega_1 + \omega_1^*$ components are high frequency and can be neglected at the output of $H_4(s)$.

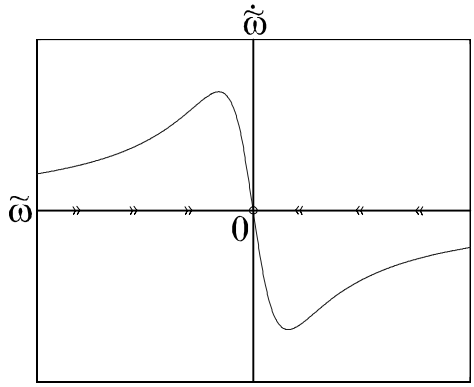

Figure 4.13. Phase plot of (4.61).

4.4.4 Modified IMFE with a constant control signal

Let

$$y(t) = u(t) + p(t) \tag{4.65}$$

The input to the IMFE consists of a sinusoidal disturbance

$$p(t) = m^* \cos(\alpha_1^*) \tag{4.66}$$

at the frequency ω_1^* as well as the constant control signal

$$u(t) = -m \cos(\alpha_1) \tag{4.67}$$

at the IMFE frequency ω_1. It is desirable to estimate the frequency of the disturbance despite the presence of the control signal. At steady-state, (4.48) becomes

$$\begin{pmatrix} x_C \\ x_S \end{pmatrix} = m^* \begin{pmatrix} \cos(\alpha_1 - \alpha_1^*) + \cos(\alpha_1 + \alpha_1^*) \\ \sin(\alpha_1 - \alpha_1^*) + \sin(\alpha_1 + \alpha_1^*) \end{pmatrix} - \begin{pmatrix} m \\ 0 \end{pmatrix} \tag{4.68}$$

The filtered signals are given by

$$\begin{aligned}\begin{pmatrix} x_1 \\ x_2 \end{pmatrix} &= m^* \begin{pmatrix} H_{4R} & H_{4I} \\ -H_{4I} & H_{4R} \end{pmatrix} \begin{pmatrix} \cos(\tilde{\alpha}) \\ \sin(\tilde{\alpha}) \end{pmatrix} - \begin{pmatrix} m \\ 0 \end{pmatrix} \\ \begin{pmatrix} x_{1F} \\ x_{2F} \end{pmatrix} &= m^* \begin{pmatrix} H_{5R} & H_{5I} \\ -H_{5I} & H_{5R} \end{pmatrix} \begin{pmatrix} H_{4R} & H_{4I} \\ -H_{4I} & H_{4R} \end{pmatrix} \begin{pmatrix} \cos(\tilde{\alpha}) \\ \sin(\tilde{\alpha}) \end{pmatrix} \\ &\qquad - \begin{pmatrix} m \\ 0 \end{pmatrix}\end{aligned} \tag{4.69}$$

where $\tilde{\alpha} = \alpha_1 - \alpha_1^*$. Now,

$$AVE\left[x_2 x_{1F} - x_1 x_{2F}\right] = -\frac{g'_\omega a_2^2 a_3 m^{*2}}{\left(\tilde{\omega}^2 + a_2^2\right)\left(\tilde{\omega}^2 + a_3^2\right)}\tilde{\omega} \tag{4.70}$$

As long as the control signal varies at the same frequency as the internally generated sinusoids of the vector (4.48), it is rejected by the estimator, and it is as though the input to the estimator consists solely of the disturbance.

4.4.5 Discrete-time implementation

Define the vector

$$\begin{pmatrix} x_C(k) \\ x_S(k) \end{pmatrix} = 2 \begin{pmatrix} \cos(\alpha_1(k)) \\ \sin(\alpha_1(k)) \end{pmatrix} y(k) \tag{4.71}$$

where

$$\alpha_1(k) = \sum_{n=0}^{k} \Omega_1(n) \tag{4.72}$$

with Ω_1 an estimate of the discrete frequency $\Omega_1^* = \omega_1^* T_S$. T_S is an appropriate sampling period. Implementation in discrete-time first requires defining the equivalent discrete-time systems

$$\begin{aligned} H_4(z) &= \tfrac{1-z_{d2}}{z-z_{d2}} \\ H_5(z) &= \tfrac{1-z_{d3}}{z-z_{d3}} \end{aligned} \tag{4.73}$$

where $z_{d2} = 1 - a_2 T_S$ and $z_{d3} = 1 - a_3 T_S$. The modified IMFE estimator is then implemented with the following equations

$$\begin{aligned} x_1(k) &= z_{d2} x_1(k-1) + (1 - z_{d2})\, x_C(k) \\ x_2(k) &= z_{d2} x_2(k-1) + (1 - z_{d2})\, x_S(k) \\ x_{1F}(k+1) &= z_{d3} x_{1F}(k) + (1 - z_{d3})\, x_1(k) \\ x_{2F}(k+1) &= z_{d3} x_{2F}(k) + (1 - z_{d3})\, x_2(k) \\ \Omega_1(k+1) &= \Omega_1(k) + g_d \left(x_2(k) x_{1F}(k+1) - x_1(k) x_{2F}(k+1)\right) \\ \alpha_{d1}(k+1) &= \alpha_{d1}(k) + \Omega_1(k+1) \end{aligned} \tag{4.74}$$

where

$$g_d = g'_\omega T_S^2 \tag{4.75}$$

4.5 Combined MPLL/IMFE Algorithm

Stability of the MPLL requires that the frequency estimate ω_1 is sufficiently close to the true frequency ω_1^*. However, the dynamics of the IMFE can be combined with the MPLL dynamics to extend the range of ω_1 for which convergence is observed. The frequency estimate of interest becomes the sum of the MPLL estimate and the IMFE estimate. To do this, add the dynamics of the IMFE frequency update and the MPLL frequency update. Also, set the IMFE phase equal to the MPLL phase. This leads to the equations

$$\begin{aligned} \dot{m} &= 2 g_m e_C \\ \dot{\omega}_1 &= -g_\omega e_S + g'_\omega \left(x_2 x_{1F} - x_1 x_{2F}\right) \\ \dot{\alpha}_1 &= \omega_1 + k \dot{\omega}_1 \end{aligned} \tag{4.76}$$

with the positive constants g_m, g'_ω, g_ω, k. (4.76) represent the slow dynamics of the system. The fast variables consist of the plant and the disturbance as described by the IMFE signals

$$\begin{aligned} \dot{x}_1 &= -a_2 x_1 + a_2 e_C \\ \dot{x}_2 &= -a_2 x_2 + a_2 e_S \\ \dot{x}_{1F} &= -a_3 x_{1F} + a_3 x_1 \\ \dot{x}_{2F} &= -a_3 x_{2F} + a_3 x_2 \end{aligned} \tag{4.77}$$

and the positive constants a_2, a_3. With the vectors

$$\begin{pmatrix} e_C \\ e_S \end{pmatrix} = 2 \begin{pmatrix} \cos(\alpha_1) \\ \sin(\alpha_1) \end{pmatrix} (y - m\cos(\alpha_1)) \tag{4.78}$$

(4.76)-(4.77) completely describe the states of the closed-loop system.

The structure of the algorithm is diagramed in Fig. 4.14. It is seen that combining the two components of the algorithm in this way is equivalent to using the IMFE estimate to bias the MPLL frequency estimate. In the next section, it is shown that doing by so, the IMFE dynamics significantly improve stability of the MPLL.

4.5.1 Averaged system for the combined algorithm

In this section, averaging is used to explore the effect of the IMFE on stability of the MPLL. The closed-loop system fits into the averaging theory for a mixed time scale system. The averaged system is found by approximating the response of the fast variables by the steady-state response, and averaging the dynamics of the slow variables over time. Defining the frequency error

$$\delta\omega_1 = \omega_1 - \omega_1^* \tag{4.79}$$

leads to the phase error

$$\delta\alpha_1 = \alpha_1 - \alpha_1^* \tag{4.80}$$

The control signal $u(t)$, which also changes with the phase α_1, is rejected by the IMFE giving the averaged IMFE dynamics as

$$AVE\left[x_2 x_{1F} - x_1 x_{2F}\right] = -\frac{a_2^2 a_3 m^{*2}}{\left(\delta\omega_1^2 + a_2^2\right)\left(\delta\omega_1^2 + a_3^2\right)} \delta\omega_1 \tag{4.81}$$

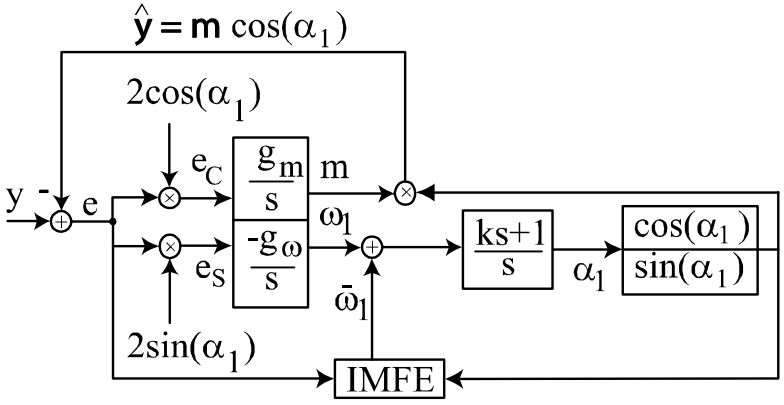

Figure 4.14. Diagram of improved MPLL algorithm.

Since the disturbance acts at the input of a plant, the magnitude of the frequency response of $P(s)$ shows up in the averaged dynamics. Recalling (3.11) allows the overall averaged system to be written

$$\begin{aligned} \dot{m} &= g_m \left(m^* \cos(\delta\alpha_1) - m\right) \\ \delta\dot{\omega}_1 &= -\tfrac{g'_\omega a_2^2 a_3 m^{*2}}{\left(\delta\omega_1^2+a_2^2\right)\left(\delta\omega_1^2+a_3^2\right)}\delta\omega_1 - g_\omega m^* \sin(\delta\alpha_1) \\ \delta\dot{\alpha}_1 &= \delta\omega_1 + k\left(\delta\dot{\omega}_1\right) \end{aligned} \tag{4.82}$$

The averaged system has an equilibrium given by

$$\begin{aligned} m &= m^* \\ \delta\omega_1 &= 0 \\ \delta\alpha_1 &= 0 \end{aligned} \tag{4.83}$$

Linearizing (4.82) around (4.83), the system's Jacobian is

$$J = \begin{pmatrix} -g_m & 0 & 0 \\ 0 & -\frac{g'_\omega m^{*2}}{a_3} & -g_\omega m^* \\ 0 & 1 - \frac{k g'_\omega m^{*2}}{a_3} & -k g_\omega m^* \end{pmatrix} \tag{4.84}$$

with corresponding characteristic polynomial

$$\det(sI - J) = (s + g_m)\left(s^2 + \left(\frac{g'_\omega m^{*2}}{a_3} + k g_\omega m^*\right) s + g_\omega m^*\right) \tag{4.85}$$

Again, the linearized system is found to be the combination of two linear time-invariant systems. As opposed to the roots of (3.13), now the poles are given by the roots of

$$\begin{aligned} s + g_m &= 0 \\ s^2 + \left(\frac{g'_\omega m^{*2}}{a_3} + k g_\omega m^*\right) s + g_\omega m^* &= 0 \end{aligned} \tag{4.86}$$

The system continues to be stable for all positive values of the design parameters g'_ω, g_ω, g_m, k. However, the combination of the MPLL with the simple dynamics of the IMFE frequency estimate has increased the damping coefficient of the frequency loop. From [49], it is known that this means the combined MPLL/IMFE can tolerate larger initial frequency estimation errors than can the MPLL by itself.

4.5.2 Discrete-time implementation

To implement the combined MPLL/IMFE algorithm in the discrete time, the discrete MPLL implementation of [13] is used in conjunction with the discrete modified IMFE implementation described in Sec. 4.4.5. The discrete time equations are given as

$$\begin{aligned} x_1(k) &= z_{d2} x_1(k-1) + (1 - z_{d2})\, e_C(k) \\ x_2(k) &= z_{d2} x_2(k-1) + (1 - z_{d2})\, e_S(k) \\ x_{1F}(k+1) &= z_{d3} x_{1F}(k) + (1 - z_{d3})\, x_1(k) \\ x_{2F}(k+1) &= z_{d3} x_{2F}(k) + (1 - z_{d3})\, x_2(k) \\ m(k+1) &= m(k) + g_{md} e_C(k) \\ \Omega_1(k+1) &= \Omega_1(k) - g_{\omega d} e_S(k) \\ &\quad + g_d \left(x_2(k) x_{1F}(k+1) - x_1(k) x_{2F}(k+1)\right) \\ \alpha_{d1}(k+1) &= \alpha_{d1}(k) + k_\alpha \left(\Omega_1(k+1) - z_\alpha \Omega_1(k)\right) \end{aligned} \tag{4.87}$$

with the vectors

$$\begin{pmatrix} e_C(k) \\ e_S(k) \end{pmatrix} = 2 \begin{pmatrix} \cos(\alpha_1(k)) \\ \sin(\alpha_1(k)) \end{pmatrix} (y(k) - m(k)\cos(\alpha_1(k))) \tag{4.88}$$

and the positive constants g_d, k_α, z_α, $g_{md} = T_S^2 g_m$, and $g_{\omega d} = T_S^2 g_\omega$. A tuning procedure for g_{md}, $g_{\omega d}$, k_α, and z_α can be found in [13].

4.5.3 Simulation example

To demonstrate the advantage of biasing the MPLL frequency loop with the IMFE estimate, the results of a simulation are presented. A sampling period of $T_S = 0.000125s$ was used, and the frequency of the input was taken as $f_1^* = 160\ Hz$. The following parameter values were used

$$\begin{aligned} g_{\omega d} &= 4.0 \times 10^{-4} \\ g_{md} &= 0.0075 \\ k_\alpha &= 267 \\ z_\alpha &= 1 - \tfrac{1}{k_\alpha} \\ z_{d2} &= 0.99 \\ z_{d3} &= 0.7 \\ g_d &= 0.125 \end{aligned} \tag{4.89}$$

In the first simulation, the MPLL estimator was used without the aide of the modified IMFE. The initial frequency estimate was chosen as $f_1(0) = 100\ Hz$. The MPLL magnitude, frequency, and phase estimates can be seen in Fig. 4.15. For an initial frequency error of 60 Hz, the frequency estimate is seen to take a full 1.5 seconds to converge to the true value. In the second simulation, the combined MPLL/IMFE was used. The initial MPLL and IMFE frequency estimates was set at $f_1(0) = 0$ and $\bar{f}(0) = 100\ Hz$, respectively, so that the initial frequency error is again 60 Hz. The results can be seen in Fig. 4.16. The combined frequency estimate is seen to converge to the true value in substantially less than 0.5 seconds.

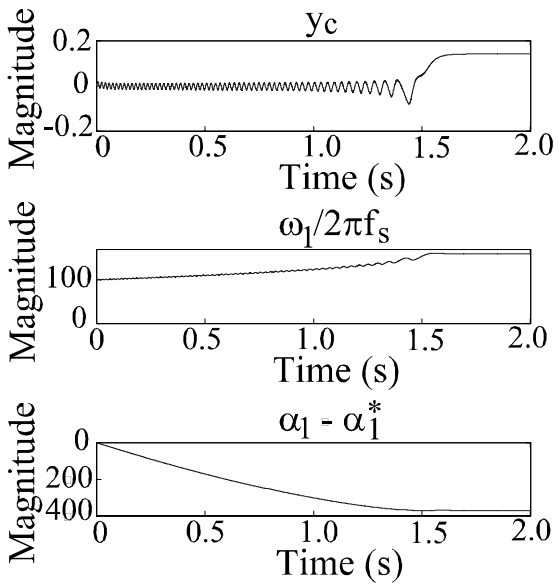

Figure 4.15. States of the MPLL frequency estimator when the MPLL alone is used.

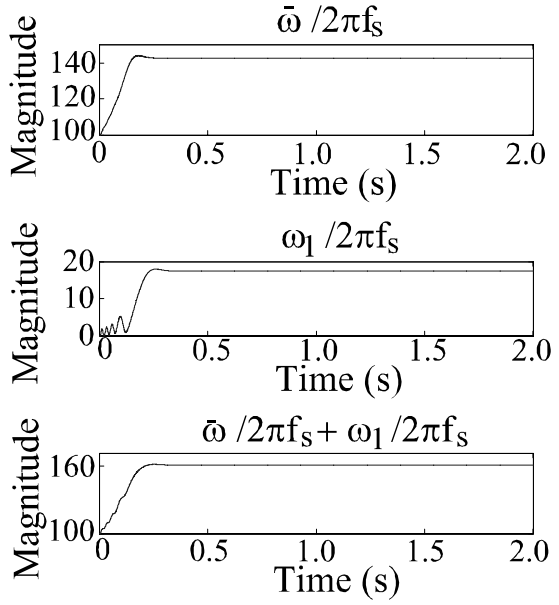

Figure 4.16. Frequency estimates of the MPLL, IMFE, and the combined estimate when the combined MPLL/IMFE estimator is used.

4.6 Sinusoidal Disturbances of Unknown Frequency Acting on an Unknown System

It has been shown that the rejection of sinusoidal disturbances of unknown frequency acting on an unknown system can be accomplished by the ADHSS algorithm. Additionally, it has been shown that when the MPLL frequency estimator is combined with the ADHSS algorithm, the two components interact such that a known phase version of the ADHSS algorithm can be used. Here it is shown how the stability of the ADHSS/MPLL algorithm can be dramatically improved by combining the known phase ADHSS with the MPLL/IMFE frequency estimator.

4.6.1 Combined ADHSS/MPLL/IMFE algorithm

The states of the ADHSS/MPLL/IMFE algorithm can be divided into a fast and a slow time scale. The slow variables are given by the states of the ADHSS, the states of the MPLL, and the IMFE frequency update. To avoid confusion with the signals of the frequency estimator, the notation x_θ is used to denote the state of the ADHSS. This gives

$$\begin{aligned} \dot{x}_\theta &= -gE(x_\theta)w_1(t)\left(w_1^T(t)E^T(x_\theta)x_\theta - y\right) \\ \dot{m} &= g_m e_C \\ \dot{\omega}_1 &= -g_\omega e_S + g'_\omega\left(x_2 x_{1F} - x_1 x_{2F}\right) \\ \dot{\alpha}_1 &= \omega_1 + k\dot{\omega}_1 \end{aligned} \tag{4.90}$$

with the positive constants g, g'_ω, g_m, g_ω, and k, as well as the algebraic expressions

$$\begin{aligned} E(x_\theta) &= \begin{pmatrix} \theta_c(x_\theta) & \theta_s(x_\theta) & 1 \\ \theta_s(x_\theta) & -\theta_c(x_\theta) & 0 \end{pmatrix}^T \\ \theta(x_\theta) &= -\tfrac{1}{x_{\theta1}^2 + x_{\theta2}^2}\begin{pmatrix} x_{\theta1}x_{\theta3} \\ x_{\theta2}x_{\theta3} \end{pmatrix} \\ \begin{pmatrix} e_C \\ e_S \end{pmatrix} &= 2\begin{pmatrix} \cos(\alpha_1) \\ \sin(\alpha_1) \end{pmatrix}\left(y - m\cos\left(\alpha_1\right)\right) \end{aligned} \tag{4.91}$$

The fast variables consist of the plant and disturbance

$$\begin{aligned}
\dot{x}_P &= Ax_P + Bu = Ax_P + Bw_1^T(t)\theta(x_\theta) \\
y &= Cx_P + m^* \cos(\alpha_1^*) = Cx_P + m^* w_1(t) \begin{pmatrix} \cos(\alpha_1 - \alpha_1^*) \\ \sin(\alpha_1 - \alpha_1^*) \end{pmatrix} \\
\dot{\alpha}_1^* &= \omega_1^*
\end{aligned} \tag{4.92}$$

as well as the IMFE dynamics

$$\begin{aligned}
\dot{x}_1 &= -a_2 x_1 + a_2 e_C \\
\dot{x}_2 &= -a_2 x_2 + a_2 e_S \\
\dot{x}_{1F} &= -a_3 x_{1F} + a_3 x_1 \\
\dot{x}_{2F} &= -a_3 x_{2F} + a_3 x_2
\end{aligned} \tag{4.93}$$

4.6.2 Averaged system

The overall system is described by a complex set of time-varying nonlinear differential equations. While the components of the algorithm have been studied separately and shown to have desirable stability properties, it remains to investigate the properties of the combined algorithm. To do this, averaging theory is employed once again. In Sec. 3.3.1, it was shown that the influence of a phase error on the ADHSS required a correction term to be added in the averaged system. Here, this is also the case. After adding the correction term, the overall averaged dynamics are given by

$$\begin{aligned}
\dot{x}_\theta &= -\tfrac{g}{2} E(x_\theta) \left(E^T(x_\theta)\left(x_\theta - x_\theta^*\right) - m^* \begin{pmatrix} \cos(\delta\alpha_1) - 1 \\ \sin(\delta\alpha_1) \end{pmatrix} \right) \\
\dot{m} &= g_m \left(m^* \cos(\delta\alpha_1) - m + x_{\theta 1}^* \theta_c + x_{\theta 2}^* \theta_s \right) \\
\delta\dot{\omega}_1 &= -\tfrac{g'_\omega a_2^2 a_3 m^{*2}}{\left(\delta\omega_1^2 + a_2^2\right)\left(\delta\omega_1^2 + a_3^2\right)} \delta\omega_1 - g_\omega \left(m^* \sin\left(\delta\alpha_1\right) - x_{\theta 2}^* \theta_c + x_{\theta 1}^* \theta_s \right) \\
\delta\dot{\alpha}_1 &= \delta\omega_1 + k\left(\delta\dot{\omega}_1\right)
\end{aligned} \tag{4.94}$$

4.6.3 Equilibrium points

The procedure for finding the equilibrium points of (4.94) is identical to finding the equilibrium points of (3.49) in Chapter 3. Namely, equilibrium points are known to satisfy the following conditions

$$\begin{aligned} m &= 0 \\ x_{\theta 3}\frac{x_{\theta 1}x^*_{\theta 1} + x_{\theta 2}x^*_{\theta 2}}{x^2_{\theta 1} + x^2_{\theta 2}} &= m^* \cos(\delta\alpha_1) \\ x_{\theta 3}\frac{x_{\theta 2}x^*_{\theta 1} - x_{\theta 1}x^*_{\theta 2}}{x^2_{\theta 1} + x^2_{\theta 2}} &= m^* \sin(\delta\alpha_1) \end{aligned} \tag{4.95}$$

Defining $\|P\|$, $\|P^*\|$, ϕ, and ϕ^* so that

$$\begin{aligned} x_{\theta 1} &= \|P\| \cos(\phi) \\ x_{\theta 2} &= \|P\| \sin(\phi) \end{aligned} \tag{4.96}$$

and

$$\begin{aligned} x^*_{\theta 1} &= \|P^*\| \cos(\phi^*) \\ x^*_{\theta 2} &= \|P^*\| \sin(\phi^*) \end{aligned} \tag{4.97}$$

the conditions become

$$\begin{aligned} x_{\theta 3}\frac{\|P^*\| \cos(\phi - \phi^*)}{\|P\|} &= m^* \cos(\delta\alpha_1) \\ x_{\theta 3}\frac{\|P^*\| \sin(\phi - \phi^*)}{\|P\|} &= m^* \sin(\delta\alpha_1) \end{aligned} \tag{4.98}$$

If $\|P\|$ and ϕ are chosen as free variables, $x_{\theta 1}$ and $x_{\theta 2}$ are given by (4.96) and $\delta\alpha_1$ and $x_{\theta 3}$ can take one of two possible values

$$\begin{aligned} \delta\alpha_1 &= \phi - \phi^* + n\pi \\ x_{\theta 3} &= (-1)^n \; m^* \tfrac{\|P\|}{\|P^*\|} \end{aligned} \tag{4.99}$$

with $n = 0$ or 1. For $n = 0$, the estimate of the magnitude of the disturbance is correct and the PLL phase error is zero if the estimate of the plant is exact. As in Chapter 3, the estimate of the magnitude of the disturbance is weighted by the ratio of the plant magnitude to the plant magnitude estimate, and the PLL phase error is equal to the plant phase error $\phi - \phi^*$. For $n = 1$, the magnitude estimate changes sign and the phase simply shifts by 180 degrees to compensate for it.

4.6.3.1 Local stability of equilibrium points

The local stability of the equilibrium points can be obtained by linearizing (3.49) around an equilibrium state. This computation and others to follow are best performed using a symbolic computation engine. With the following definitions

$$\begin{aligned} j_1 &= \tfrac{m^{*2}}{\|P\|\|P^*\|}, \quad j_2 = \tfrac{m^*}{\|P\|} \\ j_3 &= \tfrac{m^{*2}}{\|P^*\|}, \quad j_4 = \tfrac{\|P^*\|}{\|P\|} \end{aligned} \tag{4.100}$$

the Jacobian of the system evaluated around an equilibrium point can be computed to be

$$J = \begin{pmatrix} -\frac{g}{2} j_1 \cos(\phi - \phi^*) & -\frac{g}{2} j_1 \sin(\phi - \phi^*) & (-1)^n \frac{g}{2} j_2 \cos(\phi^*) \\ \frac{g}{2} j_1 \sin(\phi - \phi^*) & -\frac{g}{2} j_1 \cos(\phi - \phi^*) & (-1)^n \frac{g}{2} j_2 \sin(\phi^*) \\ (-1)^n \frac{g}{2} j_2 \cos(2\phi - \phi^*) & (-1)^n \frac{g}{2} j_2 \sin(2\phi - \phi^*) & -\frac{g}{2} j_4 \cos(\phi - \phi^*) \\ (-1)^n g_m j_2 \cos(2\phi - \phi^*) & (-1)^n g_m j_2 \sin(2\phi - \phi^*) & -g_m j_4 \cos(\phi - \phi^*) \\ (-1)^{n+1} g_\omega j_2 \sin(2\phi - \phi^*) & (-1)^n g_\omega j_2 \cos(2\phi - \phi^*) & g_\omega j_4 \sin(\phi - \phi^*) \\ (-1)^{n+1} k g_\omega j_2 \sin(2\phi - \phi^*) & (-1)^n k g_\omega j_2 \cos(2\phi - \phi^*) & k g_\omega j_4 \sin(\phi - \phi^*) \end{pmatrix}$$

$$\begin{pmatrix} 0 & 0 & -\frac{g}{2} j_3 \sin(\phi^*) \\ 0 & 0 & \frac{g}{2} j_3 \cos(\phi^*) \\ 0 & 0 & (-1)^{n+1} \frac{g}{2} m^* \sin(\phi - \phi^*) \\ \cdots \; -g_m & 0 & (-1)^{n+1} g_m m^* \sin(\phi - \phi^*) \\ 0 & -\frac{g'_\omega m^{*2}}{a_3} & (-1)^{n+1} g_\omega m^* \cos(\phi - \phi^*) \\ 0 & 1 - \frac{k g'_\omega m^{*2}}{a_3} & (-1)^{n+1} k g_\omega m^* \cos(\phi - \phi^*) \end{pmatrix} \tag{4.101}$$

This Jacobian is similar to (3.59) except for the elements in row five and six of the fifth column. These elements have changed due to the influence of the modified IMFE dynamics. The characteristic equation $\det(\lambda I - J) = 0$ has the following form

$$\lambda^2 (\lambda + g_m) \left(c_3 \lambda^3 + c_2 \lambda^2 + c_1 \lambda + c_0 \right) = 0. \tag{4.102}$$

The 2 eigenvalues at $\lambda = 0$ are associated with the two-dimensional equilibrium subset, and the stable eigenvalue at $\lambda = -g_m$ is associated with the state m, which depends on but does not influence other states. The stability of the three remain-

ing eigenvalues can be ascertained by considering the third-order polynomial with coefficients

$$\begin{aligned} c_3 &= 1 \\ c_2 &= \cos(\phi-\phi^*)\left(gj_1+\tfrac{1}{2}gj_4+(-1)^n 2kg'_\omega m^*\right)+\tfrac{g'_\omega m^{*2}}{a_3} \\ c_1 &= (-1)^n \tfrac{1}{2}gkg_\omega m^*(j_1+j_4)+\tfrac{g^2}{4}(j_1^2+j_2^2)+(-1)^n g_\omega m^*\cos(\phi-\phi^*) \\ &\quad +\tfrac{gg'^2_\omega m^{*2}}{a_3}\left(j_1+\tfrac{1}{2}j_4\right)\cos(\phi-\phi^*) \\ c_0 &= (-1)^n \tfrac{1}{2}gg_\omega m^*(j_1+j_4)+\tfrac{1}{4}\tfrac{g^2g'_\omega j_1}{m^*a_3} \end{aligned} \tag{4.103}$$

These coefficients are the same as (3.61) except for the last term in each coefficient. The last term reflects the influence of the modified IMFE dynamics. As in Chapter 3, stability of the equilibrium surface is ascertained through application of the Routh-Hurwitz test [35]. In Chapter 3, it was found that when $n = 1$, c_0 was negative indicating there are always eigenvalues in the right-half plane. Now, it is found that through the addition of the modified IMFE dynamics, it is possible to obtain eigenvalues in the left-half plane. However, for the typical gain and system parameter values used in practice, c_0 remains negative for $n = 1$, and eigenvalues remain in the right-half plane. If $n = 0$, the stability of the system is still guaranteed if and only if

$$|\phi-\phi^*| < 90^\circ \text{ and } c_2c_1 - c_3c_0 > 0 \tag{4.104}$$

The condition $c_2c_1 - c_3c_0 > 0$ is equivalent to

$$\cos^2(\phi-\phi^*)+b_1\cos(\phi-\phi^*)-b_0 > 0 \tag{4.105}$$

where (reintroducing the original variables)

$$\begin{aligned} b_1 &= \frac{\left(g^3a_3^2m^*j_6+2g^2kg_\omega a_3^2\|P\|\|P^*\|a_7\right)j_5+N_1}{gg'_\omega m^*(g+2kg_\omega\|P\|\|P^*\|m^*)j_6^2+D_1} \\ b_0 &= \frac{2gg_\omega j_5\|P\|\|P^*\|\left(a_3-kg'_\omega m^{*2}\right)}{2gg_\omega j_6\|P\|\|P^*\|(a_3+kg'_\omega m^{*2})+D_2} \end{aligned} \tag{4.106}$$

with

$$\begin{aligned} N_1 &= 4g \|P\|^2 \|P^*\|^2 m^{*2} \left(k^2 g_\omega^2 a_3^2 j_5 + g_\omega'^2 m^* j_6 + 2 g_\omega g_\omega' a_3 \|P\| \|P^*\|\right) \\ D_1 &= 4kg_\omega^2 a_3 \|P\|^2 \|P^*\|^2 m^* + 2g g_\omega a_3 \|P\| \|P^*\| j_5 \\ D_2 &= 4g^2 g_\omega' m^{*3} j_5 + \|P^*\|^2 m^* \left(4kg_\omega^2 a_3 \|P\|^2 + g^2 g_\omega' \|P^*\|^2\right) \end{aligned} \tag{4.107}$$

and

$$\begin{aligned} j_5 &= \|P^*\|^2 + m^{*2} \\ j_6 &= \|P^*\|^2 + 2m^{*2} \\ j_7 &= \|P^*\|^2 + 3m^{*2} \end{aligned} \tag{4.108}$$

As in Chapter 3, (4.104) is satisfied if and only if

$$|\phi - \phi^*| < \bar{\phi} \tag{4.109}$$

where

$$\bar{\phi} = \cos^{-1}\left(\frac{\sqrt{b_1^2 + 4b_0} - b_1}{2}\right) \tag{4.110}$$

While $\bar{\phi}$ still defines a range of ϕ about the nominal angle ϕ^* that leads to stability of the system, the modified IMFE dynamics have introduced a new mechanism for increasing the value of $\bar{\phi}$. In Chapter 3 it was shown that for k sufficiently large, the region of stability approached that of the known frequency algorithm. However, k cannot become arbitrarily large without seriously affecting stability of the frequency estimate. Now, the gain of the modified IMFE dynamics can also be used to increase the range of ϕ leading to stability. Namely, for

$$a_3 - kg_\omega' m^{*2} \leq 0 \tag{4.111}$$

stability of an equilibrium can be guaranteed. This condition is more easily satisfied. (4.111) also implies that the disturbance magnitude m^* must be sufficiently large.

A similar condition was observed in Chapter 3, where experiments showed that the algorithm was able to cope with sudden decreases in m^*.

4.7 Experimental Results

The performance of the ADHSS/MPLL/IMFE algorithm was examined through single-channel active noise control experiments. The ADHSS equations were discretized using the Euler approximation so that

$$x(k) = x(k-1) - g_\theta E(x(k-1))w_1(k)\left(w_1^T(k)E^T(x(k-1))x(k-1) - y(k)\right) \quad (4.112)$$

where $g_\theta = gT_S$, and the MPLL/IMFE was discretized as described in Sec. 4.5.2. The algorithm was coded in C and implemented in a dSPACE DS1104 digital signal processing board. A sampling frequency of 8 kHz was used. A constant amplitude sinusoidal disturbance was generated by a loudspeaker, while the control signal was produced by another loudspeaker. A microphone was used to measure the cancellation error. The plant consists of the hardware and transmission in the environment from the control signal output to the error microphone input, including the propagation effects of the surrounding air. The experiments were conducted in a small room where many signal reflections were present. In all experiments, the following parameters were used

$$\begin{aligned} g_{\omega d} &= 4.4 \times 10^{-4} \\ g_{md} &= 0.0025 \\ k_\alpha &= 800 \\ z_\alpha &= 1 - \tfrac{1}{k_\alpha} \\ z_{d2} &= 0.99 \\ z_{d3} &= 0.8 \\ g_d &= 0.125 \\ g_\theta &= \begin{pmatrix} 200 & 0 & 0 \\ 0 & 200 & 0 \\ 0 & 0 & 2 \end{pmatrix} T_S \end{aligned} \quad (4.113)$$

4.7.1 Changes in the plant

In this experiment, changes in the plant's frequency response are investigated. The frequency of the disturbance was taken as 190 Hz. The true frequency response parameters corresponding to the initial location of the microphone used to measure the system's error were

$$\begin{aligned} x_1^* &= 0.1004 \\ x_2^* &= -0.7893 \end{aligned} \tag{4.114}$$

This is equivalent to a phase angle of $\phi^* = -82.8$ degrees. The algorithm was allowed to reach steady-state and the estimated frequency response parameters were

$$\begin{aligned} x_1 &= 0.0802 \\ x_2 &= -0.3522 \end{aligned} \tag{4.115}$$

This corresponds to an estimated phase angle of $\phi = -77.2$ degrees and a phase error of $|\phi - \phi^*| = 5.6$ degrees. After reaching steady-state, the microphone used for cancellation was moved from its initial location towards a location whose true frequency response parameters were given by

$$\begin{aligned} x_1^* &= 0.3928 \\ x_2^* &= 0.1207 \end{aligned} \tag{4.116}$$

Corresponding to a phase angle of 17.1 degrees. This equals a change in the phase of the true frequency response of 99.9 degrees. In Fig. 4.17, the states of the ADHSS can be seen, and in Fig. 4.18, the phase angle corresponding to the estimated plant parameters is seen. As the error $|\phi - \phi^*|$ approaches the 90 degree barrier, oscillations begin to appear. However, at approximately 15 *seconds*, the estimated phase angle suddenly changes to approximately $\phi = 3.5$ degrees and a phase error of $|\phi - \phi^*| = 13.6$ degrees. In Fig. 4.19, the control signal u and error signal y are shown. A spike is seen in the error due to the local instability around $|\phi - \phi^*| = 90$ degrees.. However, due to the nonlinear dynamics of the ADHSS, the algorithm is able to recover. The frequency estimate can be seen in Fig. 4.20.

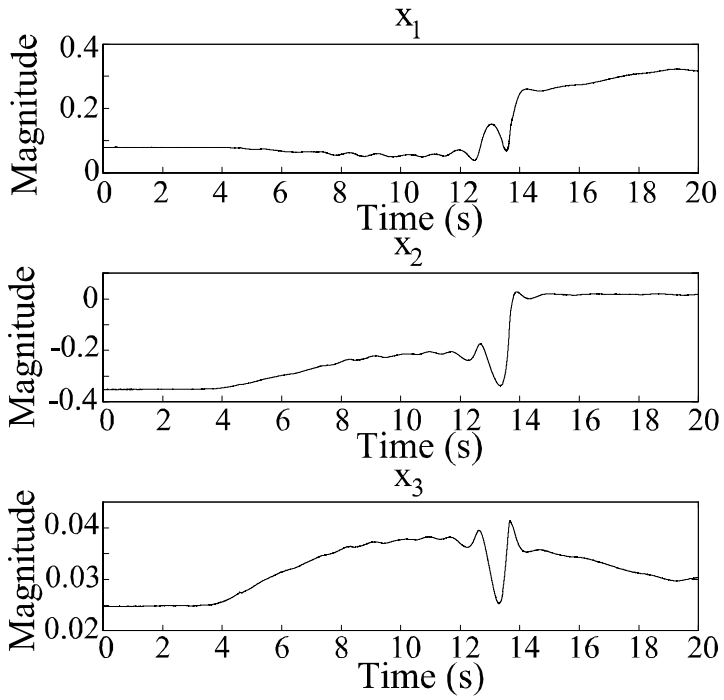

Figure 4.17. States of the ADHSS while the phase of the true plant changes by more than 90 degrees.

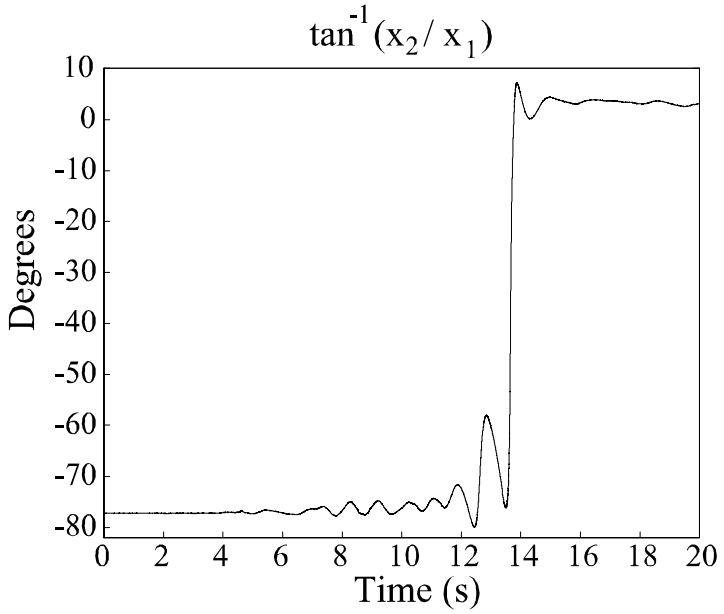

Figure 4.18. ADHSS phase estimate while the phase of the true plant changes by more than 90 degrees.

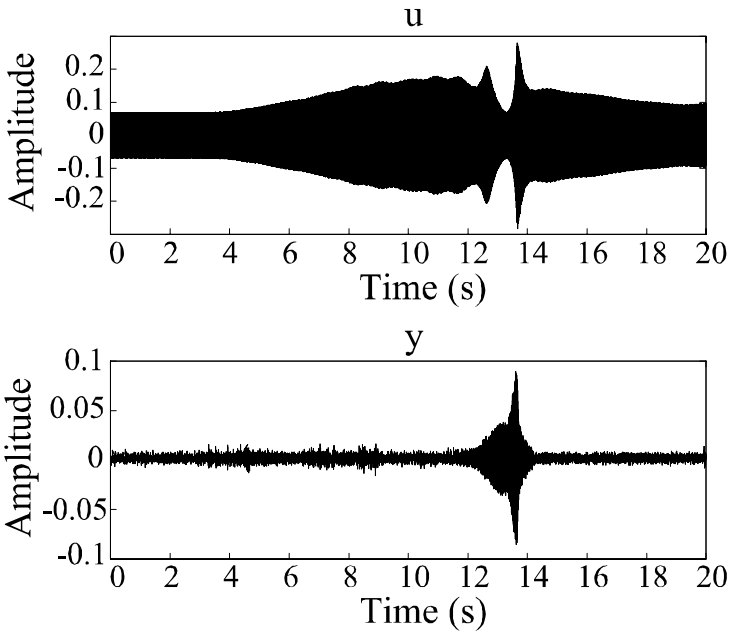

Figure 4.19. Control and error signals while the phase of the true plant changes by more than 90 degrees.

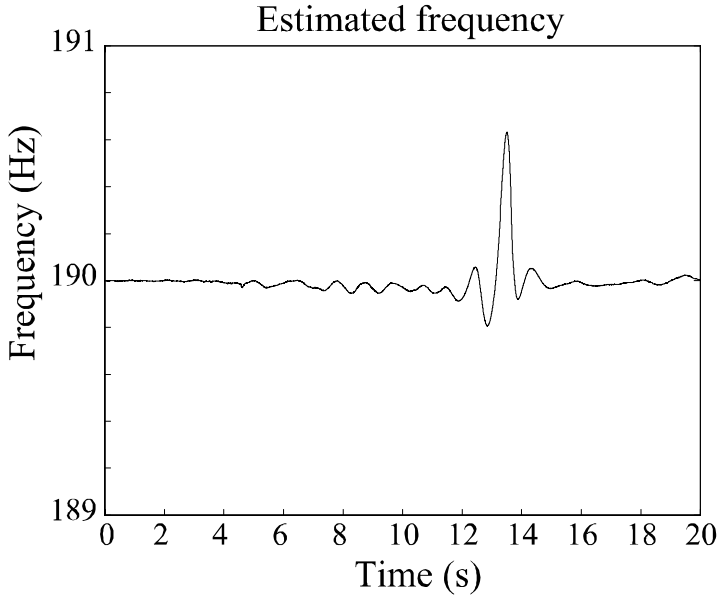

Figure 4.20. Frequency estimate while the phase of the plant changes by more than 90 degrees.

4.7.2 Changes in disturbance frequency

In this experiment, the ability of the ADHSS/MPLL/IMFE algorithm to deal with changes in the frequency of the disturbance was investigated. Initially, the frequency of the disturbance was taken to be 150 Hz. After 2 *seconds*, frequency estimation was engaged and, 3 seconds later the ADHSS was engaged and significant attenuation of the error resulted. After reaching steady-state, the frequency of the disturbance was changed to 200 Hz. This corresponds to a change of 50 Hz in the frequency of the disturbance. The results can be seen in Fig. 4.21. After some initial transients, the error is able to recover and significant attenuation of the disturbance resumes. The frequency estimate is shown in Fig. 4.22.

To demonstrate the significance of these results, the same experiment was repeated with the ADHSS/MPLL algorithm of Chapter 3. In Fig. 4.23, it is seen that this leads to poor rejection of the disturbance. In Fig. 4.24, it is seen that the frequency estimation is unable to compensate for such a large step in the disturbance frequency.

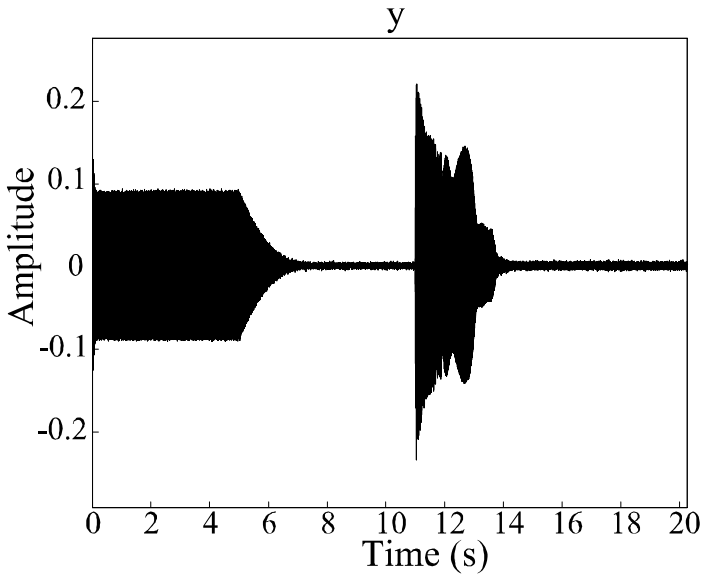

Figure 4.21. ADHSS/MPLL/IMFE error signal with large change in disturbance frequency.

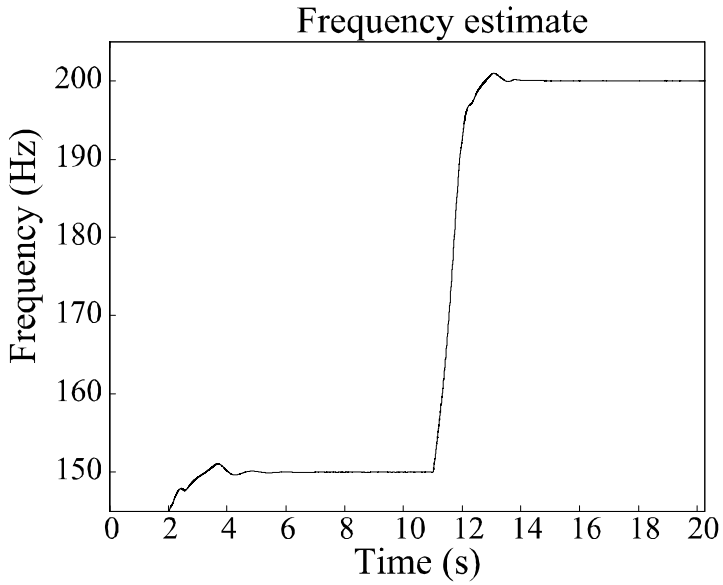

Figure 4.22. ADHSS/MPLL/IMFE estimated frequency with large change in disturbance frequency.

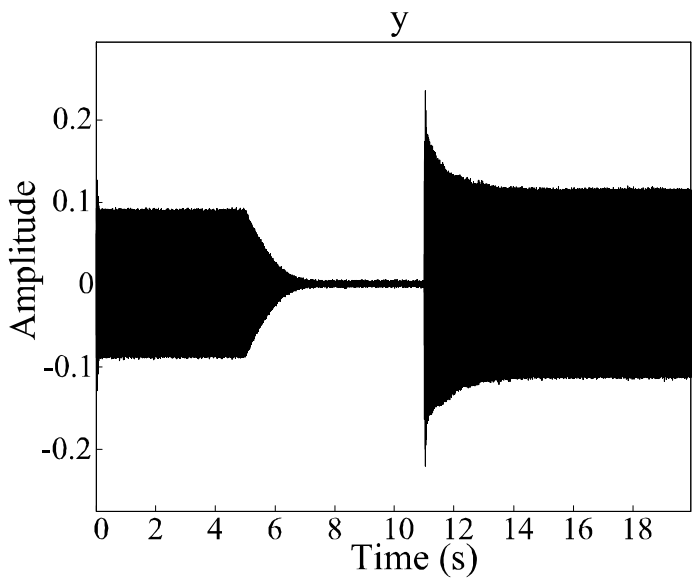

Figure 4.23. ADHSS/MPLL error with a large change in disturbance frequency.

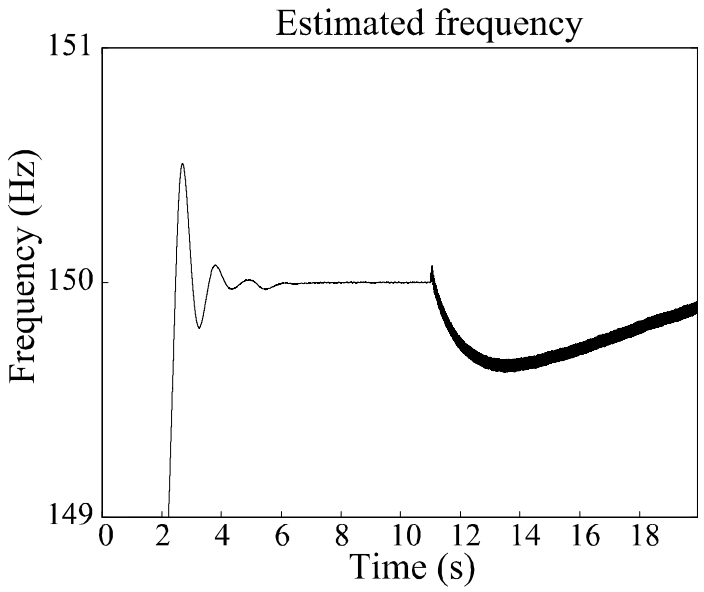

Figure 4.24. ADHSS/MPLL frequency estimate with a large change in the disturbance frequency.

4.8 Conclusions

In this chapter, a new frequency estimator was presented. Derived from the model of a two-phase induction motor under current command, the induction motor frequency estimator, or IMFE, simulated the equations of the model in the absence of load or friction effects with a sinusoidal signal of unknown frequency being used to construct the two-phase sinusoidal input to the motor. This enabled the torque equation of the induction motor model to act as a frequency estimate update. Averaging theory was used to show that global convergence (for positive initial conditions) of the frequency estimator was ensured, with local exponential stability around the nominal value. After presenting the equations needed for a discrete implementation of the estimator, the IMFE was used in two distinct disturbance rejection situations.

In the first, the plant was assumed to be known, and the IMFE was combined with a gradient-based disturbance cancellation algorithm for the rejection of sinusoidal disturbances of unknown frequency. It was found that the control signal used for disturbance cancellation introduced a bias into the frequency estimate requiring a simple fix. Specifically, the effect of the control signal at the output of the plant was

subtracted before being used as input to the IMFE. Averaging theory was used to show that the resulting disturbance cancellation algorithm was also globally convergent, with an assumption of small gains. Active noise control experiments were used to demonstrate performance of the algorithm and to verify the results of the analysis.

In the second disturbance cancellation situation, the plant was assumed to be unknown, and the IMFE was combined with the ADHSS algorithm for unknown plant. Since the plant was not known, it was not possible to implement the fix used when the plant was known. Thus, the IMFE was redesigned to obtain an unbiased estimator in the presence of a constant control signal. It was shown in Chapter 3 that the performance of the ADHSS depended upon a precise frequency estimate. While the IMFE was designed to estimate the frequency of the disturbance, the phase does not lock onto the phase of the disturbance, so that minor variations introduced by measurement noise can lead to an unstable disturbance cancellation algorithm. As such, the IMFE was combined with the MPLL to obtain a frequency estimate whose phase is locked to the disturbance phase while possessing better stability properties than the MPLL alone. An averaging analysis showed that using the IMFE with the ADHSS/MPLL algorithm of Chapter 3 provided an additional mechanism for increasing the range of allowable phase errors in the steady-state plant estimate. Active noise control experiments demonstrated the algorithm.

CHAPTER 5

CONCLUSIONS

5.1 Summary

The primary objective of the dissertation was to develop and analyze adaptive algorithms for sinusoidal disturbances acting on an unknown and possibly time-varying plant. First, an adaptive algorithm known as the so-called ADHSS algorithm was developed based on the assumption that the system's plant could be represented by its sinusoidal steady-state frequency response and that the frequency of the disturbance is known. Estimates of the plant frequency response and the disturbance magnitude and phase were obtained based on a linear parameterization of a measure at the output of the plant. Averaging theory provided justification for the steady-state assumption and provided valuable insight into the behavior of the algorithm. The system's equilibrium was described by a four-dimensional surface containing the nominal parameters and with any point on the surface other than the origin resulting in cancellation of the disturbance. It was found that the line through the origin on the equilibrium surface that is perpendicular to the line joining the origin and the nominal value of the frequency response divides the equilibrium surface into stable and unstable halves, with the nominal values residing on the stable half. A Lyapunov analysis showed that trajectories beginning in the vicinity of the unstable region of the equilibrium surface traveled along a sphere until reaching a stable equilibrium point. Numerous active noise control experiments demonstrated performance of the algorithm when the system's plant changes both rapidly or slowly with time, and a comparison with a similar implementation of the FXLMS algorithm without online plant estimation was given. Finally, extensions of the algorithm for consideration of multiple inputs and outputs as well as multiple frequency components were given and active noise control experiments demonstrated use of the extensions.

While the algorithm worked well when the frequency of the disturbance was known exactly, the presence of even a small frequency error was shown to result in periodic bursting of the control signal. To avoid bursting of the control signal and thus the measured output in cases where the disturbance frequency is uncertain, frequency estimation was added to the ADHSS algorithm. It was found that MPLL frequency estimation could be combined with the ADHSS in a special way that did not significantly increase the complexity of the algorithm. Indeed, the use of MPLL frequency estimation allowed the order of the ADHSS to be decreased from four states in the known frequency case to only three states. Combined with the three states of the MPLL, the overall algorithm for consideration of disturbances of unknown frequency involved only two additional states over the known frequency ADHSS developed in Chapter 2 of the dissertation. After exploring the reduced order ADHSS, the equations describing the overall closed-loop system consisting of ADHSS disturbance rejection and MPLL frequency estimation were given and the corresponding averaged system was found. The equilibrium of the averaged system was a two-dimensional line. Local stability of the combined algorithm was investigated by assessing the eigenvalues of the system linearized about an equilibrium point. It was found that there is always a positive range of equilibrium points around the nominal frequency response parameters for which the system is stable. The range was reduced from the $\pm$ 90 degrees in the known frequency case. However, conditions in terms of the user-defined parameters of the algorithm under which the angle approaches that of the known frequency case were given. Numerous active noise control experiments demonstrated the ability to track changes in both the plant frequency response and disturbance frequency.

While the combined ADHSS/MPLL algorithm was shown to perform well in challenging conditions, a major limitation of the algorithm was due to the local stability of the MPLL frequency estimate. As such, a new frequency estimation algorithm known as the IMFE and possessing semiglobal convergence properties in the context of averaging was introduced. Based on the theory of electric machines, it was shown that the equations of the two-phase induction motor under current

command could be used to estimate the frequency of a sinusoidal signal. Analysis of the corresponding averaged system showed that positive initial frequency estimates converged globally with convergence becoming exponential close to the true frequency. Next, the IMFE was used in an indirect adaptive disturbance cancellation algorithm for a known plant. It was found that the estimator was biased in the presence of a constant control signal, requiring a simple fix. This fix consisted of subtracting the effect of the control signal at the output of the plant from the input to the estimator. However, if the new estimator was to be used with the unknown plant ADHSS algorithm, it would be impossible to utilize this fix. Thus, a modified version of the IMFE that remains unbiased in the presence of a constant control signal was presented. Combining the modified IMFE with the MPLL resulted in an estimator with a larger stability region that still locks onto the phase of the disturbance as the frequency estimate approaches the true value. After combining the MPLL/IMFE frequency estimator with ADHSS disturbance rejection, an eigenanalysis similar to the one used in Chapter 3 for the MPLL alone combined with the ADHSS showed that local stability about an equilibrium of the algorithm was improved. Namely, the user-defined parameters of the modified IMFE could be used to increase the range of equilibrium points around the nominal frequency response parameters for which the system is stable. Active noise control experiments demonstrated the algorithm.

5.2 Future Work

5.2.1 Reduction of the ADHSS

It was shown that the excellent stability properties of the ADHSS where rooted in a fundamental over-parameterization of the system that resulted in the linearized system possessing two eigenvalues at the origin. However, if one of the eigenvalues at the origin could be eliminated while maintaining the stability properties of the algorithm, the order of the ADHSS could be reduced. Practically, this might involve fixing one of the adapted disturbance parameters at a constant value, i.e. setting $x_4 = 1$. Preliminary simulations have shown that this development still leads to convergence of the algorithm with a larger initial transient being observed. However,

at steady-state, the algorithm appeared to posses the same properties as the original algorithm. Future research might involve further development of this idea by dealing with the issue of initial convergence.

5.2.2 Convergence of the ADHSS with frequency tracking

While the local stability of the ADHSS algorithm combined with frequency estimation has been explored, no insight into the region around an equilibrium for which the local stability is valid has been provided. Due to the highly nonlinear nature of the adaptive algorithm, this insight is very difficult to obtain. However, future research could involve exploration of the region of attraction, possibly through a Lyapunov analysis. If discovery of an appropriate Lyapunov function proves elusive, a numerical study may produce useful results.

5.2.3 Extension of the algorithms

While the rejection of sinusoidal disturbances of known frequency acting on an unknown system was demonstrated for multiple inputs/outputs and multiple frequency components, only a single input/output and a single frequency component was considered in the rejection of a sinusoidal disturbance of unknown frequency acting on an unknown system. Since many disturbances consist of multiple distinct frequency components affecting a three-dimensional space, future work should involve the extension of all algorithms introduced in the dissertation. In particular, extending the semiglobally convergent IMFE to include the estimation of multiple frequency components is not at all trivial and would be extremely beneficial.

APPENDIX A

AVERAGING THEORY BACKGROUND - MIXED TIME SCALE SYSTEMS

Of particular interest to our problem is the continuous-time averaging method for mixed time scale systems as discussed in [43]. The theory is applied to systems of the form

$$\begin{aligned} \dot{x} &= \epsilon f(t, x, x_P) \\ \dot{x}_P &= A(x)x_P + h(t, x) + \epsilon g(t, x, x_P) \end{aligned} \tag{A.1}$$

For ϵ sufficiently small, x is a slow variable, while x_P varies faster, except through its dependency on x. Averaging theory shows how the trajectories of (A.1) can be related to the trajectories of the so-called averaged system

$$\dot{x} = \epsilon f_{av}(x) \tag{A.2}$$

where

$$f_{av}(x) = \lim_{T\to\infty} \frac{1}{T} \int_{t_0}^{t_0+T} f(\tau, x_\omega, v(\tau, x))d\tau \tag{A.3}$$

and

$$v(t, x) := \int_0^t e^{A(t-\tau)} h(\tau, x)d\tau. \tag{A.4}$$

Central to the method of averaging is the assumption that the limit in (A.3) exist uniformly in t_0 and x. In other words, there exists a strictly decreasing continuous function $\gamma(T)$, such that $\gamma(T) \to 0$ as $T \to \infty$ and

$$\left| \frac{1}{T} \int_{t_0}^{t_0+T} f(\tau, x, v(\tau, x)) d\tau - f_{av}(x) \right| \leq \gamma(T). \tag{A.5}$$

The function $\gamma(T)$ is called the convergence function. If the limit exists, ϵ is sufficiently small, and certain technical conditions are satisfied, the response of (A.1) is close to the response of (A.2). Specifically, the theory is based on the following assumptions.

Given some arbitrary vector $x \in R^n$ and for some $h > 0$ such that $B_h = \{x \in \mathbb{R}^n \,|\|x\| < h\}$

B1 The function f and g are a piecewise continuous function of time, and a continuous function of x and x_P. Moreover, $f(t, 0, 0) = 0$, $g(t, 0, 0) = 0$ for all $t \geq 0$, and for some $l_1,\ l_2,\ l_3,\ l_4 \geq 0$

$$\begin{aligned} |f(t, x_a, x_{P,a}) - f(t, x_b, x_{P,b})| &\leq l_1 |x_a - x_b| + l_2 |x_{P,a} - x_{P,b}| \\ |g(t, x_a, x_{P,a}) - g(t, x_b, x_{P,b})| &\leq l_3 |x_a - x_b| + l_4 |x_{P,a} - x_{P,b}| \end{aligned} \tag{A.6}$$

for all $t \geq 0$, $x_a,\ x_b \in B_h$, $x_{P,a},\ x_{P,b} \in B_h$. Also assume that $f(t, x, v(t, x))$ has continuous and bounded first partial derivatives with respect to x for all $t \geq 0$ and $x \in B_h$.

B2 The function $f(t, x, v(t, x))$ has average value $f_{av}(x)$. Moreover, $f_{av}(x)$ has continuous and bounded first partial derivatives with respect to x, for all $x \in B_h$, so that for some $l_{av} \geq 0$

$$|f_{av}(x_a) - f_{av}(x_b)| \leq l_{av} |x_a - x_b| \tag{A.7}$$

for all $x_a,\ x_b \in B_h$.

B3 Let $d(t, x) = f(t, x, v(t, x)) - f_{av}(x)$, so that $d(t, x)$ has zero average value. Assume that the convergence function can be written as $\gamma(T)\,|x|$. Additionally, $\frac{\partial d(t,x)}{\partial x}$ has zero average value, with convergence function $\gamma(T)$.

The following result can then be obtained [43]:

Lemma 1 (Perturbation Formulation of Averaging) *If the mixed time scale system (A.1) and the averaged system (A.2) satisfy assumptions B1-B4. Then, there exists a bounded function $w_\epsilon(t,x)$, whose first partial derivative with respect to time is arbitrarily close to $d(t,x)$ and a class K function $\xi(\epsilon)$ such that the transformation*

$$x = z + \epsilon w_\epsilon(t,x) \tag{A.8}$$

is a homeomorphism in B_h for all $\epsilon \leq \epsilon_1$, where $\epsilon_1 > 0$. Under the transformation, system (A.1) becomes

$$\begin{aligned} \dot{z} &= \epsilon f_{av}(z) + \epsilon p_1(t,z,\epsilon) + \epsilon p_2(t,z,x_P,\epsilon) \\ z(0) &= x(0) \end{aligned} \tag{A.9}$$

where

$$|p_1(t,z,\epsilon)| \leq \xi(\epsilon) k_1 |z| \tag{A.10}$$

and

$$|p_2(t,z,x_P,\epsilon)| \leq k_2 |x_{P,zi}| \tag{A.11}$$

for some k_1, k_2 depending on l_1, l_2, l_{av}.

A proof of *Lemma 1* can be found in [43]. This proof establishes a link between the convergence function $\gamma(T)$ and the order of the bound in (A.10). In particular, if $d(t,x)$ in assumption B3 has a bounded integral with respect to time, then $\gamma(T) \sim \frac{1}{T}$ and it can be shown that $\xi(\epsilon)$ is on the order of ϵ. The bound in (A.11) is determined by the convergence properties of $x_{P,zi} = x_P - v(t,x)$, which is the zero-input response of x_P.

Lemma 1 is fundamental to the theory of averaging. It allows a system satisfying certain conditions to be written as a perturbation of the averaged system and it shows that the perturbation terms are bounded. By imposing further restrictions, conclusions can then be drawn concerning the closeness of the original and averaged systems. Consider the additional assumptions:

B4 $A(x)$ is uniformly exponentially stable for all $x \in B_h$.

B5 Let $x_{av}(t)$ specify the solution of the averaged system (A.2). For some $h' < h$, $|x_{av}(t)| \in B_{h'}$ on the time intervals considered, and for some h_0, $x_P(0) \in B_{h_0}$.

B6 $h(t,0) = 0$ for all $t \geq 0$, and $\left\| \frac{\partial h(t,x)}{\partial x} \right\|$ is bounded for all $t \geq 0$, $x \in B_h$.

Then, the following result can be obtained.

Lemma 2 (Basic Averaging Lemma) *If the mixed time scale system (A.1) and the averaged system (A.2) satisfy assumptions B1-B6, then there is an* ϵ_T, $0 < \epsilon_T \leq \epsilon_0$ *and a class K function* $\Psi(\epsilon)$ *such that*

$$\|x(t) - x_{av}(t)\| \leq \Psi(\epsilon) b_T \tag{A.12}$$

for some $b_T > 0$ *and for all* $t \in [0, T/\epsilon]$ *and* $0 < \epsilon \leq \epsilon_T$. *Further,* $\Psi(\epsilon)$ *is on the order of* $\xi(\epsilon) + \epsilon$.

A proof of *Lemma 2* can be found in [43]. *Lemma 2* states that, for ϵ sufficiently small, the trajectories of (A.1) and (A.2) can be made arbitrarily close for all $t \in [0, T/\epsilon]$. This allows insight into the behavior of (A.1) by studying the behavior of (A.2). Also, when $d(t,x)$ in assumption B3 has a bounded integral with respect to time, $\Psi(\epsilon)$ is on the order of ϵ. This condition is satisfied for the system under consideration due to the sinusoidal nature of the signals.

B7 Assume that trajectories of the original and averaged system are such that $x_1^2 + x_2^2 \geqslant \delta$ for some $\delta > 0$.

Assumption B7 is a technical assumption that allows the theory to avoid certain singularities that sometimes occur in adaptive systems, specifically, any time the gain of the plant approaches zero.

APPENDIX B

ADHSS: VERIFICATION OF THE ASSUMPTIONS

The original system is given by

$$f(t,x,x_P) = -E(x)w_1(t)\left(w_1^T(t)E^T(x)x - Cx_P - w_1^T(t)\pi^*\right) \tag{B.1}$$

with corresponding averaged system

$$f_{av}(x) = -\frac{1}{2}E(x)E^T(x)(x-x^*) \tag{B.2}$$

and

$$\begin{aligned} d(t,x) &= f(t,x,v(t,x)) - f_{av}(x) \\ &= -E(x)\left(w_1(t)w_1^T(t) - \tfrac{1}{2}I_{2\times 2}\right)E^T(x)(x-x^*) + E(x)w_1(t)y_{tr}(t) \end{aligned} \tag{B.3}$$

where $y_{tr}(t)$ decays exponentially to zero. In the verification of B1-B6, assumption B7 will be assumed to hold. Then, we have the following:

For some arbitrary vector $x \in R^n$ and for some $h > 0$ such that
$B_h = \{x \in \mathbb{R}^n \,|\, \|x\| < h\}$

B1 Due to the sinusoidal variation of w_1, f is continuous in t. Due to assumption B7 and the BIBO stability of $P(s)$, f is a smooth continuous function in x, x_P for all $t \geq 0$ and $x, x_P \in B_h$. Again, as a result of B7, $\{\partial f/\partial[x, x_P]\}$ is bounded for all $t \geq 0$ and $x, x_P \in B_h$.

B2 In the main text it is shown that the averaged system (B.2) can be obtained from the original system (B.1) and, due to assumption B7, $\partial f_{av}/\partial x$ is continuous and bounded for all $x \in B_h$.

B3 Since averaging is done with respect to time, $d(t,x)$ and $\frac{\partial d(t,x)}{\partial x}$ have zero average value. Further, the following bounds can be derived

$$\begin{aligned} \left| \frac{1}{T} \int_{t_0}^{t_0+T} d(\tau,x) d\tau \right| &\leq \tfrac{1}{T}\gamma_1(T) \left\|x\right\| + \tilde{\gamma}(T) \\ \left| \frac{1}{T} \int_{t_0}^{t_0+T} \frac{\partial d(t,x)}{\partial x} d\tau \right| &\leq \tfrac{1}{T}\gamma_2(T) h \end{aligned} \tag{B.4}$$

where

$$\begin{aligned} \gamma_1(T) &= \tfrac{1}{2\omega \left\|\hat{P}(j\omega)\right\|^2} \left[\left\|\hat{P}(j\omega)\right\|^2 \left\|\pi\right\|^2 + \left\|\hat{\pi}\right\|^2 \left\|P(j\omega)\right\|^2 \right. \\ &\qquad \left. -2 \left\|P(j\omega)\right\|^2 \left\|\hat{P}(j\omega)\right\|^2 (\theta_c\theta_c^* + \theta_s\theta_s^*) \right]^{\frac{1}{2}} \\ \gamma_2(T) &= \tfrac{1}{2\omega \left\|\hat{P}(j\omega)\right\|^2} \left[\left\|x^*\right\|^2 + 4 \left\|P(j\omega)\right\|^2 \left(\frac{\left\|\hat{\pi}\right\|^2}{\left\|\hat{P}(j\omega)\right\|^2} - \theta_c\theta_c^* - \theta_s\theta_s^* \right) \right]^{\frac{1}{2}} \end{aligned} \tag{B.5}$$

and $\tilde{\gamma}(T)$ converges exponentially to 0 with y_{tr} for all $x \in B_h$. Then, one can write

$$\gamma(T) = \frac{1}{T} \max[\gamma_1(T), \gamma_2(T)h] \tag{B.6}$$

for all $x \in B_h$. Further, by assumption B7 and due to the sinusoidal variation of w_1, $d(t,x)$ has a bounded integral with respect to time for all $t \geq 0$ and $x \in B_h$.

B4 This assumption can be verified for the vast majority of active noise and vibration control applications for which this algorithm is designed.

B5 This assumption follows directly from the constraint on the averaged system (2.50) derived in the main text and the bounded-input bounded-output (BIBO) stability of $P(s)$.

B6 This assumption is satisfied as a consequence of the BIBO stability of $P(s)$.

B7 This assumption is satisfied as long as the magnitude of the plant frequency response does not approach zero. While the amplitude response in active noise

and vibration control applications may exhibit dramatic dips due to the interaction of signal reflections, this can be avoided by appropriate arrangement of the hardware.

REFERENCES

[1] B. D. O. Anderson, R. R. Bitmead, C. R. Johnson, P. V. Kokotovic, R. L. Kosut, I. M. Y. Mareels, L. Praly, & B.D. Riedle, *Stability of Adaptive Systems. Passivity and Averaging Analysis*. MIT Press, Cambridge, MA 1986.

[2] S. Bittanti & L. Moiraghi, "Active Control of Vibrations in Helicopters via Pole Assignment Techniques," *IEEE Trans. on Control Systems Technology,* vol. 2, no. 4, pp. 343-350, 1994.

[3] M. Bodson, "An Adaptive Algorithm with Information-Dependent Data Forgetting," *Proc. of the American Control Conference*, Seattle, WA, pp. 3485-3489, 1995.

[4] M. Bodson, "Rejection of Periodic Disturbances of Unknown and Time-Varying Frequency," *International Journal of Adaptive Control and Signal Processing*, vol. 19, pp. 67-88, 2005.

[5] M. Bodson & S. Douglas, "Adaptive Algorithms for the Rejection of Sinusoidal Disturbances with Unknown Frequency," *Automatica*, vol. 33, no. 12, pp. 2213-2221, 1997.

[6] J. Chiasson, *Modeling and High-Performance Control of Electric Machines*, New Jersey, John Wiley and Sons, 2005.

[7] J. Chanderasekar, L. Liu, D. Patt, P. P. Friedmann, & D. S. Bernstein, "Adaptive Harmonic Steady-State Control for Disturbance Rejection", *IEEE Trans. on Control Systems Technology*, vol. 14, no. 6, pp. 993-1007, 2006.

[8] H. G .M. Dötsch, H. T. Smakman, P. M. J. Van den Hof, & M. Steinbuch, "Adaptive Repetitive Control of a Compact Disc Mechanism," *Proc. of the Conference on Decision and Control*, New Orleans, LA, pp. 1720-1725, 1995.

[9] U. Emborg, "Cabin Noise Control in the Saab 2000 High-speed Turboprop Aircraft," *Proc. of the ISMA 2*3, Brussels, Belgium, pp. 13-25, 1998.

[10] G. Feng & M. Palaniswamy,"Adaptive Implementation of Internal Model Principle for Continuous Time Systems," *IEE Proceedings-D*, vol. 139, no. 2, pp. 167-171, 1992.

[11] G. Feng & M. Palaniswamy, "A Stable Adaptive Implementation of the Internal Model Principle," *IEEE Trans. on Automatic Control*, vol. 37, no. 8, pp. 1220-1225, 1992.

[12] Y. H. Guan, W. S. Shepard Jr., T. C. Lim, & M. Li, "Experimental Analysis of an Active Vibration Control System for Gearboxes," *Smart Mater. Struct.*, vol. 13, pp. 1230-1237, 2004.

[13] X. Guo & M. Bodson, "Frequency Estimation and Tracking of Multiple Sinusoidal Components," *Proc. of the Conference on Decision and Control*, Maui, HI, pp. 5360-5365, 2003.

[14] X. Guo & M. Bodson, "Analysis and Implementation of an Adaptive Algorithm for the Rejection of Multiple Sinusoidal Disturbances," submitted to *IEEE Trans. on Control Systems Technology*, 2006.

[15] X. Guo and M. Bodson, "Adaptive rejection of multiple sinusoids of unknown frequency," in Proc. Eur. Control Conf., Kos, Greece, 2007, pp. 121–128.

[16] X. Guo & M. Bodson, "Analysis and Implementation of an Adaptive Algorithm for the Rejection of Multiple Sinusoidal Disturbances," *IEEE Trans. on Control Systems Technology*, vol. 17, no. 1, pp. 40-50, 2009.

[17] S. Hall & N. Wereley, "Performance of higher harmonic control algorithms for helicopter vibration reduction," *J. Guidance Contr. Dynam.*, vol. 116, no. 4, pp. 793–797, 1993.

[18] P. Ioannou & J. Sun, *Robust Adaptive Control*, Prentice-Hall, Upper Saddle River, New Jersey, 1996.

[19] E. Kamen and B. Heck, *Fundamentals of Signals and Systems: Using the Web and Matlab, 2nd Edition*, New Jersey, Prentice Hall, 2000.

[20] H.K. Khalil, *Nonlinear Systems,* 3rd ed., Prentice Hall, New Jersey, 2002.

[21] C. R. Knospe, S. J. Fedigan, R. W. Hope, & R. D. Williams, "A Multi-Tasking Implementation of Adaptive Magnetic Bearing Control," *IEEE Trans. on Control Systems Technology*, vol. 5, no. 2, pp. 230-238, 1997.

[22] S. M. Kuo, S. Mitra, & W.-S. Gan, "Active Noise Control System for Headphone Applications," *IEEE Trans. on Control Systems Technology*, vol. 14, no. 2, pp. 331-335, 2006.

[23] S. M. Kuo & D. R. Morgan, *Active Noise Control Systems: Algorithms and DSP Implementations*, New York, Wiley, 1996.

[24] S. M. Kuo & D. Vijayan, "A Secondary Path Modeling Technique for Active Noise Control Systems," *IEEE Trans. on Speech and Audio Processing*, vol. 5, no. 4, pp. 374-377, 1997.

[25] J. Lau, S. S. Joshi, B. N. Agrawal, & J.-W. Kim, "Investigation of Periodic-Disturbance Identification and Rejection in Spacecraft," *AIAA Journal of Guidance, Control, and Dynamics*, vol. 29, no. 4, pp. 792-798, 2006.

[26] T. J. Manayathara, T.-C. Tsao, J. Bentsman, & D. Ross, "Rejection of Unknown Periodic Load Disturbances in Continuous Steel Casting Process Using Learning Repetitive Control Approach, *IEEE Trans. on Control Systems Technology*, vol. 4, no. 3, pp. 259-265, 1996.

[27] M. A. McEver, D. G. Cole, & R. L. Clark, "Adaptive Feedback Control of Optical Jitter Using Q-parameterization," *Opt. Eng.*, vol. 43, no. 4, pp. 904-910, 2004.

[28] T. Meurers, S.M. Veres, & A.C.H. Tan, "Model-free frequency domain iterative active sound and vibration control," *Control Engineering Practice*, vol. 11, pp. 1049-1059, 2003.

[29] D. R. Morgan, "An Analysis of Multiple Correlation Cancellation Loops with a Filter in the Auxiliary Path," *IEEE Trans. on Speech and Signal Processing*, vol. 28, no. 4, pp. 454-467, 1980.

[30] R. Morino & P. Tomei, "Global estimation of n unknown frequencies," *IEEE Trans. on Automatic Control*, vol. 47, no. 8, pp. 1324—1328, 2002.

[31] K.S. Narendra & A. Annaswamy, *Stable Adaptive Systems*, Prentice-Hall, Englewood Cliffs, NJ, 1989.

[32] M. Niedzwiecki & M. Meller, "A New Approach to Active Noise and Vibration Control-Part I: The Known Frequency Case," *IEEE Trans. Signal Processing*, vol. 57, no. 9, pp. 3373 -3386, 2009.

[33] M. Niedzwiecki & M. Meller, "A New Approach to Active Noise and Vibration Control-Part II: The Unknown Frequency Case," *IEEE Trans. Signal Processing*, vol. 57, no. 9, pp. 3387 -3398, 2009.

[34] D. Patt, J. Chandrasekar, D. S. Bernstein, & P.P. Friedmann, "Higher-Harmonic-Control Algorithm for Helicopter Vibration Reduction Revisited," *AIAA Journal of Guidance, Control, and Dynamics*, vol. 28, no. 5, pp. 918-930, 2005.

[35] C. Phillips & R. Harbor, *Feedback Control Systems*, New Jersey, Prentice Hall, Upper Saddle River, 2000.

[36] S. Pigg and M. Bodson, "A new algorithm for frequency estimation and disturbance cancellation inspired from induction machine theory," *to appear in Proc. of the American Control Conference,* 2011.

[37] S. Pigg and M. Bodson, "Adaptive Algorithms for the Rejection of Sinusoidal Disturbances Acting on Unknown Plants," *IEEE Trans. on Control System Technology*, vol. 18, no. 4, pp. 822-836, 2010.

[38] S. Pigg & M. Bodson, "Adaptive harmonic steady-state disturbance rejection with frequency tracking," *Proc. of the Conference on Decision and Control*, Atlanta, GA, pp. 887-892, 2010.

[39] S. Pigg & M. Bodson, "Rejection of Periodic Disturbances with Adaptation to Unknown Systems," *Proc. of the European Control Conference*, Kos, Greece, pp. 2477-2483, 2007.

[40] S. Pigg & M. Bodson, "Adaptive Rejection of Sinusoidal Disturbances of Known Frequency Acting on Unknown Systems," *Proc. of the American Control Conference*, Minneapolis, MN, pp. 4777-4781, 2006.

[41] G. O.-Pulido, B. C.-Toledo, & A. Loukianov, "A globally convergent estimator for n—frequencies," *IEEE Trans. on Automatic Control*, vol. 47, no. 5, pp. 857—863, 2002.

[42] A. Sacks, M. Bodson, & P. Khosla, "Experimental Results of Adaptive Periodic Disturbance Cancellation in a High Performance Magnetic Disk Drive," *ASME Journal of Dynamics Systems, Measurement, and Control*, vol. 118, pp. 416-424, 1996.

[43] S. Sastry and M. Bodson, *Adaptive Control: Stability, Convergence, and Robustness*, New Jersey, Prentice Hall, Englewood Cliffs, 1989.

[44] T. Söderstrom and P. Stoica, System Identification. Englewood Cliffs, NJ: Prentice-Hall, 1988.

[45] Y. Song, Y. Gong, & S. M.Kuo, "A Robust Hybrid Feedback Active Noise Cancellation Headset," *IEEE Transactions on Speech and Audio Processing*, vol. 13, no. 4, 2005, pp. 607-617.

[46] J. Spanos, Z. Rahman and G. Blackwood, "A Soft 6-Axis Active Vibration Isolator," *Proc. American Control Conference,* Seattle, WA, pp. 412-416, 1995.

[47] M. Steinbuch, "Repetitive control for systems with uncertain period-time," *Automatica*, vol. 38, no. 12, pp. 2103-2109, 2002.

[48] G. Tao, *Adaptive Control Design and Analysis*, Wiley, Hoboken, New Jersey, 2003.

[49] B. Wu and M. Bodson, "A Magnitude/Phase-locked Loop Approach to Parameter Estimation of Periodic Signals," *IEEE Trans. on Automatic Control*, vol. 48, no. 4, pp. 612-618, 2003.

[50] B. Wu & M. Bodson, "Multi-Channel Active Noise Control for Periodic Sources – Indirect Approach," Automatica, vol 40, no. 2, pp. 203-212, 2004.

[51] S.C. Wu & M. Tomizuka, "Repeatable Runout Compensation for Hard Disk Drives Using Adaptive Feedforward Cancellation," *Proc. of the American Control Conference*, Minneapolis, MN, pp. 382-387, 2006.

[52] Y. Xiao, L. Ma, & K. Hasagawa, "Properties of FXLMS-Based Active Noise Control with Online Secondary Path Modeling," *IEEE Trans. Signal Processing*, vol. 57, no. 8, pp. 2931-2949, 2009.

[53] Y. Xu, M. de Mathelin, & D. Knittel, "Adaptive Rejection of Quasi-Periodic Tension Disturbances in the Unwinding of a Non-Circular Roll," *Proc. of the American Control Conference*, Anchorage, AK, pp. 4009-4014, 2002.

[54] M. Zhang, H. Lan, & W. Ser, "An Improved Secondary Path Modeling Method for Active Noise Control Systems," *IEEE Signal Processing Letters*, vol. 7, no. 4, pp. 73-75, 2000.

[55] M. Zhang, H. Lan, & W. Ser, "Cross-updated Active Noise Control System with Online Secondary Path Modeling," *IEEE Trans. on Speech & Audio Processing*, vol. 9, no. 5, pp. 598-602, 2001.

[56] Y. Zhang, P. G. Mehta, R. R. Bitmead, & C. R. Johnson, "Direct Adaptive Control for Tonal Disturbance Rejection," *Proc. of the American Control Conference*, Philadelphia, PA, pp. 1480-1482, 1998.

[57] H. Zhong, V. Kulkarni, & L. Pao, "Adaptive Control for Rejecting Disturbances with Time-varying Frequencies in Tape Systems," *Proc. of the American Control Conference*, Portland, OR, pp. 533-538, 2005.